UNIVERSITÀ
DEGLI STUDI
DI PADOVA

Sede Amministrativa: Università degli Studi di Padova

Dipartimento di Biologia

SCUOLA DI DOTTORATO DI RICERCA IN: BIOSCIENZE E BIOTECNOLOGIE
INDIRIZZO: NEUROBIOLOGIA
CICLO: XXVIII

SIGNALING AND TRANSCRIPTOMICS AT THE DEGENERATING-REGENERATING NEUROMUSCULAR JUNCTION

Direttore della Scuola: Ch.mo Prof. Paolo Bernardi
Supervisore: Dott.ssa Ornella Rossetto

Dottorando: Samuele Negro

SOMMARIO

La giunzione neuromuscolare è una regione anatomica altamente specializzata in cui i segnali elettrici che corrono lungo l'assone del motoneurone sono convertiti in segnali chimici, che vengono a loro volta riconosciuti dalle cellule muscolari causandone la contrazione. E' composta dal terminale assonico del motoneurone, dalle cellule di Schwann perisinaptiche che avvolgono quest'ultimo, dalla fibra muscolare e dalla lamina basale. La giunzione neuromuscolare non è protetta da barriere anatomiche e pertanto può essere bersaglio di differenti patogeni come virus, batteri, tossine. Inoltre la giunzione può essere affetta da diverse patologie quali la sclerosi laterale amiotrofica o la Sindrome di *Guillain-Barrè* di origine autoimmune. Per questi motivi e per la sua funzione fisiologica essenziale per la vita degli animali, non sorprende dunque la capacità della giunzione neuromuscolare di rigenerare e recuperare la sua funzionalità a seguito di differenti tipi di danno. Questa abilità si è mantenuta durante l'evoluzione animale, e differenzia le sinapsi del sistema nervoso periferico da quelle del centrale, che non hanno invece capacità rigenerativa.

In seguito a denervazione le cellule di Schwann perisinaptiche mostrano una grande plasticità, de-differenziando ed iniziando a proliferare. Esse partecipano attivamente ai processi di rigenerazione nervosa, contribuendo al rilascio di diversi fattori in grado di agire sul terminale nervoso degenerato promuovendone la ricrescita ed il pieno recupero della sua funzionalità. Sono ancora poco conosciuti gli eventi intra- ed inter-cellulari che avvengono alla giunzione durante la degenerazione e soprattutto quelli che governano il processo rigenerativo del terminale nervoso.

A tale scopo, nel nostro laboratorio è stato messo a punto un approccio sperimentale innovativo che permette di studiare la degenerazione e rigenerazione della giunzione neuromuscolare sfruttando il meccanismo d'azione di una neurotossina presinaptica animale, α-Latrotoxin, presente nel veleno dei ragni del genere *Latrodectus*. Questa tossina agisce selettivamente a livello della membrana presinaptica del motoneurone, inducendo un danno acuto e localizzato del terminale nervoso. Il terminale degenera rapidamente ma in breve tempo, in seguito alla rimozione dei detriti neuronali da parte delle cellule di Schwann, è in grado di ricrescere e di riacquisire una piena funzionalità.

L'azione di tali neurotossine rappresenta quindi un sistema appropriato e controllato per indurre una degenerazione acuta, localizzata e reversibile del terminale nervoso, evitando il coinvolgimento di molti tipi cellulari e mediatori dell'infiammazione come accade nel corso della degenerazione indotta da *cut/crush* del nervo sciatico, tradizionalmente utilizzato fino ad

oggi. Questo approccio può dunque aiutare a definire i meccanismi molecolari ed identificare i segnali intra- ed inter-cellulari alla base della degenerazione e rigenerazione nervosa.
Con lo scopo di identificare molecole in grado di promuovere la rigenerazione del terminale nervoso, abbiamo messo a punto un protocollo che ci ha permesso di ottenere per la prima volta un'analisi trascrizionale a livello di giunzione neuromuscolare durante le diverse fasi di degenerazione e rigenerazione del terminale nervoso periferico in seguito ad intossicazione con α-latrotoxin. Abbiamo isolato e sequenziato da un numero adeguato di giunzioni RNA codificanti e non. Tra i diversi trascritti abbiamo selezionato quelli che presentavano un basso valore di espressione nel controllo, un aumento durante le fase rigenerativa per poi tornare ad un livello basale quando la rigenerazione è conclusa. Tra questi abbiamo approfondito lo studio della chemochina CXCL12, dimostrando che viene prodotta dalle cellule di Schwann terminali durante la degenerazione nervosa, e che l'iniezione intraperitoneale di un anticorpo neutralizzante comporta un ritardo nel processo rigenerativo. Inoltre abbiamo dimostrato che questa chemochina è in grado di promuovere la crescita dei neuriti di motoneuroni in coltura. Questi risultati suggeriscono come CXCL12 sia un importante fattore rilasciato dalle cellule di Schwann perisinaptiche con un ruolo cruciale nei processi rigenerativi del terminale nervoso.

Parallelamente abbiamo indagato quali potessero essere i segnali di *allarme* rilasciati dal terminale nervoso in degenerazione in grado di attivare le cellule di Schwann e di promuovere la rigenerazione nervosa. Abbiamo dimostrato che l'ATP viene rilasciato da neuroni in seguito ad intossicazione con α-latrotoxin, ed è in grado di attivare nelle cellule di Schwann diverse vie di segnalazione intracellulari quali il calcio, l'AMP ciclico, ERK1/2, CREB, importanti per il recupero della funzionalità nervosa in seguito a danno.

I dati presentati in questa tesi identificano l'ATP come importante molecola segnale nella comunicazione tra il terminale nervoso in degenerazione e le vicine cellule di Schwann perisinaptiche, ed estendono tale ruolo anche ad altre forme di degenerazione del terminale nervoso presinaptico.

SUMMARY

The neuromuscular junction (NMJ) is a specialized tripartite synapse that allows the transmission of an electrical impulse travelling along the axon to the muscle. It is composed of the motor axon terminal (MAT), covered by perisynaptic Schwann cells (PSCs), and the muscle fibre (MF), which are separated by a basal lamina. The NMJ is not protected by anatomical barriers: it can be therefore exposed to traumas, to the attack of many pathogens including neurotoxins, and affected by many neuromuscular diseases such as amyotrophic lateral sclerosis and immune-mediated disorders, such as the Guillain-Barré and Miller Fisher syndromes. For these reasons and for its essential role in life and survival the NMJ has retained throughout vertebrate evolution an intrinsic ability for repair and regeneration, differently from central synapses. After nerve injury the glial cells of the NMJ, the PSCs, acquire a regenerative phenotype and release a series of factors that act on the stump of the MAT, providing several cues to promote neuronal regeneration. Following peripheral nerve injury, many changes taking place at the NMJ have been reported so far, but the inter- and intra-cellular signaling that occur during MAT degeneration and, more importantly, those governing the ensuing regeneration are not completely understood.

We have recently established a model to study NMJ degeneration and regeneration in mice based on the specific action of α-latrotoxin, a presynaptic neurotoxin isolated from the venom of the black widow spider, which targets specifically the presynaptic terminal causing its complete degeneration. Following intoxication and the subsequent clearing of MAT debris by PSCs, the axon stump regrows in few days in mice allowing complete NMJ recovery. This toxin represents therefore a simple and controlled method to induce an acute, localized and reversible nerve terminal degeneration not blurred by inflammation, and can help to identify molecules involved in the intra- and inter-cellular signalling governing NMJ regeneration.

In the search of candidate molecules involved in triggering and sustaining nerve recovery we choose to perform a transcriptomic analysis of the mouse NMJs at different time points after injection of α-latrotoxin. This approach has been very challenging: to our knowledge a transcriptomic analysis of the sole NMJ was never reported before. We succeeded in collecting a number of NMJs suitable for RNA isolation and sequencing of both coding and non–coding RNAs. Among the coding transcripts we selected a series of messenger RNAs (mRNAs) that are expressed at low level in controls, at higher levels during regeneration, and then return to basal when substantial regeneration is attained and we selected the mRNA encoding for the chemokine CXCL12. We found that CXCL12 is produced by PSCs during

nerve degeneration, and that intraperitoneal injection of a neutralizing antibody for CXCL12 slows down the regeneration process. Moreover, the exposure of primary motor neurons to the recombinant chemokine stimulates neurite growth.

These data suggest that CXCL12 is an important factor released by PSCs with a crucial role in the nerve terminal regeneration process.

Parallely, we looked for molecules released by injured neurons that could activate SCs and stimulate nerve regeneration. We found that ATP released by intoxicated neurons activates a series of intracellullar signaling pathways in SCs including Ca^{2+}, adenylate cyclase, ERK 1/2 and CREB, that are of fundamental importance for the recovery of nerve function. We propose ATP as an important *alarm* signal partecipating in the cross-talk between degenerating nerve terminals and adjacent PSCs not only in a model of degeneration by a spider toxin, but also in different forms of neurodegeneration of the presynaptic nerve terminal.

TABLE OF CONTENTS

ABBREVIATIONS

PNS: peripheral nervous system

SCs: Schwann cells

BL: basal lamina

EPP: end plate potential

NMJ: neuromuscular junction

ACh: acetylcholine

PSCs: perisynaptic Schwann cells

ATP: adenosine triphosphate

CAMs : cell adhesion molecules

CNS: central nervous system

mPTP: mitochondrial permeability transition pore

P0: protein 0

ECM: extracellular matrix

IGF: insulin-like growth factor

MAT: motor axon terminal

MF: muscle fibre

MFCs: Microfluidic chambers

MBP: myelin basic protein

GFAP: glial acidic fibrillary protein

GAP-43: growth associated protein 43

MCP-1:chemoattractantprotein-1

NGF: nerve growth factor

LIF: leukemia inhibitory factor

LDH: lactate dehydrogenase

LCM: laser microdissection

BDNF: brain derived neurotrophic factor

GDNF: glial cell-line derived neurotrophic factor

NT-3: neurotrophin 3

NT-4: neurotrophin 4

ATF-3: cyclic AMP-dependent transcription factor

CREB: cyclic AMP-responsive element-binding protein

STAT: signal transducers and activators of transcription

ALS: amyotrophic lateral sclerosis

α-Ltx: α-Latrotoxin

NO: nitric oxide

NRX: neurexin

ROS: reactive oxygen species

WD: Wallerian degeneration

LPH1: latrophilin 1

PTPσ: protein tyrosin phosphatase σ

PLC: phospholipase C

IP_3: inositol triphosphate

PKC: protein kinase C

NT-3: neurotrophin 3

MIP-1a : macrophage inflammatory protein-1a

mRNA: messanger RNA

ncRNA: non-coding RNA

miRNA: microRNA

lncRNA: long non-coding RNA

MNs: motoneurons

CGNs: cerebellar granular neurons

SEM: Scanning electron micrograph

VAChT : vesicular Ach transporter

mtDNA: mitochondrial DNA

Cyt c: cytochrome c

PTPs: protein tyrosine phosphatases

ERK: extracellular-signal regulated kinase

MAPK: mitogen activated protein kinase

LAL: *Levator Auris Longus*

EJPs: evoked junction potentials

P2Y: metabotropic purinergic receptors

P2X: ionotropic purinergic receptors

CD68: cluster of differentiation 68

CFP: cyan fluorescence protein

YFP: yellow fluorescence protein

GFP: green fluorescence protein

Introduction

The neuromuscular junction (NMJ) is the specialized anatomical structure where the electric signal transmitted along the myelinated axon is converted into a chemical message, the neurotransmitter, which is released into the intersynaptic space, permeates through the basal lamina (BL), a structured form of extracellular matrix, and binds to post-synaptic receptors causing muscle contraction. The regulation of voluntary and involuntary movements, which relies on this transmission, is crucial for many physiological functions such as breathing, moving and feeding.

This synapse consists of three main components: motor axon terminal (MAT), muscle fiber (MF), and perisynaptic Schwann cells (PSCs). MAT is covered by a multi-cellular carpet of PSCs, and the NMJ is enveloped by the largely permeable BL separating MAT from MF.

Most NMJs are exposed to mechanical traumas and represent the main target of several pathogens: indeed during evolution, both animals and bacteria have developed several toxins which selectively interfere with nerve-muscle transmission, causing paralysis and in most severe cases death. Moreover in many neuromuscular diseases such as amyotrophic lateral sclerosis and immune-mediated disorders, including the Guillain-Barré and Miller Fisher syndromes, the synaptic transmission between motor neurons and muscle cells is compromised, with demyelination and axonal degeneration.

For these reasons and for its essential role in life and survival the NMJ, at variance from most mammalian tissues, has retained through evolution the capacity to regenerate. Damaged MATs regenerate readily (unlike those in the central nervous system), and form new NMJs that look and perform as the original ones. PSCs are main players of NMJ regeneration and provide fundamental cues that trigger neuronal regenerative responses. Following injury PSCs de-differentiate and acquire phagocytic properties, remove cellular debris and guide axon growth to its original site with recovery of function (Son et al., 1996; Jessen et al., 2015). This complex response is governed by molecular signals that are exchanged among the three cellular components of the NMJ and the BL, whose nature is largely unknown.

This work has been focused on the setting up of an innovative experimental system to define the NMJ transcriptome profile and the crosstalk between the different components of NMJ during nerve degeneration\regeneration. The final purpose was to identify pathways involved in the recovery of NMJ functionality, and to find out molecules released by PSCs and MF capable of promoting the growth of the axonal stump for the reconstitution of a functional MAT and of an active NMJ.

The unravelling of the complex interplay of inter- and intra-cellular signaling occurring among the three cellular partners of the NMJ is essential to devise more effective therapies for the treatment of patients affected by motor neuron peripheral degenerations of any kind.

1. The neuromuscular junction

Motor neurons in the brain stem and in the spinal cord have axons that branch intramuscularly to provide peripheral single nerve terminals at each muscle fibre. The motor neuron and the innervated muscle fibre form a motor unit. A muscle fibre can be innervated by one motor neuron only, except for the extraocular muscle fibre, which can be innervated by axons from multiple motor neurons. The neuromuscular junction (NMJ) is a specialized chemical synapse where transmission of information takes place between the axon of a motor neuron and a skeletal muscle fibre. This synapse consists of three main components: motor axon terminal (MAT), muscle fiber (MF) and perisynaptic Schwann cells (PSC) (Fig.1). Moreover the synaptic cleft of NMJ contains a structured form of extracellular matrix known as basal lamina (BL), that separates the MAT from the MF, but includes PSCs. The nerve terminal branches are covered by non-myelinating PSCs (Sanes and Lichtman, 1999). The synaptic cleft is about 60 nm wide.

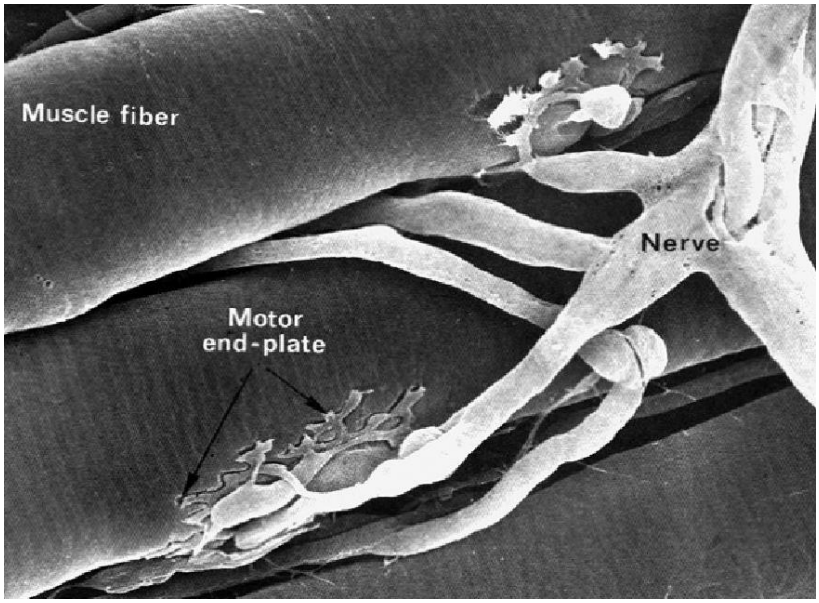

Fig.1. Scanning electron micrograph (SEM) of a motor nerve and two motor end plates (arrows).

1.1 Pre- and postsynaptic specializations of NMJ

The NMJ contains highly specialized pre- and postsynaptic sites, with different organization and roles in neurotransmission. In vertebrate NMJs the neurotransmitter is acetylcholine (ACh), which is synthesized in the cytosol of the nerve endings from acetyl coenzyme A and choline by choline acetyltransferase. A single nerve terminal has approximately 200,000

synaptic vesicles, each containing ACh. Under controlled conditions fusion of a pool of vesicles with the presynaptic membrane results in neurotransmitter release into the synaptic cleft. The neurotransmitter diffuses in about 0.5 ms across the extracellular synaptic space and binds to nicotinic ACh receptors (nAChRs) on the postsynaptic cell. After activation of the nAChRs the neurotransmitter is catabolized by acetylcholinesterase in the extracellular synaptic space. The postsynaptic membrane is specialized to respond adequately to the released neurotransmitter. It contains nAChRs, which are ligand-gated ion channels, clustered in lipid rafts. Clustering is dependent, amongst others, on agrin, muscle-specific kinase, and rapsyn (Zhu et al., 2006; Chen et al., 2007). The AChR is a Na+ / K+ channel. When activated by ACh binding, the channel opens and allows for a relative large influx of Na+ ions and a smaller flow outwards of K+ ions: the net influx of positivity leads to a depolarization of the muscle membrane. These changes in the electric properties of the membrane are termed "end plate potential" (EPP). If the EPP is sufficiently large, a muscle fibre action potential is triggered by opening of the voltage-gated Na+ channels, leading to contraction of the muscle. The total charge of an EPP required to produce an action potential has to overcome a threshold value. During normal activity the amount of neurotransmitter released is abundantly greater than the required threshold, allowing a safety margin for more stressful situations, and ensuing the NMJ to be a reliable synapse (Wood and Slater, 2001).

1.2 Basal lamina

BL is composed of extracellular matrix (ECM) proteins that reside within the synaptic cleft at the NMJ. It plays an essential role in almost all aspects of synaptic development including synaptic initiation, topography, ultrastructure, maturation, stability and transmission. BL is an ordered ECM structure that contains laminin and collagen IV as its main protein constituents, along with heparan sulfate glycosaminoglycans, which in muscle include agrin and perlecan, and other ECM proteins, including tenascin, fibronectin and nidogen (Yurchenco et al., 2004). McMahan and colleagues, in the late 1970s, demonstrated that, after injury of either the pre- or postsynaptic NMJ components, ECM proteins of the synaptic BL help to dictate the topography of synapses on regenerated cell membranes (McMahan et al., 1978; Burden et al., 1979). Denervation of motor axons, coupled with muscle destruction, leads to re-innervation of original synaptic sites on the BL, while postsynaptic differentiation of regenerated muscle occurs at the original synaptic sites on the BL even in the absence of the nerve.

Thus, the synaptic BL not only marks the location of the NMJ during development, but also provides trophic support to allow NMJ regeneration, and contains essentially indelible markers of synaptic localization and differentiation.

1.3 Perisynaptic Schwann cells

PSC (also termed terminal SCs) are the glial cells at NMJ that share markers with other glial cells, such as S-100 (Son and Thompson, 1995). At mammalian and amphibian NMJs, there are typically 3 to 5 PSCs.

PSCs are non-myelinating SCs, traditionally believed to play passive roles at the synapse. By contrast, it has become clear that PSCs roles at NMJ are more dynamic than originally thought. Indeed, PSCs display a higher number of neurotransmitter receptors and ion channels than myelinating SCs. In this regard, PSCs are more analogous to CNS astrocytes than to myelinating SCs. For instance, they have functional L-type voltage-dependent Ca^{2+} channels (Robitaille et al., 1996), muscarinic (Robitaille et al., 1997), purinergic (Robitaille, 1995), and substance P (SP) receptors (Bourque and Robitaille, 1998). PSCs express receptors for ACh and ATP. Moreover, they contain and/or can synthesize numerous potential neuromodulatory substances, including nitric oxide (NO) (Descarries et al., 1998), and glutamate (Pinard et al., 2003). The anatomical relationship between PSCs and the presynaptic and postsynaptic elements of the NMJ, and the presence of receptors able to detect neurotransmitters and neuromodulators suggest that synaptic activity is controlled by PSCs, and this might indirectly contribute to synaptic stability. Additionally, PSCs play a direct role in the competition during NMJ development. PSCs are indeed present at the neonatal junction (Brill et al., 2011) where they play a major role in the removal of losing axons once they are eliminated from the muscle surface (Bishop et al., 2004). As losing axons withdraw from the synapse, forming so-called retraction bulbs (Riley, 1977), PSCs phagocytose pieces of them (Bishop et al., 2004). PSCs are also important for the maintenance of axon terminals, as their ablation in frog tadpoles reduces the growth of NMJs (Reddy et al., 2003). SCs deletion in mice (Wolpowitz et al., 2000) results in loss of muscle innervation and motor neuron death.

Hence PSCs are important for an activity dependent continuum of synaptic efficacy, stability, and plasticity at the NMJ. We expect that this relationship helps to maintain synaptic efficacy under normal conditions and contributes to reestablishing synaptic connections after denervation. Indeed, non-traditional executive roles for PSCs are being recognized during recovery after nerve injury. Following denervation PSCs de-differentiate to an earlier

developmental stage, becoming "reactive" PSCs, and start proliferating. These reactive PSCs actively participate in the process of nerve degeneration and regeneration: they undergo changes in their gene expression and acquire macrophagic-like activities, thus contributing to the removal of nerve debris as well as to the recruitment of macrophages, by releasing cytokines and chemokines. Moreover, following nerve terminals degeneration, PSCs at denervated end-plates extend long processes that find innervated endplates, where they then induce a terminal sprout and guide nerve regrowth to the denervated endplate.

In conclusion, the NMJ is a complex structure where an intense cross talk occurs among the cellular partners during its development and maturation (Fig.2). The identification of the inter- and intra-cellular signaling among the components of this specialized synapse is essential to molecularly define the mechanism of nerve degeneration/regeneration, and to devise more effective therapies for the treatment of patients affected by motor neuron degeneration of any kind.

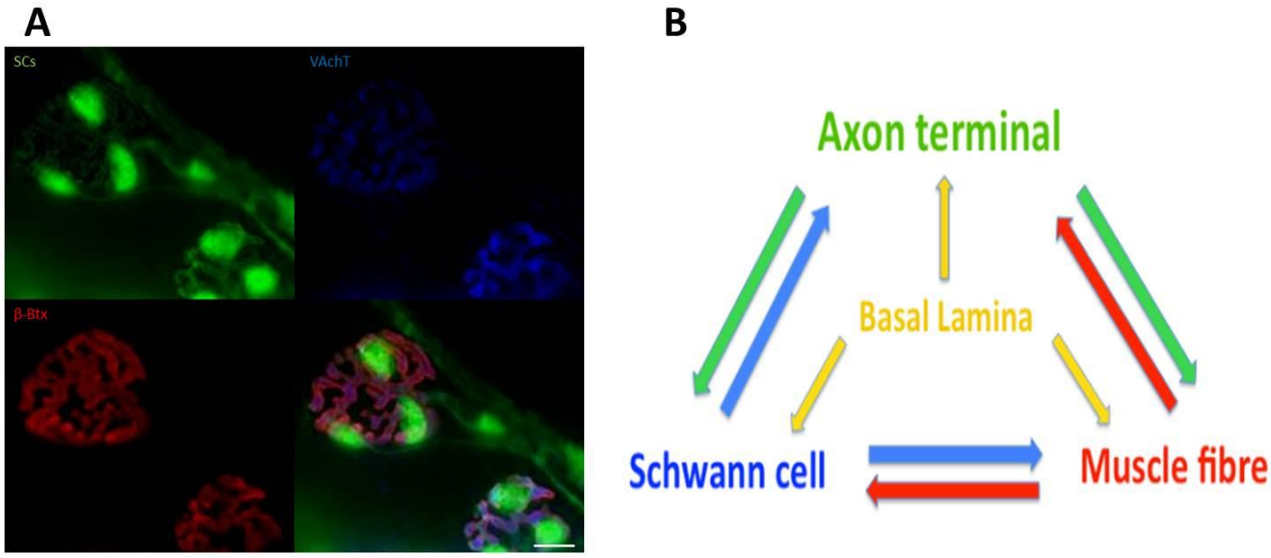

Fig.2. Mammalian NMJs. A: Immunohistochemistry of *Levator Auris Longus (LAL)* muscle of a transgenic mouse expressing GFP in the cytosol of SCs under the *plp* promoter (green). Presynaptic nerve terminals are labelled with an antibody against the vesicular Ach transporter (VAChT, blue), while the muscle end-plate is stained by α-Bungarotoxin (α-Btx) Alexa 555-conjugated (red). Scale bar: 10 μm. **B**: Diagram of molecular signaling between MAT, PSCs, BL and MF.

2. Peripheral nerve degeneration

Disruption of axonal integrity during injury to the peripheral nerve system (PNS) sets into motion a cascade of responses including inflammation, SCs mobilization, and degeneration of the nerve fibres distal to the injury site. There are different types of axonal degeneration. In 1850, Augustus Waller described changes in axons of cranial nerves after they were disconnected from their cell bodies (Waller, 1850; reprinted in Stoll et al., 2002). Those phenomena have been collectively termed Wallerian degeneration (WD), the simplest model of axonal degeneration, which includes the rapid disintegration of the distal axons, with the subsequent recruitment of immune cells that clear nerve debris. This process is required for successful regeneration to occur in the PNS (Gaudet et al., 2011). In the central nervous system (CNS), regeneration is inhibited in part because WD occurs much more slowly, and because myelin contains inhibitory molecules (Vargas and Barres, 2007; Filbin et al., 2003). The inhibitory environment in the CNS is the greatest challenge for regeneration of CNS axons. WD usually begins within 24-36 hours from the lesion. Early pathological changes in the distal stump include failure of synaptic transmission, target denervation and granular disintegration of the axonal cytoskeleton. Within minutes after damage to the axonal membrane, Ca^{2+}-mediated proteolytic activity by calpain initiates fragmentation of axonal cytoskeleton, leading to a massive decrease of microtubular and neurofilament protein levels (Coleman, 2005; Glass et al., 2002) and inner organelles, together with axolemma swelling; bead-like formation leading to the breakdown of axons occurs within 48 h (Beirowski et al., 2005). Early alterations also include endoplasmic reticulum degradation, and accumulation of swelled mitochondria at the paranodal regions at the site of injury (Conforti et al., 2014). Mitochondria have been proposed to have key roles in WD: in the earliest phase they swell, accumulate at paranodal sites and lose their membrane potential. Mitochondrial disfunction lowers ATP levels, generates reactive oxygen species (ROS) and impairs calcium buffering, leading to cellular homeostasis imbalance, mitochondrial permeability transition pore opening, release of pro-apoptotic signals and activation of other cell death mechanisms. Indeed ROS scavengers delay WD and axon pathology associated with neurodegenerative disorders (Press et al., 2008). However, whether these changes are a cause or simply a consequence of degeneration remains unclear (Conforti et al., 2014).

At the end of the process the axon undergoes complete fragmentation; the rate of degradation depends on the type of injury. Another factor affecting degradation rate is axon length: in longer axons cytoskeleton degrades more slowly, thus longer axons take longer to degenerate.

The second, and more delayed injury-induced signaling phase is mediated by signaling complexes transported in a retrograde manner back to the cell body. A key aspect of the increased retrograde transport following peripheral nerve injury is the increased expression or activation of adaptor molecules that facilitate the association of transcription factors with the dynein motor proteins of the retrograde transport (Ben-Yaakov, et al.,2012). Clinically, WD is observed following traumatic or ischemic nerve injury.

Another type of nerve degeneration is called "Wallerian-like", pathologically reminiscent of WD but not necessarily due to nerve transection. It is observed in a variety of disease states that may involve focal axonal interruption (Glass, 2002). Examples include inflammatory and demyelinating diseases, as well as degenerative diseases that result in formation of large axonal swellings or spheroids or disruption of axonal transport (Coleman, 2005). The third type of axon degeneration comprises the so-called "dying-back" neuropathies, in which axon degeneration is most prominent in distal nerves (Cavanagh et al., 1964)(Fig.3). It includes peripheral neuropathies that may result from a variety of insults including diabetes mellitus, exposures to toxics, HIV infection, nutritional deficiencies, aging and neurodegenerative diseases such as ALS and autoimmune neuropathies, including the Guillain-Barré and Miller Fisher syndromes (Coleman et al., 2005). In these types of nerve degeneration many molecular changes influencing motor neuron degeneration are thought to occur at the NMJ at very early stages of the disease prior to symptom onset (Moloney et al., 2014).

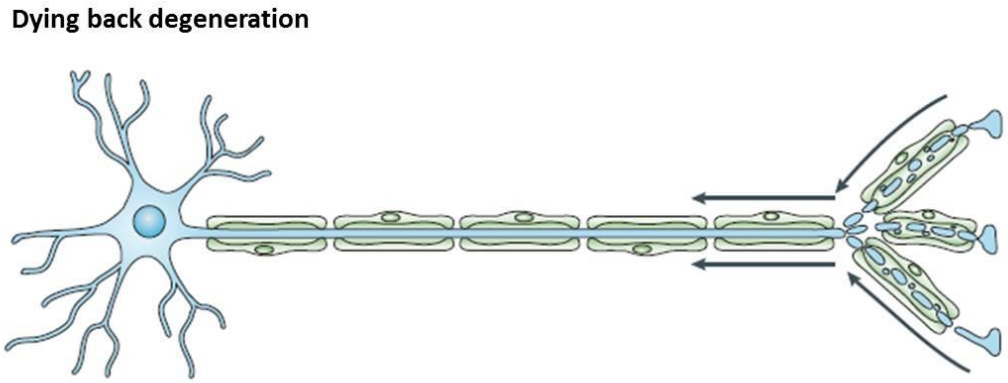

Fig.3. Dying back model of axon degeneration. The 'dying back' model (top) proposes that degeneration of each axon starts at the distal end and moves retrogradely. (Coleman et al., 2005)

However axonal degeneration due to a diverse array of insults seems to share common features: (1) impaired axonal transport, (2) mitochondrial failure, and (3) rise in axonal Ca^{2+}, with calpain activation and degradation of axonal components. While the proximal cause(s) of

axonal degeneration in peripheral neuropathies and degenerative motor neuron diseases are unknown, substantial evidence supports the idea that degeneration ultimately proceeds through these pathways (Coleman, 2005).

Another feature in common to different types of nerve degeneration is that, immediately after peripheral nerve injury, SCs dissociate from axons, dedifferentiate to a progenitor-like state, become "reactive", and start proliferating (Clemence et al., 1989). They undergo changes in gene expression, down-regulate structural proteins such as protein zero (P0), myelin basic protein (MBP) and myelin associated glycoprotein, whilst up-regulate cell-adhesion molecules and glial fibrillary acidic protein (GFAP), along with growth factors (Thomson et al., 1993). Following peripheral nerve injury, specific laminin subunits are up-regulated by SCs (Doyu et al. 1993; Wallquist et al., 2002), favoring the formation of different laminins to support nerve growth. Indeed, genetic deletion of the gamma1 (γ1) laminin subunit causes a significant decrease in regenerating nerve fibres crossing into the distal fragment of crushed sciatic nerves (Chen and Strickland, 2003). The myelin sheaths separate from the axons, rapidly deteriorate and shorten to form bead-like structures. Moreover, reactive SCs acquire macrophagic-like activities and start clearing up the axonal and myelin debris (Stoll et al.,1989); they secrete cytokines and chemokines, such as chemoattractantprotein-1 (MCP-1) or leukemia inhibitory factor (LIF), that promote infiltration of macrophages, thus improving the clearing rate of cell debris (Tofaris et al., 2002). Indeed, the influx of macrophages has proved to be a critical step in nerve regeneration (Rotshenkeret al., 2011). Macrophages also produce growth factors and regulate the constituents of the extracellular matrix (ECM) (Griffin et al., 1993; Shen et al., 1998). Macrophages recruited to the site of peripheral nerve injury seem to be of the M2 phenotype, and act to both suppress inflammation and promote repair (Ydens et al., 2012).

The disruption of normal innervation results in an extensive array of PSCs responses which includes: de-differentiation, proliferation, invasion of the synaptic cleft, release of Ach, changes in neurotransmitter receptor properties, expression of growth-associated, cytoskeletal, and other proteins, and extensive process extension. Within 24 h from denervation growth-associated protein 43 (GAP-43) is upregulated in PSCs at the rat NMJ, and its levels drop following reinnervation (Woolf et al., 1992). GAP-43 expression is not dependent on neurotransmission, but likely results from a loss of nerve contact or degeneration products (Hassan et al., 1994). Moreover, PSC immunoreactivity for the p75 neurotrophin receptor increases during denervation (Reynolds and Woolf, 1992). PSCs at degenerating NMJs, once completed the clearing of MAT debris, occupy the denervated synaptic cleft and start

releasing ACh, giving rise to miniature endplate potentials in the muscle fibre (Auld and Robitaille 2003).

3. Peripheral nerve regeneration

The injured PNS differs from the injured CNS in its remarkable capacity of self-recovery, which depends on the extent and type of nerve injury. Regeneration involves a series of molecular events involving the injured neuron and associated SCs that leads to axon regrowth, remyelination, and functional restitution. Over time, the understanding on the PNS regeneration process has increased significantly. Injured axons form proximal regenerative buds that, in a process largely governed by factors produced by SCs, sprout and grow toward their distal targets. Furthermore, the importance of degeneration as the rate limiting step in the process of recovery has also been elucidated. After PNS injury, there is exponential migration of glia and macrophages to the lesion site for the purpose of removing debris. This process clears the path for the growing axons. Once the debris is cleared, the proximal end of the injured axon can sprout, leading to regenerative buds. If an axon is able to survive following nerve injury, it urgently needs to regain its ionic homeostasis through the rapid repair of the ruptured membrane. This occurs in two stages: first, plasma membrane at the cut end collapses, thereby reducing the diameter of the ruptured membrane and in some cases even leading to fusion of the cut end; second, vesicles move to the ruptured plasma membrane to form multivesicular structures that fuse with the plasma membrane, the so-called “sealing patch”. After closure of the interrupted plasma membrane, the assembly of a growth cone apparatus can begin (Bradke et al., 2012).

Growth cones are highly motile structures that explore the extracellular environment, guide and promote the extension of the axon and determine the direction of growth. The main morphological characteristic of a growth cone is a sheet-like expansion of the growing axon at its tip, called lamellipodium. The highly dynamic nature of growth cones allows them to respond to the surrounding environment by rapidly changing direction and branching in response to various stimuli. Overall, axon elongation is the product of a process known as tip growth. This process requires the recruitment of membrane and its insertion into the neurolemma. The source of this membrane is mostly anterogradely transported vesicles that derive from the Golgi apparatus (Erez et al., 2007); it is conceivable that a fraction of the retrieved plasma membrane from the cut axonal end is reused for the growth process (Schaefer et al., 2008). Laminins of the BL interact with the integrins of the growth cone to

promote the forward movement of the axon tip. Additionally, axon outgrowth is also supported by the stabilization of the proximal ends of microtubules, which provide the structural support for the axon. Many of the molecules that are necessary for immediate growth cone assembly are provided by recycling axonal material; however, growth cones also contain proteins that are not part of the structure of mature axon shafts. These new proteins could arrive via axonal transport or through local protein translation. Indeed, some axons in mammalian PNS contain messenger RNAs (mRNAs), ribosomal proteins and Golgi-like structures and can synthesize proteins within the axon (Sotelo-Silveira et al., 2008; Yoo et al., 2010).

SCs play a crucial role in repair of peripheral axons. Within the distal nerve stump, SCs undergo several changes that are required to support growth cone outgrowth. After the initial injury, they transdifferentiate, loose their myelinating phenotype, and become repair cells. Their expression of myelin protein is downregulated, and growth-promoting genes, including those encoding cell adhesion molecules, growth factors such as NGF, BDNF, GDNF and NT-3 and their receptors, are upregulated (Hoke et al., 2002; You et al., 2007). These changes in SCs after injury might be actively triggered by an injury signal, or might occur as a result of loss of axonal signals. During their proliferation phase, SCs begin to form a line of cells called Bands of Bungner, within the basal laminar tube, which guide and encourage axon growth in the proper direction (Sheib et al., 2013).

Also PSCs at NMJs greatly contribute to axonal regeneration after nerve injury. After full denervation, PSC processes were shown to extend between adjacent endplates and often form fasciculated bundles (Son et al., 1995). During reinnervation, regenerating axons that follows myelinating SCs tubes do not stop once found the endplates on the muscle. They keep on growing beyond the endplate region, where they follow PSC extensions very closely (Son et al., 1995). In this manner, the processes act as bridges between endplates for reinnervating axons. These bridges precede axons, and instances were observed where PSC processes extended well beyond the limit of their associated axon (Son and Thompson, 1995). By contrast, axons were not observed extending past their associated PSC processes. Thus, processes guided reinnervating axons to endplates. Following partial denervation, nerve sprouts from undamaged axons extend from terminals to innervate denervated muscle fibres (Brown et al., 1981). In addition to nerve sprouting, PSCs extend numerous long processes after partial denervation (Mehta et al., 1993; Son and Thompson 1995; Love and Thompson, 1999). They contact other endplates, and the vast majority of connections are formed by processes from denervated endplates contacting innervated endplates. Interestingly, all nerve

sprouts resulting from partial denervation were associated with PSC processes. Moreover, PSC processes always extend beyond their associated nerve sprouts, giving the impression that they were leading the growing sprouts. Of the nerve sprouts that had reinnervated endplates, most were associated with PSC processes from denervated endplates (Love and Thompson, 1999). These data suggest that PSC processes from denervated endplates find innervated endplates, inducing a terminal sprout and guide it to the denervated endplate. Because most bridges exist between denervated and innervated endplates, PSC processes appear to select innervated endplates, which is clearly an advantage for facilitating reinnervation of their denervated endplate. It is not clear if this is achieved through selective guidance or stabilization by signals from innervated endplates.

4. Factors that positively influence nerve regeneration

The growth of axons, their guidance to the original synaptic sites on denervated fibers and the functional recovery from peripheral nerve injury are complex processes that involve many still unknown factors, both intrinsic and extrinsic to neurons. Neuronal survival after injury is a prerequisite for regeneration and is facilitated by an array of trophic factors from multiple sources, including neurotrophins, cytokines, chemokines, insulin-like growth factors (IGFs), and glial-cell-line-derived neurotrophic factors (GDNFs). Axotomized neurons must switch from a transmitting mode to a growth mode and express growth-associated proteins, such as GAP-43, tubulin, and actin, as well as an array of novel neuropeptides and cytokines, all of which have the potential to promote axonal regeneration. After peripheral injury also SCs express cytokines and chemokines important for successful nerve regeneration. These dedifferentiated SCs upregulate synthesis and secretion of the chemokine monocyte chemoattractant protein-1 (MCP-1, now referred to as CCL2, chemokine C–C motif ligand 2) and macrophage inflammatory protein-1a (MIP-1a, also known as CCL3), with a peak in mRNA expression at 1 d after injury (Subang and Richardson, 2001; Perrin et al., 2005). It was recently shown that during degeneration MAT releases signaling molecules such as mtDNA and Cyt c, which in turn activate PSCs and promote nerve regeneration (Duregotti et al., 2015).

SCs in the distal stump undergo proliferation and phenotypical changes to prepare the local environment for axonal regeneration. They increase the expression of surface cell adhesion molecules (CAMs) such as *N*-CAM, Ng-CAM/L1, N-cadherin, and L2/HNK-1, they elaborate a basement membrane that contains many ECM proteins such as laminin, fibronectin, and

tenascin, creating a permissive environment to axonal growth and playing an important role in the promotion of post injury nerve regeneration. Laminin for instance, the major component of the ECM in the PNS, exhibits clear stimulatory effects on axonal growth, and is able to counteract inhibitory myelin influences (Lemons et al., 2005). Numerous studies have demonstrated that laminin not only improves neurite growth but also mediates SCs migration, proliferation, or remyelination (Tucker et al., 2008; Previtali et al., 2001). Moreover, denervated SCs of the distal nerve fragment up-regulate trophic factors, such as nerve growth factor (NGF), brain-derived neurotrophic factor (BDNF) and neurotrophin-4 (NT4), that support neuronal survival and axon growth (Gordon et al., 2009). Even the interactions between neurotransmitters, such as Ach and ATP, released by nerve terminal and their receptors expressed in PSCs play an important role in the regeneration of axons. Indeed after blockade of nicotinic AChRs and purinergic P2Y receptors of injured peripheral nerves, fewer axons grow into the peripheral nerve stump than in untreated (Vrbova et al., 2009), indicating that the interactions between transmitters released from the growth cones and SCs in the distal stump are important for nerve regeneration.

Several transcription factors are thought to be important for promoting the regenerative phenotype, including ERK (Duregotti et al., 2015), c-Jun (Arthur Farraj et al., 2012), cyclic AMP-dependent transcription factor ATF-3, members of the cyclic AMP-responsive element-binding protein (CREB) family of transcription factors, signal transducers and activators of transcription (STAT) proteins, and NF-κB (Scheib and Höke 2013). One transcription factor essential for nerve regeneration is c-Jun, a component of transcription factor AP-1. After injury, c-Jun is upregulated in repair SCs. When c-Jun is inactivated in SCs of mice, these cells become less supportive of regeneration: myelin debris persists, neuronal death increases, bands of Büngner are not maintained, and functional recovery is impaired (Arthur-Farraj et al., 2012). Non-coding RNAs (ncRNAs), especially microRNAs (miRNAs) and long non-coding RNAs (lncRNAs), have been reported to be dysregulated following a variety of peripheral nerve injury (Yu et al., 2015).

In addition to the classic mechanisms of intercellular signaling, the possibility of communication through secreted vesicles has been poorly explored to date. Recent findings suggest the occurrence of a lateral transfer mediated by vesicles from glial cells to axons that could have important roles in axonal growth and axonal regeneration (Lopez-Verrilli et al., 2013). In the following paragraphs I will describe more in detail some of the molecules important for nerve regeneration.

4.1 ATP

ATP is well known as a free energy source involved in many biochemical pathways, but it is also recognized as an extracellular messenger. ATP was found co-released with ACh at NMJs more than 30 years ago (Silinsky, 1975), and interacts with both neurons and SCs. A number of different receptors are expressed at the NMJ by the presynaptic nerve terminal, the postsynaptic muscle, and PSCs (Fig.4). They include P1 adenosine receptors on presynaptic terminals (Baxter et al., 2005) and PSCs (Robitaille 1995), and P2 receptors on PSCs (Robitaille 1995), nerve terminals (Grishin et al., 2005), and muscle fibres (Collet et al., 2002). Purinergic signaling in the PNS and at the NMJ takes place during development of NMJ, PNS myelination, and neuron-glia interactions (Todd and Robitaille, 2006). ATP is a functionally important extracellular signaling molecule in the CNS also during nerve injury. A recent study revealed that both resting and activated microglia express P2X4, P2X7, and P2Y12 receptors after nerve injury, and that released ATP can trigger significant Ca^{2+} entry into the cytoplasm, thus contributing to the activation of resting microglia (Fields and Burnstock, 2006). In *vitro* findings demonstrate that cultured SCs respond to ATP with a transient increase in intracellular calcium that is blocked by the P2 purinoreceptor antagonist suramin (Ansellin et al., 1997). These observations, together with the presence of purinergic receptors, provide further evidence that SCs respond to ATP released by nerve terminals. However, the mechanism of ATP release after peripheral nerve axons injury and its effects are not well known. In particular, it is not clear whether ATP released from injured nerve induce the activation of denervated SCs in the distal nerve stumps, and if this interaction plays a role in peripheral nerve regeneration.

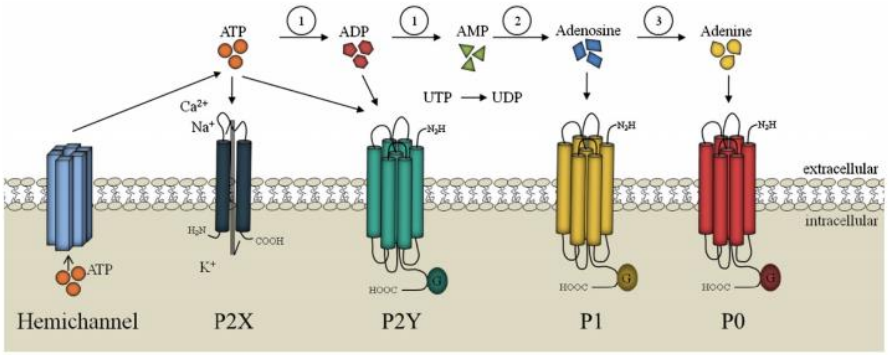

Fig.4. Purinergic receptors and their natural ligands. Purinergic receptors are divided into P2 receptors, activated by a variety of nucleotides, which can be further subdivided into ionotropic P2X receptors activated by ATP and the metabotropic G-protein-coupled receptors (P2Y) stimulated by nucleotides, di- or triphosphates, purines or pyrimidines. In contrast, metabotropic P1 receptors are preferentially activated by adenosine. Recently, evidences for the functional expression of adenine receptors, designated as P0 receptors, have been found. At NMJ both P1 and P2 receptors are expressed.

5. Experimental model

The classical experimental approach used to study nerve degeneration/regeneration is the *in-vivo* cut or crush of sciatic nerves in rats or mice. This approach leads to WD with consequent inflammation, and involvement of many cell types and mediators. This surgically-induced nerve degeneration closely mimics the cascade of events observed following traumatic or ischemic nerve injury, such as impaired axonal transport, mitochondrial failure, and cytoskeletal fragmentation of injured nerves, thus representing a well-established model to characterize these pathological conditions.

However in several motor neuron diseases, collectively referred to as "dying-back" neuropathies, axon degeneration is most prominent in distal nerves. Many molecular changes influencing motor neuron degeneration are thought to occur at the NMJ at very early stages of the disease, prior to symptoms onset (Moloney et al., 2014). Dying-back axonopathies include ALS and autoimmune neuropathies such as the Guillain-Barré and Miller Fisher syndromes. The ability of injured peripheral nerves to regenerate and re-innervate their original targets is characteristic of the PNS. Successful regeneration at NMJ is a consequence of well arranged interactions between injured nerve, non-neuronal cells, especially PSCs, MF and BL. Hence, further characterization of pathological events that occur peripherally during initial denervation may provide insight into disease onset, help in the discovery of pre-symptomatic diagnostic disease markers, lead to the identification of additional pathways involved in the recovery of NMJ functionality, and hopefully of new therapeutic targets.

To this purpose, we induced a very specific and localized damage to the MAT in order to avoid the activation of many cell types (including myelinating SCs), and the production of a massive inflammatory response. This localized damage mimics the main pathological events that lead to nerve terminal degeneration in injured patients and in other neurodegenerative conditions. The original and novel experimental approach described here employs a presynaptic neurotoxin, α-Latrotoxin (α-Ltx), a pore forming toxin from black widow spiders, to provide an acute and localized damage of MAT, that is much more controllable than classical methods and is fully repaired within a short time.

5.1 α-Latrotoxin

Black widow spiders (genus *Latrodectus*) are largely diffused in many parts of the world. The venom of *Latrodectus spp.* contains at least 86 unique proteins (Duan et al., 2006), including several homologous latrotoxins (LTXs) which play a role in its toxicity towards insects and crustaceans, with only one component, alpha-Latrotoxin (α-Ltx), targeting vertebrates specifically (Grishin, 1998).

The toxin almost always exists as a stable dimer in which the monomers are associated "head to tail" (Orlova et al. 2000). Association of dimers, strongly catalysed by Mg2+, produces a cyclical structure that can contain four monomers only. The tetramer has C4 rotational symmetry and resembles a bowl, in which the bottom is formed by the "horizontal" parts of the bodies (Fig.5). This part is important for penetration into lipid bilayers, and it is likely that structural rearrangements required for tetramerisation expose the surface regions favourable to interaction with lipid bilayers. In addition, this part represents the intracellular mouth of the channel, with a large (30 Å) central hole in its center. Above this, in the centre of the "bowl", the four heads form a cylindrical assembly surrounding the channel, which is restricted at one point to 10 Å; this constriction probably corresponds to the cations binding site of the α-Ltx channel. The role of tetramerisation in toxin pore formation has been vividly illustrated by mutagenesis. Indeed mutated α-Ltx fails to incorporate into the membrane and form pores, providing a powerful argument that the tetramer is the molecular species that inserts into membranes. (Ashton et al., 2001; Volynski et al., 2003).

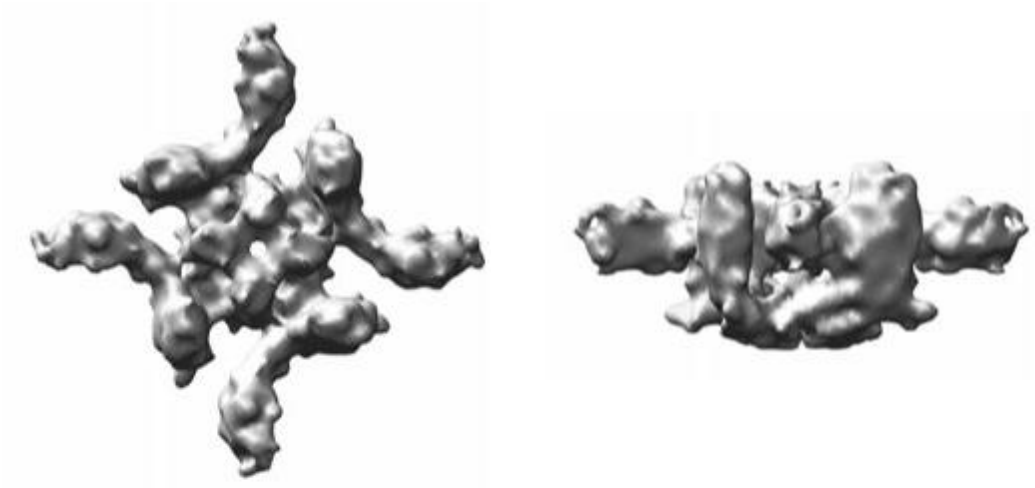

Fig.5. reconstructions of the α-Ltx tetramer, viewed from the top and side. The tetramer is the active form of α-Ltx (Ushkaryov, 2008).

Although α-Ltx is able to insert into pure lipidic membranes, reconstituted receptors greatly enhance the rate of insertion (Scheer et al., 1986). Biological membranes seem even more refractive to the toxin: when cells do not possess α-LTX receptors, no pore formation can be detected (Volynski et al., 2000), whereas expression of exogenous receptors allows abundant α-LTX insertion and concomitant channel formation. It is not clear whether some receptors are directly involved in membrane insertion, if they simply concentrate toxin near membrane or if they organise membrane lipid domains to make them accessible to α-Ltx. However till now, three surface-proteins have been identified to be selectively bound by α-Ltx: neurexin (NRX) (calcium-dependent interaction), latrophilin 1 (LPH1) and protein tyrosin phosphatase σ (PTPσ) (calcium-independent interaction). Such receptors are present mostly in the brain, but they have also been found, though in small amounts, in other secretory tissues such as pancreas, lung and kidney. Thus, receptors confer specificity to the pore-mediated effects of α-Ltx (Ushkaryov, 2008). Moreover, the makeup of lipid bilayer seems to influence the rate of α-Ltx insertion into lipid membranes (Robello et al., 1984). All α-Ltx actions in biological systems require receptors, which provide binding sites for the toxin on the cell surface. Once bound to its target membrane, α-Ltx can cause both calcium-dependent and -independent release of neurotransmitters. Part of its calcium-dependent action is due to the pore formation and resulting calcium influx; this mechanism triggers the release of both the readily releasable and the reserve pools of vesicles (Ashton et al., 2001). Another action is based on receptor-mediated signaling, which involves stimulation of PLC, production of IP_3 and diacyl glycerol, with release of stored calcium and activation of protein kinase C (PKC) respectively. This mechanism, most likely mediated by LPH1, affects the readily releasable vesicles only. Both the pore and receptor mediated signals can be amplified by the release of intracellular calcium, for istance mitochondria can contribute to the increase in intracellular [Ca^{2+}], and the extracellular calcium influx (Ushkaryov, 2008).

Electrophysiologically, α-Ltx causes an increase in the frequency of spontaneous miniature postsynaptic potentials (mepps), and it also affects evoked action potentials (epps) and synchronous release in a time-dependent manner, eventually inhibiting them, thus leading to skeletal muscles paralysis (Capogna et al., 1996).

Electron microscopy studies at mouse soleus muscles show that, within 30 minutes from intoxication, motor nerve terminals become markedly swollen, as a consequence of the toxin-mediated entry of cations, and depleted of synaptic vesicles, due to the massive vesicle fusion (Fig.6). Mitochondria appear also swollen and rounded (Duchen et al., 1981; Matteoli et al., 1998; Tedesco, Rigoni et al., 2009). The massive calcium influx cause the activation of

calcium-dependent calpains, triggering cytoskeletal fragmentation (Duregotti et al., 2013), and eventually to nerve terminals degeneration.

By 6 hours from intoxication motor nerve terminals are disrupted and engulfed by SCs. By 24 hours end-plates are denervated. Noteworthy, MAT regenerates in a short time, with fully recovery of the NMJ (Duchen et al., 1981).

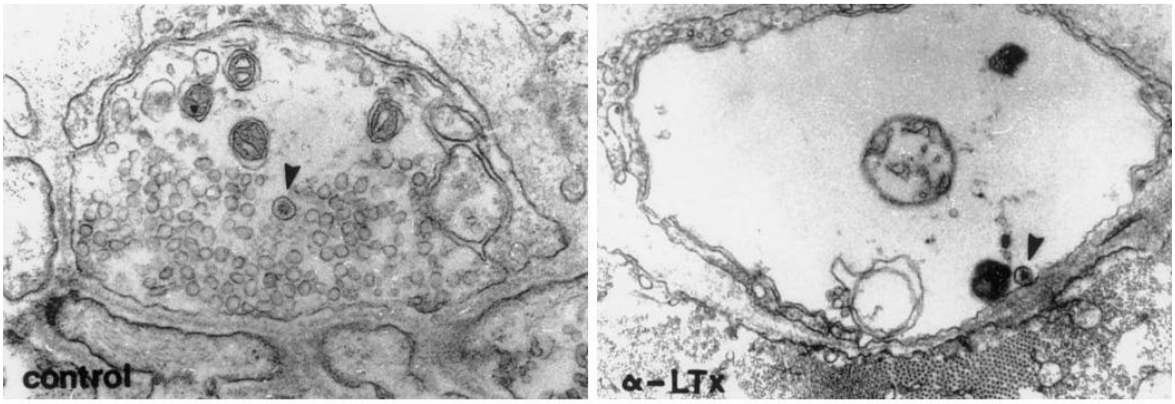

Fig.6. Electron microscopy of mouse NMJs treated or not with α-Ltx. A: A control terminal densely populated by synaptic vesicles. **B**: Exposure to α-Ltx causes a massive release of small synaptic vesicles. This results in an enlargement of the plasmalemma and a total depletion of the neurotransmitter-containing vesicles (Matteoli et al., 1998).

6. AIM

Injured nerve terminals at NMJs can regenerate. This complex response is governed by molecular signals that are exchanged among the main cellular components of the NMJ: motor axon nerve terminal (MAT), perisynaptic schwann cells (PSC), muscle fibre (MF), and the basal lamina.

Although clearly documented, the regeneration of MAT is still ill-known in many cellular and molecular aspects. Here we have used the spider toxin α-Latrotoxin (α-Ltx), which targets specifically the presynaptic terminal causing its complete degeneration, to further investigate the mechanisms underlying peripheral neuroregeneration. This neurotoxin induces a very specific and localized damage of MAT, and its action mimics the cascade of events that leads to nerve terminal degeneration in injured patients and in other neurodegenerative conditions. Strikingly, after the clearing of MAT debris by PSCs, the axon stump grows allowing complete NMJ recovery. Therefore this toxin represents a simple and controlled method to induce an acute, localized and reversible MAT degeneration followed by full regeneration of the NMJ.

The aim of the present work is to define the transcriptomic profile of the NMJ during neurotoxin- induced degeneration and regeneration in mouse. This is a major effort that could allow to identify additional pathways involved in the recovery of NMJ functionality, and to find out molecules released by PSCs and MF involved in MAT regeneration. This experimental approach will allow to characterize the cross-talk between degenerating MAT and adjacent PSCs and, in particular, to identify the molecular mediators released by MAT that might be involved in PSCs activation.

7. MATERIALS AND METHODS

7.1 MATERIALS

Toxins. α-Ltx was purchased from Alomone. The purity of the toxins was checked by SDS-PAGE and their neurotoxicity by *ex-vivo* mouse nerve-hemidiaphragm preparation as previously described (Rigoni *et al.*, 2005).

Chemicals. Unless otherwise stated all reagents were purchased from SIGMA.

Animal strains. C57BL/6 mice expressing cytosolic GFP under the *plp* promoter (Mallon et al., 2002; Brill et al., 2011) were kindly provided by Dr. W.B. Macklin (Aurora, Colorado) via the collaboration of Dr. T. Misgeld (Munchen, Germany). All experiments were performed in accordance with Italian animal care guidelines, law no. 116/1992. Experiments using Wistar rats (Plaisant Srl) were performed in accordance with the Council Directive 2010/63/EU of the European Parliament, the Council of 22 September 2010 on the protection of animals used for scientific purposes, and approved by the Italian Ministry of Health.

7.2 METHODS

7.2.1 Laser microdissection

α-Ltx (5 µg/kg) was diluted in 15 µl of physiological saline (0.9% w/v NaCl in distilled water) and injected subcutaneously in proximity of *Levatoris auris longus* (LAL) muscle of anesthetized transgenic C57BL/6 male mice (expressing a cytosolic GFP under the *plp* promoter) of around 20-25 gr. Control animals were injected with saline. LAL muscles were sacrificed, subcutaneously fixed in 4% PFA in PBS for 5 min and then dissected at different time points after injections. Muscles were then incubated with fluorescent α-bungarotoxin in sterile PBS for 30 min at 37°C and then frozed in liquid nitrogen. Crio-sections (7 µm thick) were transferred to UV treated microscope glass slides (six to eight sections per slide). Microdissection was performed under direct microscopic visualization with PALM RoboMover automatic laser microdissector (Carl Zeiss, Oberkochen, Germany).

7.2.2 RNA isolation

LCM samples were incubated with 50 µl of lyisis buffer PKD (Qiagen, Venlo, Netherlands) and 10 µl of proteinase K (Promega, Madison, WI, USA) at 55 °C over night with the sample upside down. The day after samples were centrifuged for 10 minutes at 10000 rpm, and RNA extracted with the automated system Maxwell 16 (Promega, Madison, WI, USA) using the Maxwell® 16 LEV RNA FFPE Purification Kit. The protocol was followed starting from the DNase treatment. It was not possible to measure the concentration of the RNA extracted from LMD samples, even with Qubit RNA HS assay kit, because of the low amount of material.

7.2.3 Ribosomal RNA Removal

Because of the too low amount of starting material, ribosomal RNA (rRNA) was not removed before retro-transcription into cDNA, but only at the time of data analysis, using appropriate filters.

7.2.4 cDNA Synthesis

To prepare the library we used the SMARTer Universal Low Input RNA kit.

It was not possible to check the quality of the cDNA libraries with Agilent 2100 Bioanalyzer instrument because of the low quantity of the starting material.

7.2.5 Adapters Ligation, Size Selection and Amplification

Only samples from fresh tissues were fragmented with Ion TargetSeq Exome Enrichment kit, using the Ion Shear Plus Reagents for 3-5 minutes at 37 °C. Ligation of the adapters and of the barcodes to the cDNA samples was then performed (two libraries were loaded together in the same chip doing a pooled library), following the instruction for the Ion TargetSeq Exome Enrichment (Life Technologies). Samples were purified with Agencourt AMPure XP Reagent (Beckman Coulter, Indianapolis, IN).

The unamplified libraries were run on the E-Gel SizeSelect 2% Agarose Gel (Life Technologies, Grand Island, NY) to obtain about 270 bp library DNA. The size-selected fragment library was then amplified with Platinum PCR SuperMix High Fidelity (Life Technologies, Grand Island, NY) with this PCR cycling program: 95 °C for 15 seconds of denaturation; 95 °C for 15 seconds, 58 °C for 15 seconds, 70 °C for 1 minute (22 cycles) and 70 °C for 5 minutes. and purified. The quality and the quantity of the amplified library was

checked with Agilent 2100 Bioanalyzer instrument with the Agilent High Sensitivity DNA Kit.

Our libraries were ready for template preparation in Ion OneTouch 2 Instrument (Ion Torrent, Life Technologies, Grand Island, NY).

7.2.6 Template Preparation

cDNA was amplified using emulsion PCR performed via Ion OneTouch 2 Instrument (Ion Torrent, Life Technologies, Grand Island, NY). One DNA molecule per Ion Sphere particle in an oil emulsion was obtained. The cDNA library was diluted to 10 pM and loaded in the Ion PI Plus Reaction Filter Assembly (Ion Torrent). The run was performed overnight in the Ion OneTouch 2 Instrument. The day after the template-positive Ion PI Ion Sphere Particles (ISPs) were recovered, the unenriched template ISPs were measured by the Qubit 2.0 Fluorometer (Invitrogen, Life Technologies, Grand Island, NY) with the V3.10 firmware and the Ion Sphere Quality Control Assay (Ion Torrent, Life Technologies, Grand Island, NY). The non-templated ISPs were removed from the template ISPs by the Ion OneTouch ES Instrument (Ion Torrent, Life Technologies, Grand Island, NY), which uses magnetic bead technology to isolate template-positive ISPs.

7.2.7 Sequencing on the Ion Proton

Unlike Illumina and 454, Ion proton sequencing does not make use of optical signals; instead, it is based on the release of a H^+ ion each time a dNTP is added to a DNA polymer. As in other kinds of Next generation sequencing, the input DNA or RNA is fragmented, ~200bp fragments. Adaptors are added to fragments and one molecule is placed onto a bead. The molecules are amplified on the bead by emulsion PCR. Each bead is placed into a single well of a slide.

Like 454, the slide is flooded with a single species of dNTP, along with buffers and polymerase, one NTP at a time. The pH is detected by sensors at the bottom of each well, as each H^+ ion released will decrease the pH. The changes in pH allow us to determine if that base, and how many thereof, was added to the sequence read.

The Ion PI Sequencing 200 kit was employed for sequencing (Ion Torrent, Life Technologies, Grand Island, NY). The Ion PI Chip (Ion Torrent, Life Technologies, Grand Island, NY) was prepared and calibrated for loading. The Ion PI Chip (Ion Torrent, Life Technologies, Grand Island, NY) was loaded with the template-positive ISPs and run on Ion Proton Sequencer.

7.2.8 Bioinformatic Analysis

Bioinformatics analysis was carried out using several command line software included in Bio-Linux (http://nebc.nerc.ac.uk/tools/bio-linux/bio-linux-7-info), a custom version of Ubuntu 12.04 LTS. Fastq files were extracted from the Torrent Server and previously analysed for quality, length and presence of contaminants, by using the software Fastqc (http://www.bioinformatics.babraham.ac.uk/projects/fastqc/) and FastqScreen (http://www.bioinformatics.babraham.ac.uk/projects/fastq_screen/).

Using Star aligner the reads, previously filtered for the quality, length and contaminants, were processed and aligned to *Mus musculus* reference genome. The unmapped reads, generated from the first step, were re-aligned by using Bowtie2 with the preset options "local" and "very sensitive" selected. The reads mapped with Star and Bowtie2 were then merged by using the Picard command SamMerge. The quality of the mapping was evaluated by using the SamStat software.

7.2.9 NMJ immunohistochemistry

α-Ltx injection in LAL muscles was performed as described for sample preparation for laser microdissection. Muscles were dissected at different time points and fixed in 4% PFA in PBS for 30 min at RT. Samples were quenched, permeabilized and saturated for 2 h in 15% goat serum, 2% BSA, 0.25% gelatin, 0.20% glycine and 0.5% Triton X-100 in PBS. Incubation with the following primary antibodies was carried out for at least 48 h in blocking solution: anti-VAChT (rabbit polyclonal Synaptic Systems, 1:200), anti-CD68 (mouse monoclonal, Santa Cruz, 1:200). Muscles were then washed and incubated with secondary antibodies (Alexa-conjugated, 1:200 in PBS, Life Technologies). For CXCL12 detection incubation with the primary antibody (mouse monoclonal anti-CXCL12, R&D, 1:50) was carried out for 72 h and the tyramide signal amplification kit (Perkin Elmer) was used.

To stain acidic compartments, LAL muscles collected after 4 h of intoxication were loaded *ex-vivo* with LysoTracker Red DND-99 (1:5000, Life Technologies) for 2-3 min (Song et al., 2008), while being continuously perfused with oxygenated Neurobasal A medium (Life Technologies). Samples were then fixed and processed for indirect immunohistochemistry as described above. Images were collected with a Leica SP5 Confocal microscope equipped with a 63x HCX PL APO NA 1.4. Laser excitation line, power intensity and emission range were chosen accordingly to each fluorophore in different samples in order to minimize bleed-through.

7.2.10 Electrophysiological recordings

Electrophysiological recordings were performed in oxygenated Krebs-Ringer solution on soleus muscles using intracellular glass microelectrodes (WPI, Germany) filled with one part of 3 M KCl and two parts of 3 M CH_3COOK. Measurements were done on muscles from control mice, from mice locally injected with the toxin (α-Ltx 5 µg/kg), and from mice that were i.p. injected with 100 µg of anti-CXCL12 antibody (diluted in 40 µl physiologic solution 0,2 % gelatine) prior to local injection of α-Ltx. Different time points were analysed.
Evoked neurotransmitter release was recorded in current-clamp mode and resting membrane potential was adjusted with current injection to −70 mV. Evoked junction potentials (EJPs) were elicited by supramaximal nerve stimulation at 0.5 Hz using a suction microelectrode connected to a S88 stimulator (Grass, USA). To prevent muscle contraction after dissection samples were incubated for 10 min with 1 µM µ-Conotoxin GIIIB (Alomone, Israel). Signals were amplified with intracellular bridge mode amplifier (BA-01X, NPI, Germany), sampled using a digital interface (NI PCI-6221, National Instruments, USA) and recorded by means of electrophysiological software (WinEDR, Strathclyde University). EJPs measurements were carried out with Clampfit software (Molecular Devices, USA), statistical analysis with Prism (GraphPad Software, USA).

7.2.11 Cerebellar granular neurons

Rat cerebellar granular neurons (CGNs) were prepared from 6-days-old Wistar rats as described elsewhere (Levi et al., 1984). Briefly, neurons were isolated from freshly dissected cerebella by mechanical disruption in the presence of trypsin (0,08% m/w) and DNase I (0,08 mg/ml) and then seeded onto 24-wells culture plates coated with poly-L-lysine (10 µg/ml). Cells were seeded at a density of 3 x 10^5/well in BME (Life Technologies) supplemented with 10% FBS (Euroclone), 25 mM KCl, 2 mM glutamine and 50 µg/ml gentamycin. Cultures were maintained at 37 °C in a humidified atmosphere of 95% air, 5% CO_2. Cytosine arabinoside (10 µM) was added to the culture medium 18-24 hours after plating to arrest the growth of non-neuronal cells. Experiments were performed at 6 days *in-vitro*.

7.2.12 Spinal motoneurons

Primary rat spinal motoneurons (MNs) were isolated from Sprague-Dawley rat embryos (embryonic day 14) and cultured following previously described protocols (Arce et al., 1999). Briefly, spinal cords were dissected from E14 rat embryos, treated with trypsin (0,025% m/w) and DNase (0,1 mg/ml) and collected under a bovine serum albumin (BSA) cushion. Cells were then resuspended in Neurobasal medium (Life Technologies) supplemented with 2% B27 supplement (Life Technologies), 2% horse serum (Euroclone), 0,5 mM glutamine, 25 µM 2-mercaptoethanol, 10 ng/ml CNTF (R&D Systems), 100 pg/ml GDNF (R&D Systems), 5 µg/ml Pen/Strep and 25 µM L-glutamic acid, and seeded on poly-ornithine and laminin coated plates. Cultures were maintained at 37 °C in a humidified atmosphere of 95% air, 5% CO_2, and experiments were performed at 6 days *in-vitro*.

7.2.13 Primary Schwann cells

Primary SCs were purified from sciatic nerves of six P3 Wistar rats. Briefly, sciatic nerves were dissected and tissues digested in 0.1% w/v collagenase, 0.25% w/v trypsin in L15 medium (Life Technologies) plus 0.3% BSA for 1 h. Dissociated cells were seeded onto uncoated Petri dishes in DMEM (Life Technologies) 10% FBS and 50 µg/ml gentamycin; 24 h after seeding 10 µM arabinoside C was added to the medium and kept for 2 days to prevent fibroblasts mitosis. Five days after seeding an immunopanning with an anti-Thy1.1 antibody (1:500, 30 min at 37 °C) followed by rat complement addition (1:10, 2 hours) were performed to eliminate contaminating fibroblasts. Purified SCs were subsequently plated on poly-L-lysine-coated dishes and allowed to grow in Expansion Medium consisting of DMEM, supplemented with 10% FBS, 2 µM forskolin and 10 nM heregulin β-1. SCs were then seeded on laminin-coated 24 wells-dishes (2×10^4 cells/well) and kept in Expansion Medium.

7.2.14 Neurons-SCs co-cultures

CGNs and spinal MNs were used to set up co-cultures with primary SCs. Briefly, 4 days after primary neurons seeding, primary SCs were added to neuronal cultures at an average density of 1×10^4 cells/cm^2. Co-cultures were kept for 2-3 days in CGNs or MNs medium respectively.

7.2.15 Cell treatments

CGNs or spinal MNs plated onto 24 wells-plates were exposed for 24 h to recombinant CXCL12 (100, 250, 500 or 700 ng/ml, R&D) at 37°C in in Neurobasal medium supplemented with 2% B27 supplement, 2% horse serum, 0,5 mM glutamine, 25 µM 2-mercaptoethanol, 10 ng/ml CNTF, 100 pg/ml GDNF, 5 µg/ml Pen/Strep and 25 µM L-glutamic acid. A low density motor neuron culture system was chosen to easily compare the effects of CXCL12 on axon growth. AMD3100 (10 µM, SIGMA), a CXCR4 antagonist, was added to MNs together with CXCL12.

Primary SCs were exposed to 100 µM ATP for different incubation times in KRH at 37°C.

In some experiments primary neurons, SCs or co-cultures were pre-incubated for 5 min with 1,5 U/well apyrase before toxin addition and apyrase was kept throughout the experiments. Samples were then processed for Western blotting or immunofluorescence.

7.2.16 Microfluidic chambers

Microfluidic chambers (MFCs) were produced using established methods (Park et al.,2006). Polydimethylsiloxane (Dow Corning) inserts were sterilized and fixed to 50 mm glass-bottomed WillCo dishes (IntraCel) using plasma cleaning. MFCs were blocked with 0.8% BSA in PBS overnight at 37°C and then coated with poly-L-ornithine and laminin. Spinal MNs were plated in the somatic compartment of the MFC and left to adhere before the full medium was applied. The chemokine CXCL12 (500 ng/ml) was added in the distal compartments. Immunofluorescence analysis were performed after 5 days of treatments.

7.2.17 Western Blot

Primary cell cultures were treated as described above, then lysed in Lysis Buffer (Hepes 10 mM, NaCl 150 mM, SDS 1%, EDTA 4 mM, protease inhibitors cocktail (Roche), and phosphatase inhibitor cocktail). Samples were then denatured at 95°C for 5 min, loaded on precast 4-12% SDS-polyacrylamide gels (Life Technologies) and transferred to a nitrocellulose membrane in a refrigerated chamber. Following saturation, membranes were incubated o.n. with primary antibodies (rabbit polyclonal anti-Phospho-CREB, Cell Signaling, 1:1000, mouse monoclonal anti-Hsc70, Synaptic Systems, 1:10000) followed by a

secondary antibody HRP-conjugated (Life Technologies, 1:10000). Chemiluminescence was developed with Luminata TM Crescendo (Millipore) or ECL Advance western blotting detection system (GE Healthcare), and emission measured with ChemiDoc XRS (Bio-Rad). For densitometric quantification the software Quantity One (Bio-Rad) was used, and the bands of interest were normalized to the housekeeping protein Hsc70. None of the bands reached signal saturation.

7.2.18 Immunofluorescence

Following treatments, primary MNs, primary SCs or co-coltures were fixed for 15 min in 4% PFA in PBS, quenched (0.38% glycine, 0.24% NH_4Cl in PBS) and permeabilized with 0.3% Triton X-100 in PBS for 5 min at RT. After saturation with 3% goat serum in PBS for 1 h, samples were incubated with primary antibodies (polyclonal anti-β3 tubulin, SIGMA 1:200); polyclonal anti-CXCR4 Abcam 1:500, rabbit polyclonal anti-Phospho-CREB, Cell Signaling, 1:800, mouse monoclonal anti-S100, SIGMA, 1:200) diluted in 3% goat serum in PBS o.n. at 4°C, washed, and then incubated with the correspondent secondary antibodies (Alexa-conjugated, 1:200, Life Technologies) for 1 h at RT. Coverslips were mounted in Mowiol and examined by confocal (Leica SP5) or epifluorescence (Leica CTR6000) microscopy.

7.2.19 Extracellular ATP measurement

ATP in cell culture supernatant was quantified using ATP Lite One-Step kit (Perkin-Elmer, Waltham, MA, USA). Quick centrifugation of the plates was performed to get rid of cell debris. Luminescence was measured with a luminometer (Infinite M200 PRO, Tecan) and ATP concentration determined using a standard curve.

7.2.20 Cytosolic Calcium Determination with Fluo-4.

SCs or co-cultures were loaded with 5 μM Fluo-4 (Molecular Probes, Invitrogen) in saline for 10 min, then washed. After being loaded with dye, cells were moved to the stage of an inverted fluorescence microscope (Eclipse-Ti; Nikon Instruments) equipped with the perfect focus system (PFS; Nikon Instruments) and with high numerical aperture oil immersion objectives (60X). Calcium signals were recorded with excitation of the fluorophore performed at 465-495 by means of an Hg arc lamp (100 W; Nikon). Emitted fluorescence was

collected at 515-555 nm. Fluorescence was measured in a selected region of interest (ROI) containing cell cytosol corrected for background.

7.2.21 FRET

SCs alone or in co-cultures, plated on glass coverslips, were transfected with 0,5 μg of the regulatory (pCDNA3-RIIRI-CFP) and catalytic subunit(pCDNA3-RIIRI-CFP) of cAMP-binding protein kinase A (PKA) based sensor or with 1 μg of the FRET sensor *Epac (Exchange protein directly activated by cAMP)-based* in Opti-MEM, using 6 μl of Lipofectamine 2000 (Invitrogen). This is a new sensor for cAMP with an increased affinity, consisting of the cAMP-binding Rap-1 activating protein Epac, sandwiched between a suitable donor protein mTurquoise2- and an acceptor fluorescent protein cp137Venus (*Klarenbeek et al., 2015*). The construct was transfected 24 hours prior to experiments. Cells were monitored using an inverted fluorescence microscope (Eclipse-Ti; Nikon Instruments) equipped with the perfect focus system (PFS; Nikon Instruments). Excitation of the fluorophore was performed by means of an Hg arc lamp (100 W; Nikon) using a 435-nm filter (10- nm bandwidth). YFP and CFP intensities were recorded by means of a cooled CCD camera (C9100-13; Hamamatsu) equipped with a 515-nm dichroic mirror at 530 nm (25-nm bandwidth) and 470 nm (20-nm bandwidth), respectively. Signals were digitized and FRET was expressed as the ratio between donor and acceptor signals. YFP and CFP intensities were corrected for background by defining two corresponding regions of interest (ROIs) in each channel: one relatively, taking care that the cell selected remained within the ROI, and a smaller ROI located near the border of the image for background recordings. FRET ratio was set = 1 at the onset of the experiment. SCs were treated with ATP (25 μM) and co-cultures with α-Ltx (0,1 nM) after 3 min of recordings, and stimulated with 25 μM forskolin at the end of each experiment to maximally raise the cAMP levels.

7.2.22 Statistical analysis

The sample size (N) of each experimental group is described in each corresponding figure legend, and at least with three biological replicates were performed. GraphPad Prism software was used for all statistical analyses. Quantitative data displayed as histograms are expressed as means ± SEM (represented as error bars). Results from each group were averaged and used to calculate descriptive statistics. Significance was calculated by Student's t-test (unpaired, two-side). P- values less than 0.05 were considered significant.

8. RESULTS

8.1 Isolation of mouse NMJs

For transcriptomic analysis several NMJs have been collected at different time-points during nerve terminal degeneration/regeneration using the Laser microdissection technique (LCM), that allows the isolation of single cells or tissue areas from a variety of tissue samples (Fig.7). The microdissected samples are then available for further molecular biological procedures such as PCR, real-time PCR, transcriptomics, proteomics and other analytical techniques.

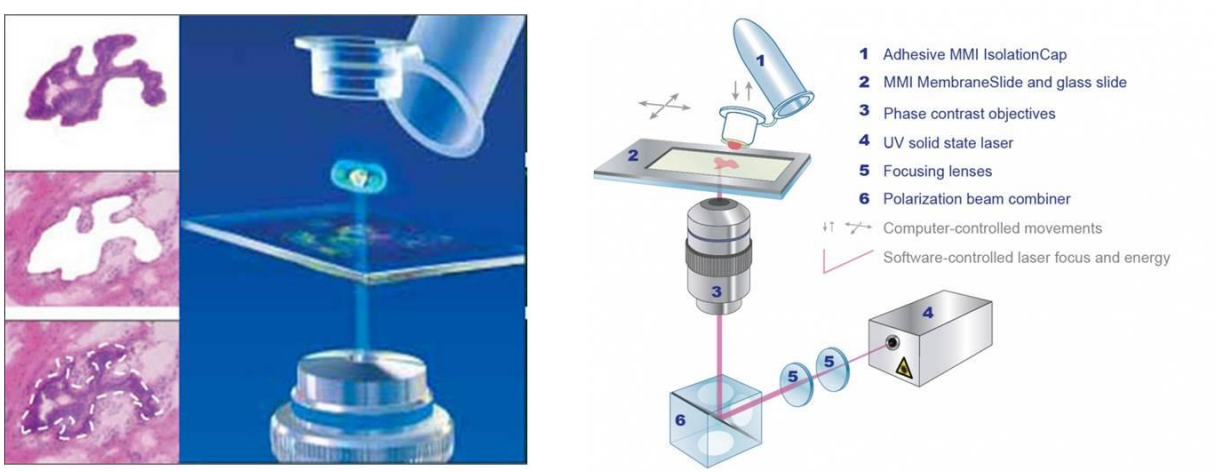

Fig.7. Laser microdissection technology. A laser is coupled into a microscope and focuses onto the tissue on the slide. By movement of the laser by optics or the stage the focus follows a trajectory which is predefined by the user. This trajectory is then cut out and separated from the adjacent tissue. The laser cutting width is usually less than 1 µm, thus the target cells are not affected by the laser beam. The technology used in our approach (Carl Zeiss PALM) cuts around the sample then collects it by a "catapulting" technology. The section is catapulted from a slide, by a defocused U.V laser pulse which generates a photonic force, to a collection cap positioned directly on the cut tissue section.

A fundamental step in LCM is to develop a specimen preparation technique that perfectly balances the dissection of specimens and the downstream analysis. The first step is the choice of the most suitable mice muscle. Initially we chose the *soleus*, since we had already defined its kinetic of degeneration/regeneration following α-Ltx injection, both by electrophysiological recordings and by immunostaining. We then realized that, despite the huge number of slices that could be obtained by cryo-sectioning, only in few of them the NMJs were concentrated; therefore a time-consuming screening of the NMJ-positive slices was required. Indeed we moved to the *Levator Auris Longus* (LAL), a very thin muscle located behind mice ears, ideal for *imaging* (Angaut-Petit et al., 1987). Although very thin,

this muscle can be longitudinally cryo-sectioned, and the majority of the slices contain a high number of NMJs, allowing their easy collection by LCM. We injected α-Ltx subcutaneously at the level of LAL of anesthetized C57BL/6 mice which express a cytosolic GFP in SCs, that allows to recognize the NMJs (together with the post-fixation staining by α-bungarotoxin). To prevent RNA degradation, we fixed LAL muscles with a subcutaneous injection of 4% PFA in PBS before dissection. We also tested alternative fixatives such as acetone and methanol, more suitable for RNA analysis (Yan et al., 2010), but they led to GFP loss and, in some cases, to muscle fibre damage. After muscle fixation and dissection, a proper care needs to be taken to preserve tissues and to achieve optimal staining. One method of tissue preservation involves the muscle embedding with paraffin wax. However this method failed to preserve the morphology of LAL muscles, and RNA extracted from paraffin sections resulted often fragmented. Hence we moved to frozen tissues. Following collection, LAL muscles were flash frozed in liquid nitrogen without embedding medium. Muscles were then cryo-sectioned (7 μm) and NMJs collected by LCM. This method provides a superior morphology preservation and an high quality RNA recovery.

8.2 Transcriptomic analysis of mouse neuromuscular junction during nerve degeneration and regeneration

Nerve regeneration could be supported by intrinsic factors of the motor neuron but also by molecules produced by surrounding cells, i.e. skeletal muscle and/or PSCs. Only few of them have been identified so far. Hence we decided to perform a transcriptomic analysis of NMJ during nerve degeneration and regeneration to try to identify additional molecules important for the regenerative process. These molecules could be involved in various aspects of cell-cell signaling and/or cell adhesion, govern axon guidance, axon growth and/or synapse formation. As the first step α-Ltx was subcutaneously injected at the level of the *Levator auris longus* (LAL) muscle in transgenic mice expressing GFP in SCs. After local fixation, muscles were collected at different time points during degeneration/regeneration for the transcriptomic analysis (Fig.8). These time points were chosen on the basis of the kinetic of degeneration/regeneration previously determined in the same muscle (Duregotti et al., 2015)

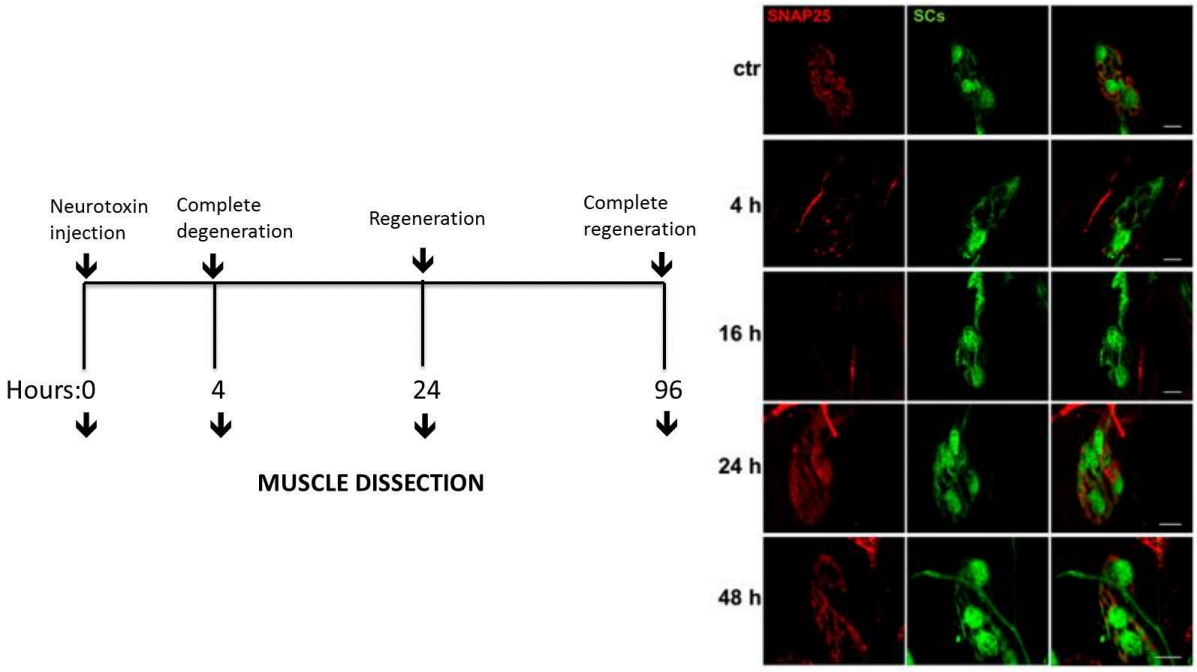

Fig.8. Kinetic of degeneration and regeneration of α-Ltx-poisoned NMJs of LAL muscles. **A**: Time points selected for transcriptomic analysis. **B**: SNAP-25 labeling, a presynaptic marker (red), was used as marker to monitor degeneration and regeneration of nerve terminals. Muscles were collected after 4, 16, 24 and 48 h, and representative images are shown. (Scale bars: 10 μm.).

Samples were frozen, cryosectioned, and fluorescent NMJs were isolated from cryoslices by laser microdissection, collected and pooled (40 to 50 NMJs/sample). GFP-expressing PSCs

and the post-synaptic staining by fluorescent α-bungarotoxin allowed the identification of the NMJs. (Fig.9)

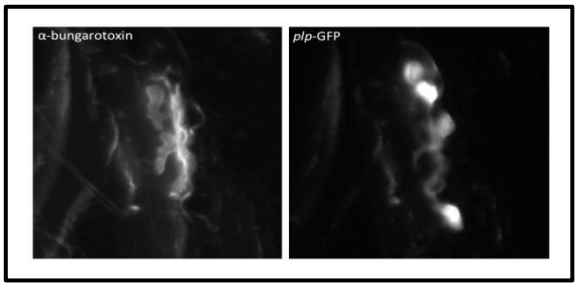

Fig.9. Double visualization of mouse NMJs in cryosections from LAL muscles of transgenic mice. Fluorescent α-bungarotoxin stains the postsynaptic element, while GFP-positive cells are SCs.

Total RNA was extracted, purified, retro-transcribed, amplified and sequenced with the Ion Proton technology in collaboration with the Laboratory of Genoproteomics of the Fondazione Pisana per la Scienza. Ion Proton system uses semiconductor sequencing technology. When a nucleotide is incorporated into the DNA molecules by the polymerase, a proton is released. By detecting the change in pH, Ion Proton recognized whether the nucleotide is added or not. Each time the chip was flooded with one nucleotide after another, if it is not the correct nucleotide, no voltage will be found; if there is 2 nucleotides added, there is double voltage detected. By this approach we have obtained a dataset for each time point of coding (and non-coding) RNAs which are significantly down- or up-regulated during the degeneration/regeneration process ($p<0,05$) (Fig.10). The full dataset analysis obtained by this approach will be not presented in this thesis because still unpublished.

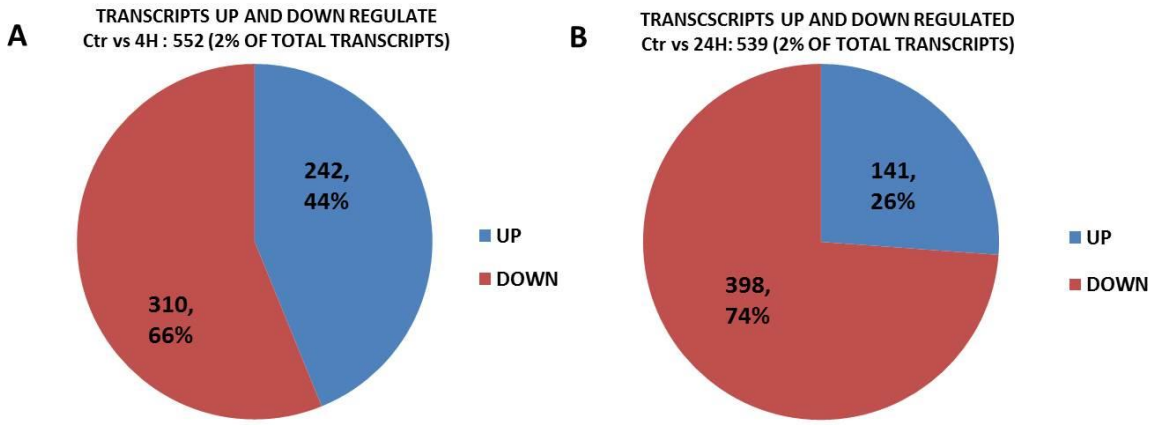

Fig.10. Coding RNAs which are significantly down- or up-regulated after transcriptomic analysis of NMJ during nerve degeneration and regeneration ($p<0,05$). **A**: Transcripts up and down regulated; ctr vs 4h. **B**: Transcripts up and down regulated; ctr vs 24h.

We decided to focus for first to coding RNA: among the different mRNAs that significantly change their abundance with time, we selected via bioinformatic analysis (Uniprot and Target P1 tools) those encoding for putative secreted factors, with the aim of identifying molecules that PSCs and/or MF produce to stimulate MAT regeneration. This analysis led to the identification of several hits, among which we selected the mRNA encoding for the chemokine CXCL12, which results up-regulated during nerve degeneration. Previous reports indicate that this molecule is involved in different pathways, among them axon guidance, growth and branching in some central neurons, but its involvement in NMJ formation and regeneration was not reported before. Therefore we decided to focus our further investigations on this molecule beginning with the validation of the transcriptomic data.

8.3 Perisynaptic Schwann cells express CXCL12 during nerve degeneration

By LCM we collect tissues deriving from MAT, MF and PSCs at the same time, and therefore the cellular origin of a given RNA molecule cannot be easily attributed. In addition, not all mRNAs are translated into proteins in a cell; therefore, the validation of the transcriptomic data by independent approaches is crucial. One way is to use specific antibodies, that provide information about the expression and localization of a given transcript product. Alpha-Ltx was injected in LAL muscles; 4, 24 and 96 hours later muscles were dissected and processed for indirect immunohistochemistry. We found CXCL12 overexpressed by PSCs 4h after α-Ltx injection, during the degeneration phase, confirming the transcriptomic data. No CXCL12 was detected in PSCs at 24 and 96 hours, when regeneration is well under way (Fig. 11).

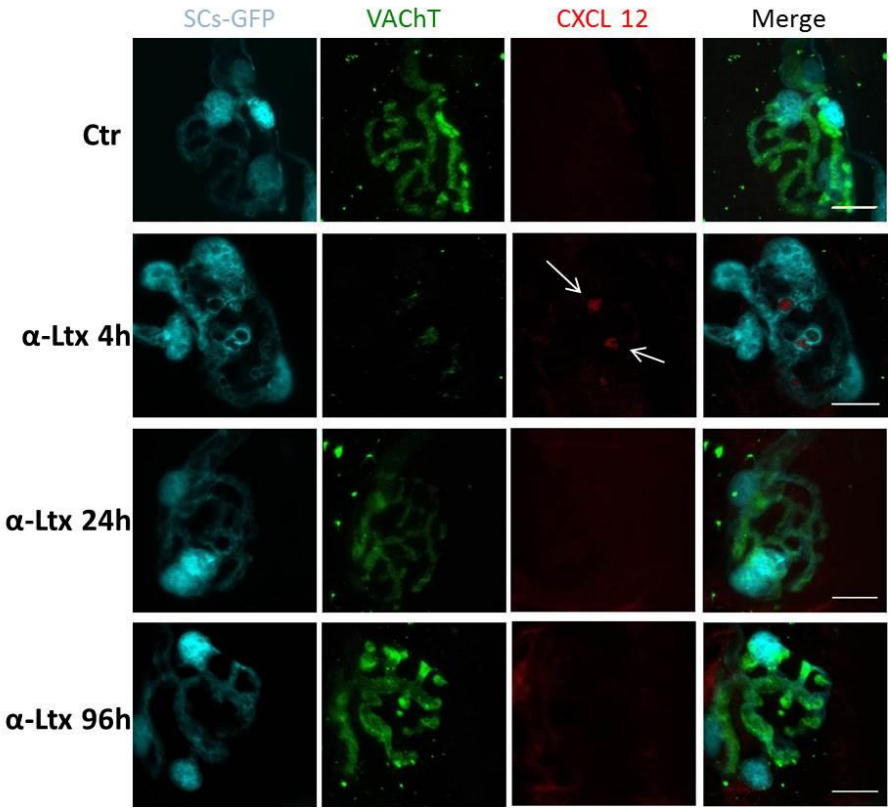

Fig.11. PSCs express CXCL12. LAL muscles from transgenic mice were injected with α-Ltx, collected at different time points (4, 24 and 96 h), and processed for indirect immunohistochemistry. PSCs (cyan) show intracellular structures (white arrows) positive for CXCL12 (red) after 4h of intoxication. Presynaptic nerve terminal is stained with VACht (green). (Scale bars: 10 μm)

Surprisingly, CXCL12 appears to localize within intracellular structures, that result Lysotracker-positive, speaking in favour of an acidic nature of such compartments(Fig.12).

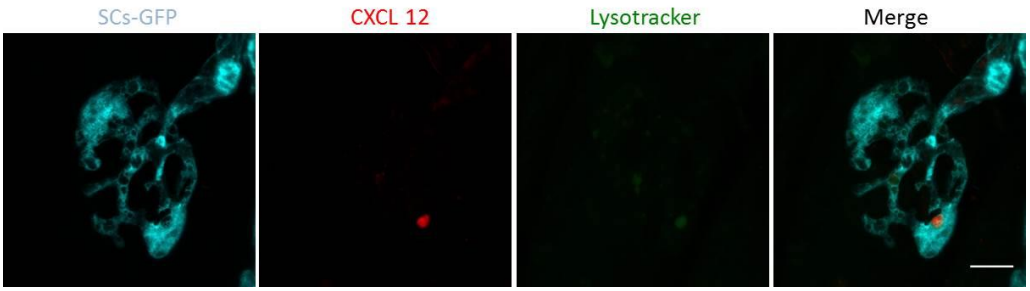

Fig.12. ***Ex vivo*** **Lysotracker staining (red) of α-Ltx-treated LAL (4 h) confirms the acidic nature of intracellular vacuoles** (Scale bar: 10 μm).

These intracellular structures are reminiscent of phagosomes involved in the clearance of nerve debris during nerve degeneration (Duregotti et al., 2015). In order to investigate whether CXCL12 is expressed in phagocytic structures, we performed an immunostaininig for CD68, a lysosomal glycoprotein associated with phagocytic function (Ramprasad et al., 1996), and involved in the lysosomal traffic (Holness and Simmons, 1993). After α-Ltx injection, PSCs of LAL NMJs do express CD68 in the same intracellular structures were the chemokine is localized (Fig.13). These observations suggest a possible role of such acidic compartments in CXCL12 secretion, similar to the one involved in IL-β1 release (Piccioli and Rubartelli, 2013).

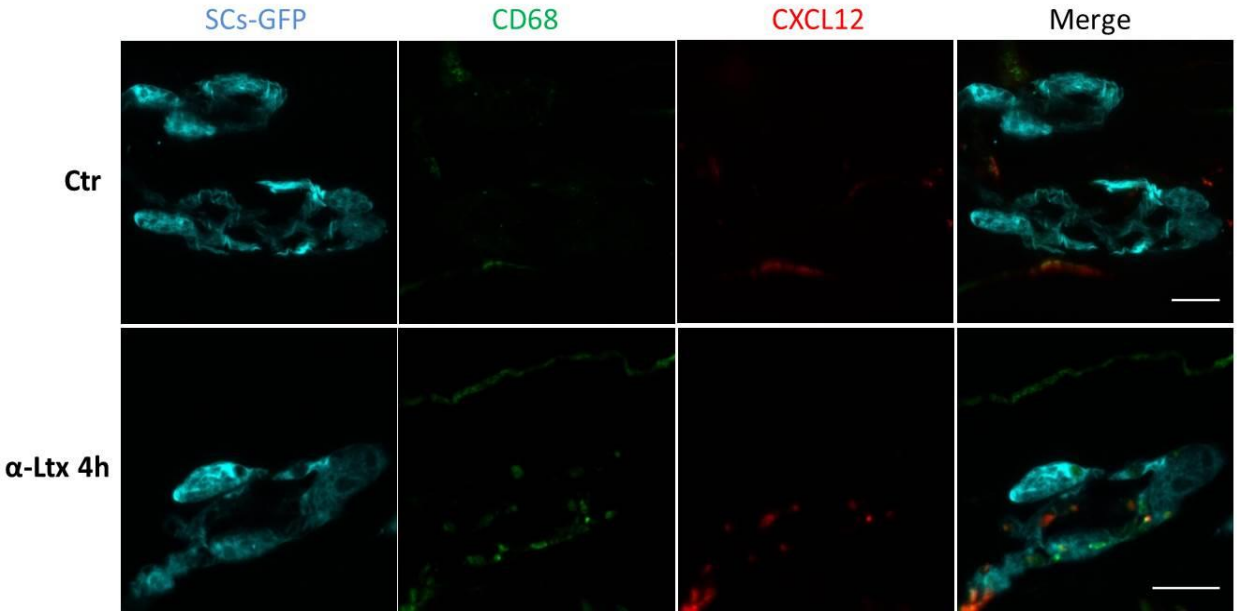

Fig.13. The chemokine CXCL12 localizes in phagocytic structures in PSCs during nerve degeneration. LAL muscles from transgenic mice were injected with α-Ltx, collected at 4h and processed for indirect immunohistochemistry. PSCs (cyan) in intoxicated NMJs become positive for both CXCL12 (red) and the phagocytic marker CD68 (green), which stains intracellular vesicular structures. No CD68 signal is detected in control NMJs (Scale bars: 10 μm).

8.4 Anti-CXCL12 antibodies delay the NMJ recovery of function

CXCL12 knock-out mice are non viable (Nagasawa et al., 1996); to evaluate whether CXCL12 produced by PSCs upon nerve injury is important for functional regeneration, we injected a specific anti-CXCL12 neutralizing antibody intraperitoneally in mice after local toxin administration in the *soleus* muscle. By electrophysiological recordings we compared the kinetics of functional regeneration in muscles injected with α-Ltx pre-treated or not with the anti-CXCL12 antibody (Fig.14).

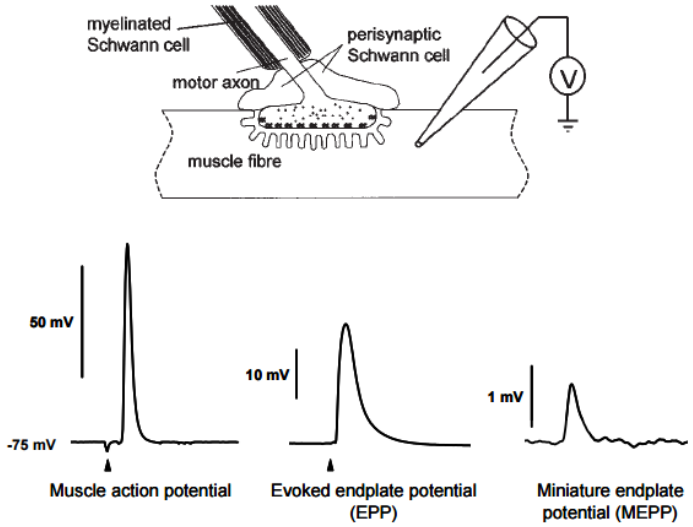

Fig.14. Electrophysiological recordings at the NMJ. Top scheme of motor endplate is adapted from O'Hanlon et al. (2002) and shows the micro-electrode (on the right) inserted into the muscle fibre. This way, alterations in the membrane potential of the muscle fibre can be recorded. These alterations are the result of ACh molecules that have been released from the motor nerve terminal (spontaneously or evoked) and bound to postsynaptic receptors. Below, examples traces of the three signals that can be measured at the NMJ are shown: The membrane potential baseline is -75 mV. Successful transmission results in a muscle action potential. When a selective muscle sodium channel blocker is applied (μ-conotoxin), the action potential is reduced to an EPP. A MEPP is the result of the spontaneous release of a quantum ACh from a single vesicle of ACh. In our experiments we measured Evoked endplate potentials.

As showed in Fig.15 in both conditions no evoked junction potentials (EJPs) were detected 48 hours after toxin treatment, meaning that nerve degeneration took place successfully. Muscles pre-treated with the neutralizing antibody alone showed EJPs indistinguishable from the control. Three to 4 days after treatment, fibres injected with α-Ltx plus anti-CXCL12 showed EJPs with significantly smaller amplitudes than those injected only with the toxin, indicating a slowdown of the regeneration process.

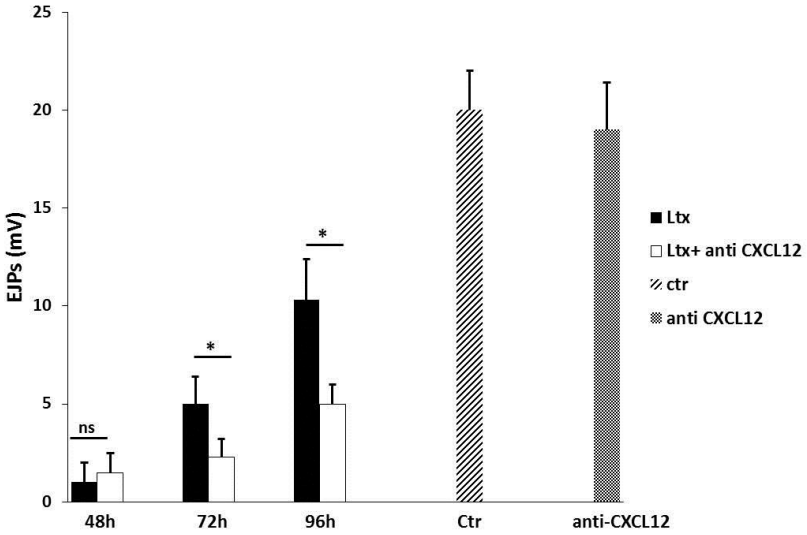

Fig.15. CXCL12 is crucial for nerve regeneration. Electrophysiological recordings of EJPs at soleus NMJs treated with α-Ltx alone (black bars) or with α-Ltx plus anti-CXCL12 (white bars). At 72 and 96 h EJP amplitudes of fibres exposed to the toxin plus anti-CXCL12 are significantly smaller than those exposed to the sole toxin. Data are mean ± s.e.m. from four independent experiments. > 15 fibers analyzed per muscle. **P* < 0.05 (student's *t*-test), ns: not significant.

After EJPs recordings, soleus muscles were processed for immunohistochemistry: to monitor the structural degeneration of nerve terminals we used an antibody specific for the presynaptic marker *vesicular acetylcholine transporter* (VAChT). At 48 hours VAChT completely disappears from poisoned NMJs, meaning that nerve terminal degeneration and debris clearing have occurred successfully in both conditions. However, at 96 hours MAT regeneration appeared delayed in muscle injected with toxin plus anti-CXCL12, with VAChT signal still missing in the vast majority of the NMJs analysed (Fig.16).

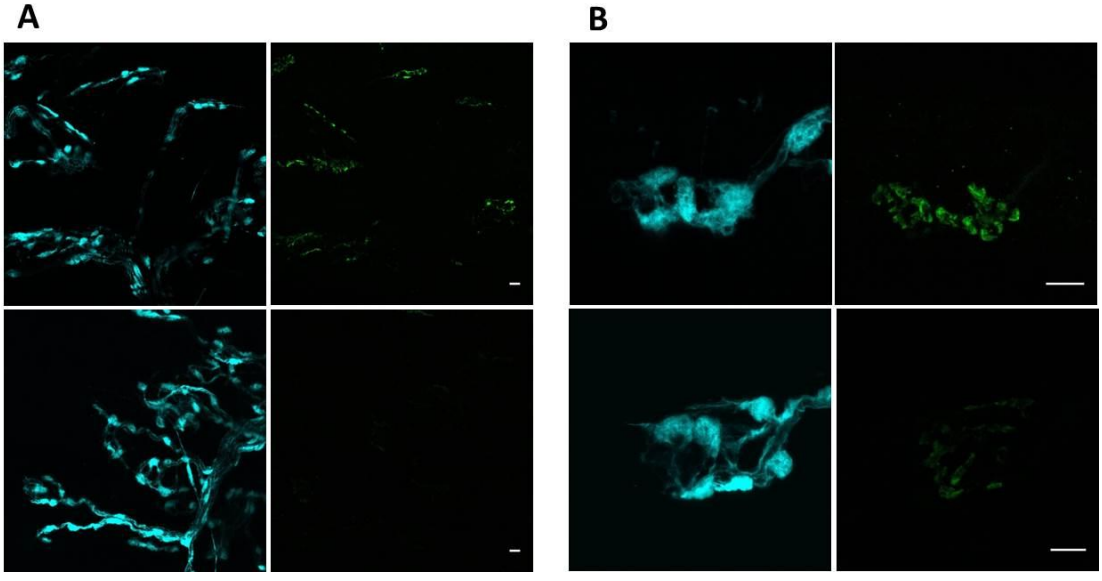

Fig.16. Regeneration of poisoned presynaptic nerve terminals is delayed by neutralization of CXCL12. VAChT labeling (green) was used as *read-out* to monitor degeneration and regeneration of nerve terminals. *Soleus* muscles were s.c. injected with α-Ltx or i.p. injection of anti-CXCL12 was performed prior to toxin administration. Muscles were collected after 96 h. Representative images at low (**A**) and high (**B**) magnification are shown (Scale bars: 10 μm).

Taken together, these data strongly support the idea that CXCL12 is an important factor released by PSCs, with a crucial role in nerve terminal regeneration.

8.5 CXCL12 promotes axon growth of spinal motor neurons

Primary MNs were exposed to different concentrations of recombinant CXCL12, and axon length monitored after 24h. We chose a low density motor neuron culture system to easily compare the effects of CXCL12 on axon growth. Fig.17 A shows that CXCL12 has a remarkable ability to promote axon elongation. This effect has been quantified and is shown in Fig. 17 B. A concentration of 500 ng/ml was effective.

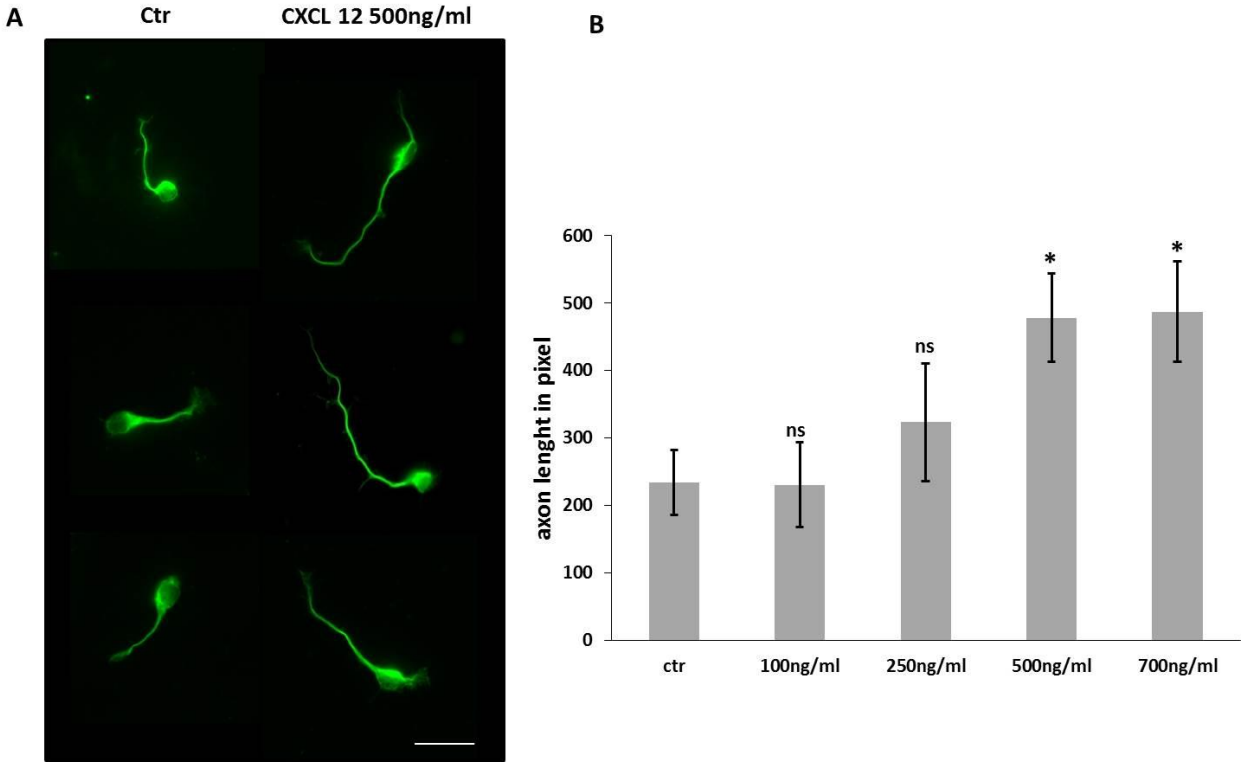

Fig 17. CXCL12 stimulates motor axon growth. MNs were plated and exposed to recombinant CXCL12. After 24h MNs were fixed and processed for immunofluorescence with β3-tubulin (green). Axon length was measured with NeuronJ. **A**: 500 ng/ml of CXCL12 is effective in promoting motor axon growth (Scale bars: 10 μm). **B**: quantitative estimation of the effect. Data are mean ± s.e.m. from three independent experiments. **P* < 0.05 (student's *t*-test), ns: not significant.

The same approach was performed in microfluidic chambers consisting of two compartments, a somatic one where neurons are plated, and a distal one connected by parallel micrometer size grooves along which axons can grow (Fig.18).

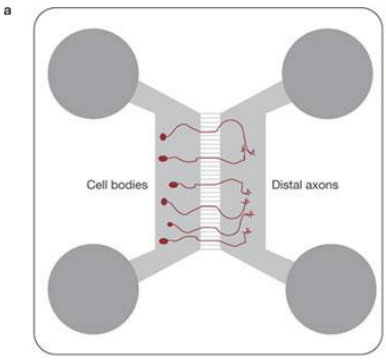

Fig.18. Schematic representation of a microfluidic chamber. Neurons are plated in the left compartment (cell body compartment), and extend their axons through microgrooves into the right compartment (axonal compartment) (Hengst et al., 2009).

Spinal MNs were plated in the somatic compartment whilst recombinant CXCL12 was added in the distal one; 5 days after plating axon length was measured. By this approach we confirmed the role of the chemokine in promoting axon growth (Fig.19).

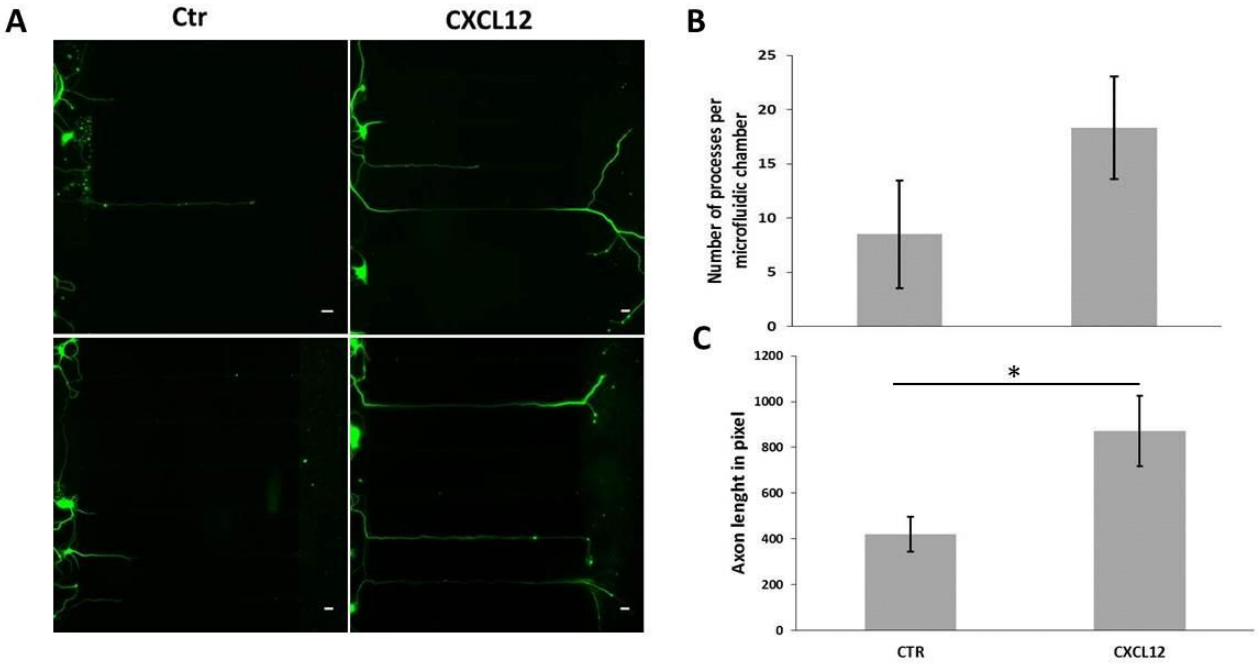

Fig.19. CXCL12 stimulates motor axon growth. MNs were cultured for 5 days in microfluidic chambers. Cells were plated in the somatic compartment whilst recombinant CXCL12 was added in the distal one. Axon length was measured with NeuronJ. After 5 days MNs were fixed and processed for immunofluorescence with β3-tubulin (green) **A**: CXCL12 promotes the motor axon growth into the grooves (Scale bars: 10 μm). **B, C**: quantitative estimation of the effect. Data are mean ± s.e.m. from three independent experiments **P* < 0.05 (student's *t*-test).

8.6 The CXCL12-CXCR4 axis controls axonal growth

CXCL12 signals via the CXCR4 receptor (Nagasawa et al., 2014), which is expressed in different cell types including neurons (McGrath et al., 1999; Opatz et al., 2009). We found that this receptor concentrates on the growing tip of MN axons starting from 1 day of culture (Fig.20 A). To demonstrate that the increase in axon length is induced by the CXCL12-CXCR4 axis we treated MNs with CXCL12 alone in the presence or absence of AMD3100, a well known CXCR4 antagonist. Our preliminary results show that in the presence of AMD3100 mixed with CXCL12, the axonal length was similar to values in the control (Fig.20 B, C), suggesting that the effects of CXCL12 on axon growth are mediated through binding to CXCR4. Further experiments are required.

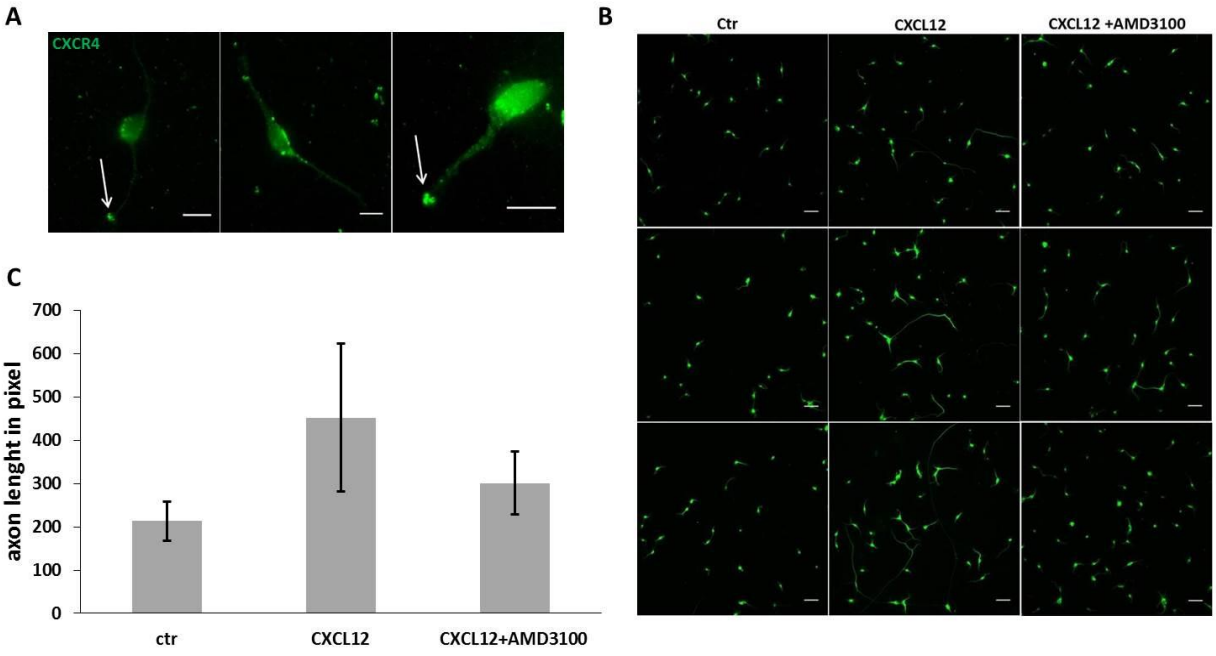

Fig.20. AMD3100 reduces the effect of CXCL12 on axonal growth. A: MNs were plated and after 24h MNs were fixed and processed for immunofluorescence with CXCR4 (green). White arrows indicate CXCR4 receptor concentrates on the growing tip of MN axons and exposed to recombinant CXCL12 (Scale bars: 10 μm). **B:** MNs were plated and exposed to recombinant CXCL12 in presence or not of AMD3100. After 24h MNs were fixed and processed for immunofluorescence with β3-tubulin (green). Axon length was measured with NeuronJ (Scale bars: 50 μm). **C**: quantitative estimation of the effect. Data are mean from two independent experiments.

8.7 Degenerating neurons release ATP

Adenosine triphosphate (ATP) is not only an intracellular energy source but also as an extracellular messenger. ATP is an important signaling molecule in the PNS, where it plays a crucial role in chemical communication between several cell types. A first evidence indicating the ability of neurons to communicate with glial cells through ATP was obtained at the frog NMJ (Robitaille, 1995; Rochon et al., 2001). At this synapse, the pre- and post- synaptic compartments are covered by PSCs. During synaptic activity ATP, which is co-released with Ach from nerve endings, evokes calcium responses in PSCs by activating P2 receptors (Robitaille, 1995), which enable these cells to detect ATP escaping the synaptic cleft. Through ATP and Ach sensing, PSCs are able to detect and monitor synaptic activity. We wondered whether PSCs could be activated by ATP released upon NMJ injury, and which downstream signalling pathways become activated in these cells.

To address this question, we performed experiments on primary cultured CGNs and spinal MNs, well-established models to study the processes of intoxication by α-Ltx *in*-vitro (Tedesco, Rigoni et al., 2009; Duregotti et al., 2015)**.** To quantify extracellular ATP released from neuronal culture after intoxication, we used the luminescence ATPLite assay system which is based on the production of light caused by the reaction of ATP with luciferase and D-luciferin. CGNs were intoxicated with α-Ltx, the supernatant collected and ATP measured. We found that by 10 minutes intoxication there is an increasing release of ATP (Fig.21). After 20 min the extracellular level of ATP decreases probably due to ATP hydrolysis by ectonucleotidases.

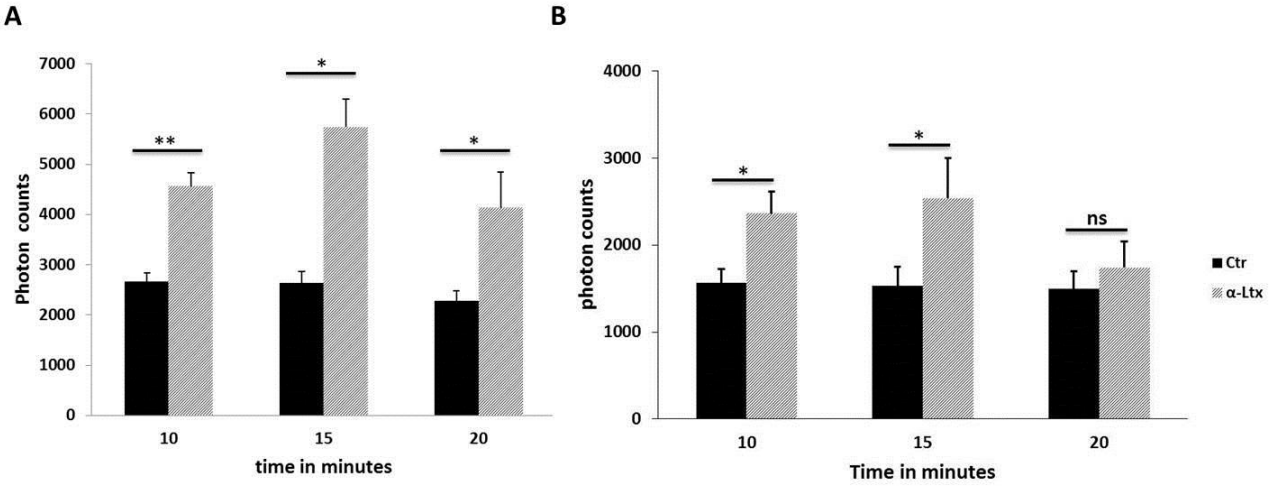

Fig.21. ATP is released following MAT injury. ATP in cell culture supernatant from control and neurons treated with the toxin was quantified by a luciferase–luciferin assay. Intoxication by α-Ltx triggers ATP release. **A**: CGNs, **B**: MNs. *P < 0.05; **P < 0.01; n = 5.

The LDH and calcein assays on neuronal supernatant were performed to exclude a loss of membrane integrity (Fig. 22), supporting the idea of an active mechanism for ATP release by injured neurons.

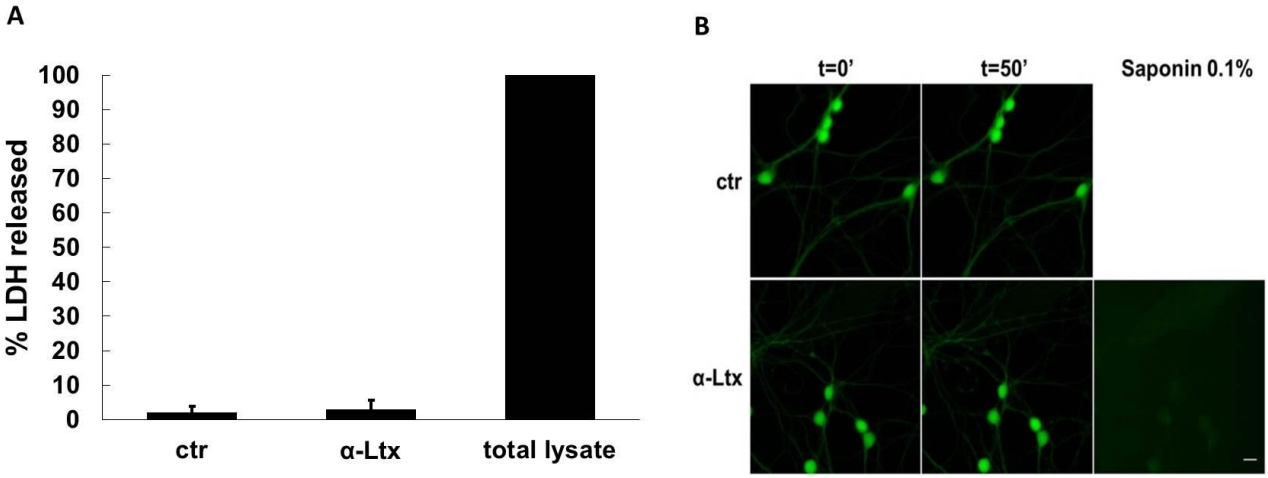

Fig.22. ATP is released from intact membranes. A: LDH enzymatic activity was determined in the supernatants of neurons exposed to α-Ltx. LDH release is an index of loss of membrane integrity. Data represent the mean of three independent experiments. **B**: Membrane integrity was also assessed by calcein-AM retention in CGNs treated with α-Ltx. Calcein staining is lost after saponin-induced membrane permeabilization (Scale bar: 10 μm).

8.8 Neuronal ATP triggers calcium waves in Schwann cells co-cultured with degenerating neurons

At NMJ PSCs respond to neuronal ATP, that is co-released with Ach during neurotransmission, by increasing their cytoplasmic calcium concentration, and ATP triggers calcium increase in different cell types (Nobile et al., 2003; Cheng et al., 2011), with consequent activation of downstream signaling pathways. ATP acts through an extended family of nucleotide receptors that can be divided in two different subfamilies, the ionotropic P2X and the metabotropic P2Y receptors. Since SCs express some of them, we wondered whether ATP might play a role in the crosstalk between degenerating neurons and SCs.

Primary SCs loaded with the calcium indicator Fluo-4 AM respond to micromolar ATP concentrations by increasing their intracellular calcium levels, as reported by *live imaging* experiments (Fig.23)

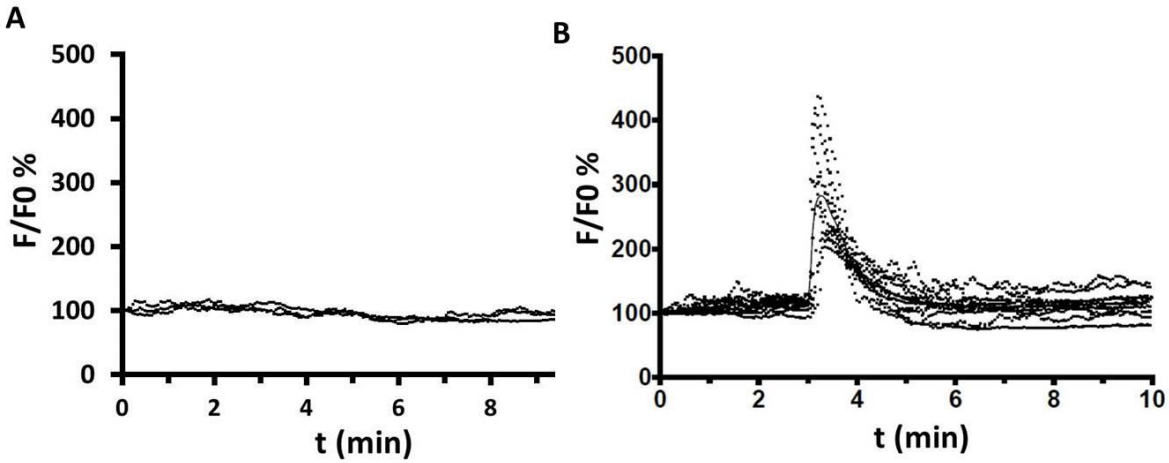

Fig.23. ATP addition triggers calcium increase in Schwann cells. Primary SCs were loaded with Fluo4 AM. ATP (3µM) was added after 30 sec and intracellular calcium levels measured. **B**: Calcium increase was detected in SCs (black dots) with a peak around 4 minutes. Data are representative of eleven independent experiments. **A**: in controls no calcium increase was detected in SCs (n=3).

We next loaded CGNs-SCs co-cultures with Fluo-4 AM, and then α-Ltx was added (at t=3 min). As expected from previous results, calcium started increasing first in neurites, in correspondence to *bulges*, hallmarks of intoxication (Rigoni et al., 2004, 2007); soon after calcium spikes were detected in the cytoplasm of SCs (Fig.24 B). In control experiments no calcium increase was detectable either in neurons nor in SCs (Fig.24 A). These experiments suggest that molecules released by degenerating neurons trigger a calcium response in nearby SCs.

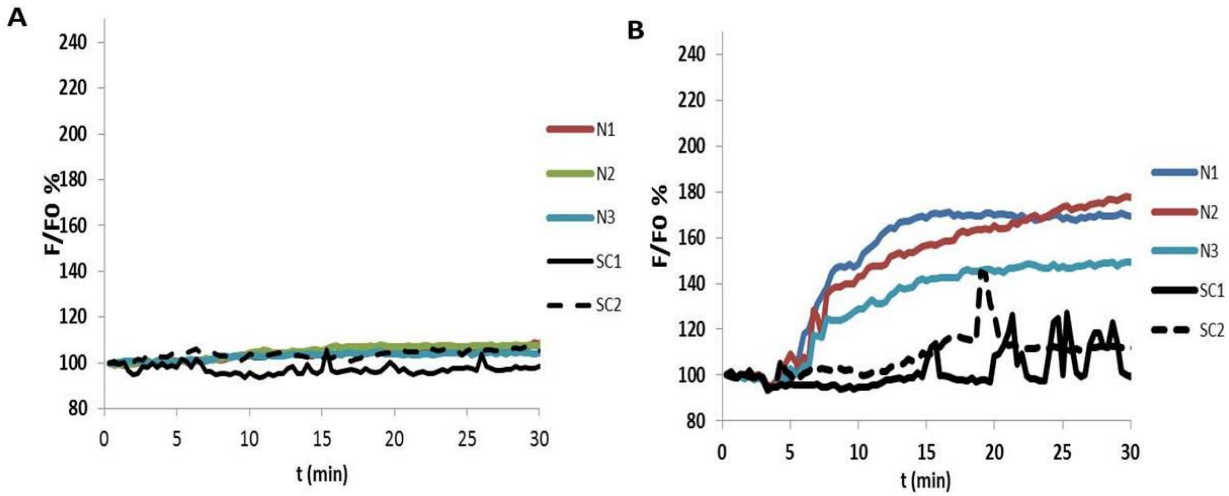

Fig.24. Intoxication of neurons-SCs co-cultures triggers calcium waves in Schwann cells. Co-cultures of primary SCs and neurons were loaded with Fluo4 AM, then exposed to α-Ltx, and intracellular calcium levels measured. A: In controls no calcium increase was detected either in neurons (colored lines) nor in SCs (black lines). B: In intoxicated co-cultures after a progressive calcium increase in neurons (colored lines), calcium spikes were detected in SCs (black lines).

Pre-incubation of co-cultures with apyrase, which hydrolases ATP in AMP and inorganic phosphate, strongly reduces calcium transients in SCs, leaving calcium levels in neurons unaffected (Fig.25). Our results indicate that ATP released by degenerating neurons is one of the signals responsible for Ca^{2+} increase in nearby SCs.

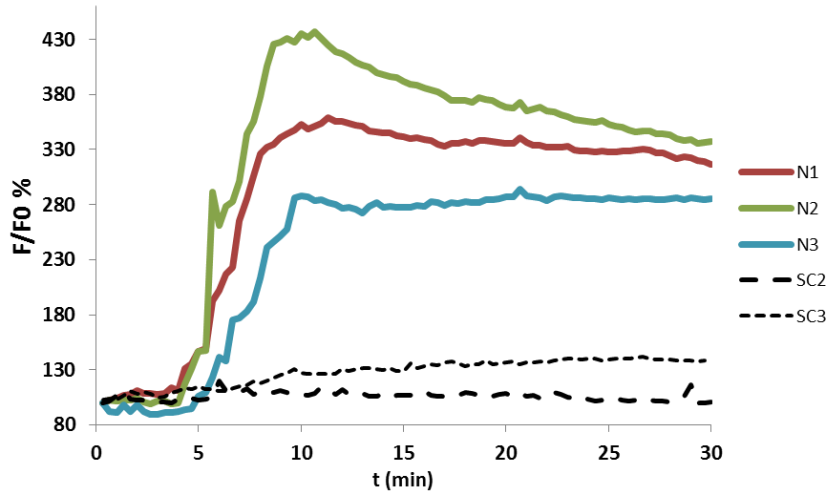

Fig.25. Calcium spikes in SCs are reduced by apyrase. Co-cultures of SCs and neurons loaded with Fluo4 AM were incubated with apyrase, then exposed to α-Ltx and calcium measured. The addition of the toxin was performed after 3 min. After the initial increase of calcium in neurons (colored lines), no calcium spikes were detected in SCs (black lines).

8.9 Neuronal ATP induces cAMP increase in Schwann cells

Purinergic receptors convert the extracellular input ATP into intracellular signalling via the activation of various intracellular pathways, including cAMP signaling (Knott et al., 2014) (Fig.26). We tested this possibility in the present case using FRET to image cAMP levels in isolated SCs exposed to extracellular ATP, and in SCs co-cultured with neurons before and after toxin exposure.

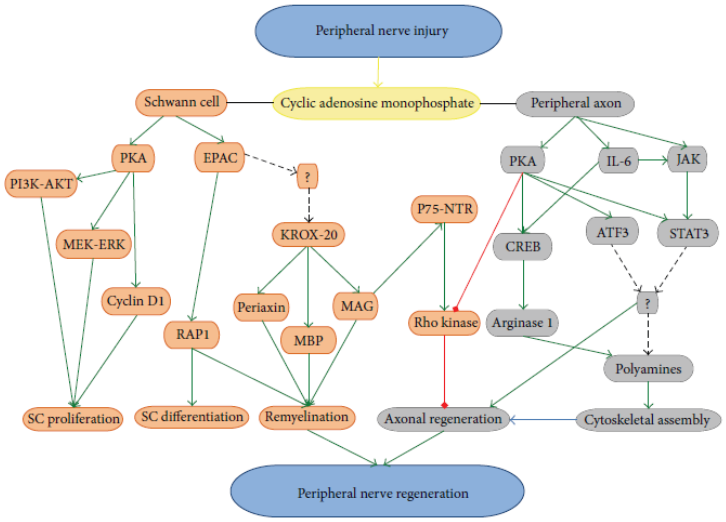

Fig.26. Role of cAMP in peripheral nerve injury. Following PNS injury, cyclic AMP is involved in a variety of positive (green line), inhibitory (red line), and as yet to be identified (dashed line) signaling mechanisms within the injured neurons and their accompanying glia that culminates in PNS regeneration (Knott et al., 2014).

In a first set of experiments SCs were transfected using Lipofectamine 2000 with a fluorescent sensor based on the cAMP-binding protein kinase A (PKA). This probe was generated by fusing the regulatory and catalytic subunit of PKA to the cyan (CFP) and the yellow (YFP) variants of the green fluorescent protein, respectively. In quiescent cells, the CFP and YFP subunits are associated in a complex and FRET occurs among them, but a rise in cAMP induces their separation with loss of FRET. Exposure of primary SCs to 25 μM ATP led to a significant cAMP increase as show in Fig.27B. At the end of experiment SCs were stimulated with forskolin to raise cAMP to maximal levels.

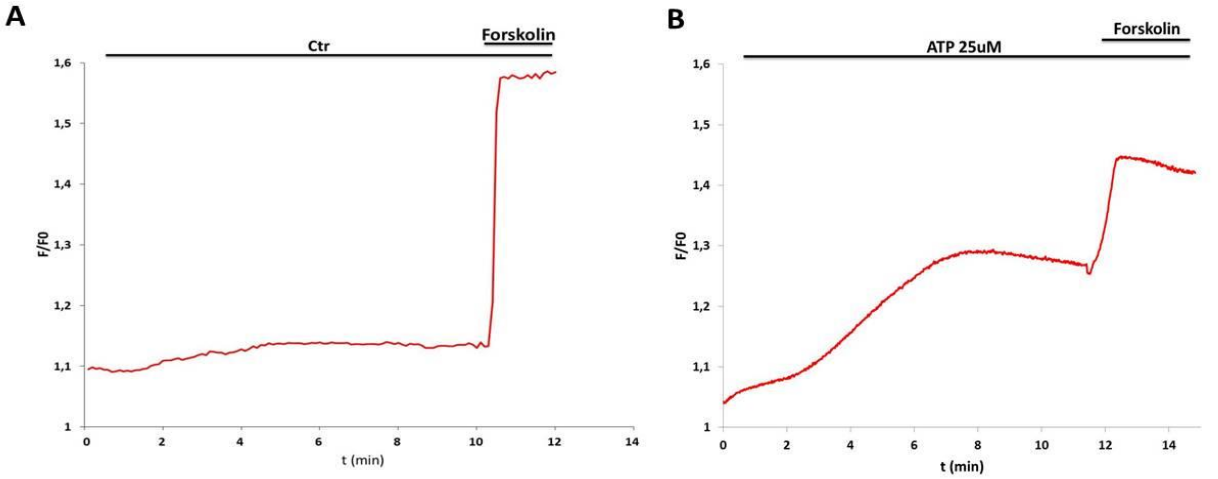

Fig.27. FRET sensor PKA-based. B: ATP was added after 30 sec, forskolin after 10 min. FRET was expressed as the ratio (F/F0) between donor and acceptor signals (YFP and CFP intensities) corrected for background (F0). **A**: in controls no cAMP increase was detected in SCs.

Co-cultures were then transfected with the FRET sensor (SCs only expressed the probe) and cAMP levels measured after α-Ltx exposure. We observed a very small and progressive rise in cAMP in SCs after few minutes from toxin addition (Fig.28).

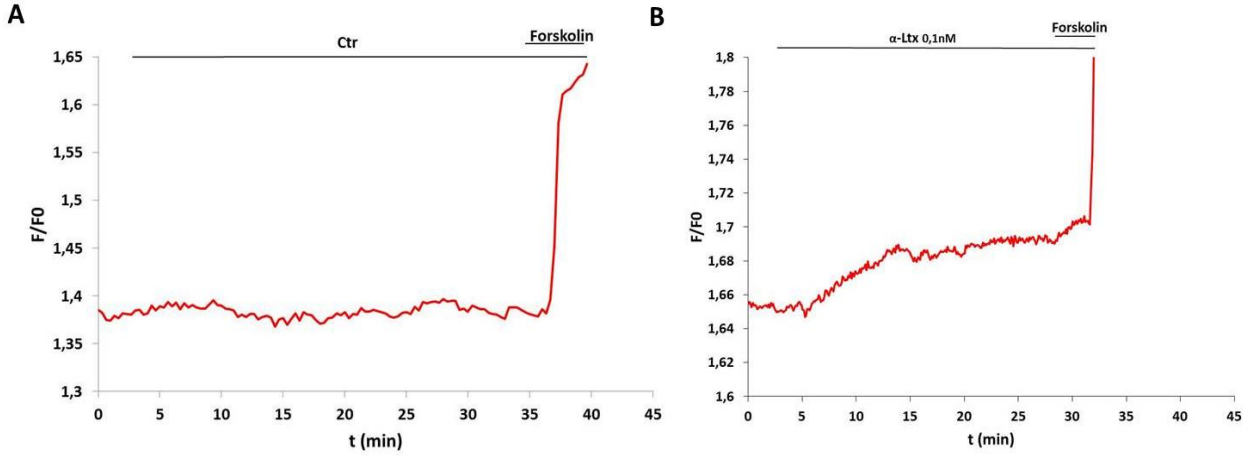

Fig.28. Intoxication of co-cultures induces a small increase in cAMP in Schwann cells. Co-cultures were transfected with the FRET sensor and then exposed to α-Ltx (**B**, t = 3 min). Forskolin was added after 35 min as positive control. FRET (F/F0) was expressed as the ratio between donor and acceptor signals (YFP and CFP intensities) corrected for background (F0). **A**: in controls no cAMP increase was detected in SCs.

To exclude that the very low cAMP increase was due to the low sensitivity of the sensor PKA-based, we switched to the improved FRET sensor *Epac (Exchange protein directly activated by cAMP)-based*, kindly provided by Prof. Jalink (Klarenbeek et al.,) which has an increased affinity for cAMP. Hence co-cultures were transfected with new probe and then exposed to α-Ltx. Cyclic AMP starts increasing significantly in SC cytoplasm after 15-20 minutes from toxin addition (Fig.29B) No cAMP increase was observed in controls.

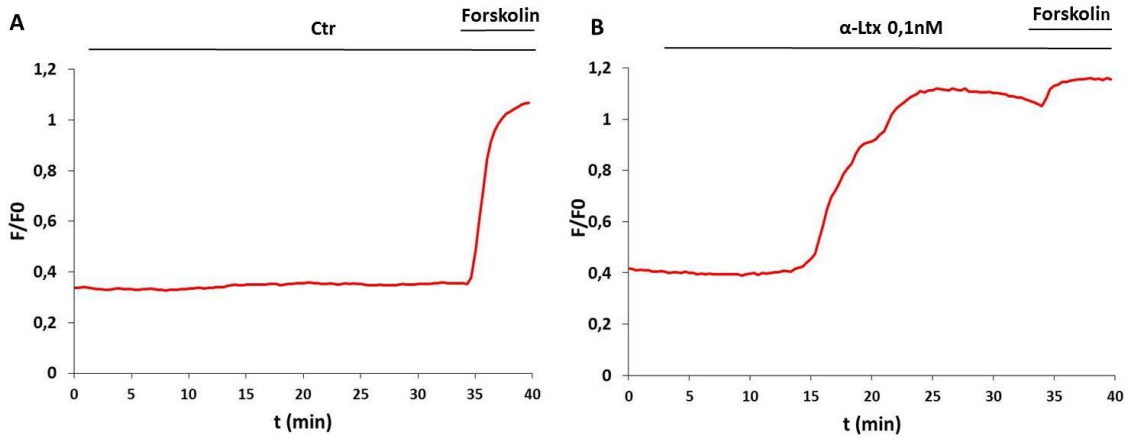

Fig.29. Intoxication of co-cultures induces cAMP increase in Schwann cells. Co-cultures of SCs and neurons were transfected with the FRET sensor and then exposed to α-Ltx **(B**, t = 3 min). Forskolin was added after 35 min as positive control. FRET (F/F0) was expressed as the ratio between donor and acceptor signals (YFP and CFP intensities) corrected for background (F0). **A**: in controls no cAMP increase was detected in SCs.

These results suggest that molecules released by degenerating neurons activate adenylate cyclase within SCs. To address whether ATP is among these molecules, co-cultures were pre-incubated with apyrase and then exposed to α-Ltx: both a reduction and a delay in cAMP rise were observed in SCs (Fig.30).

.

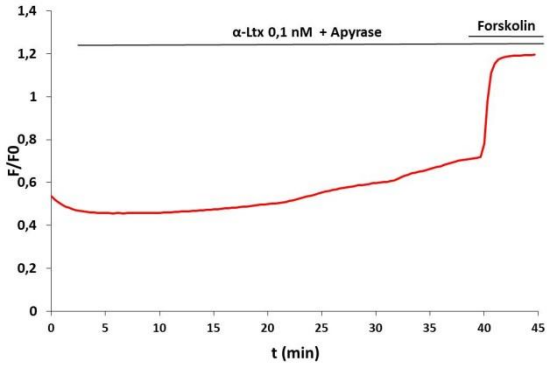

Fig.30. Neuronal ATP contributes to cAMP increase in SCs. Co-cultures transfected for FRET measurements were pre-treated with apyrase, and then exposed to α-Ltx (0,1nM). Forskolin was added after 35 min as positive control. FRET (F/F0) was expressed as the ratio between donor and acceptor signals (YFP and CFP intensities) corrected for background (F0).

Our results demonstrate that ATP released by degenerating neurons indeed contributes to cAMP increase in SCs.

8.10 Neuronal ATP induces ERK 1/2 and CREB phosphorylation in Schwann cells co-cultured with degenerating neurons

The MAPK signaling pathway plays a central role in controlling SCs plasticity and peripheral nerve regeneration via the activation of ERK1/2 and JNK (Napoli et al., 2012; Arthur-Farraj et al., 2012). We have recently reported that mitochondrial alarmins released by degenerating neurons activate SCs via the ERK 1/2 pathway, among which hydrogen peroxide appears to be the stronger inducer (Duregotti et al., 2015). We therefore wondered whether also ATP contributes to MAP kinase activation. Isolate SCs respond to ATP by phosphorylating ERK 1/2 very rapidly (Fig.31A, B). ERK 1/2 phosphorylation in SCs in co-cultures exposed to α-Ltx is reduced in the presence of apyrase (Fig. 31C, D), thus demonstrating the involvement of ATP in the engagement of the MAP kinase signaling pathway.

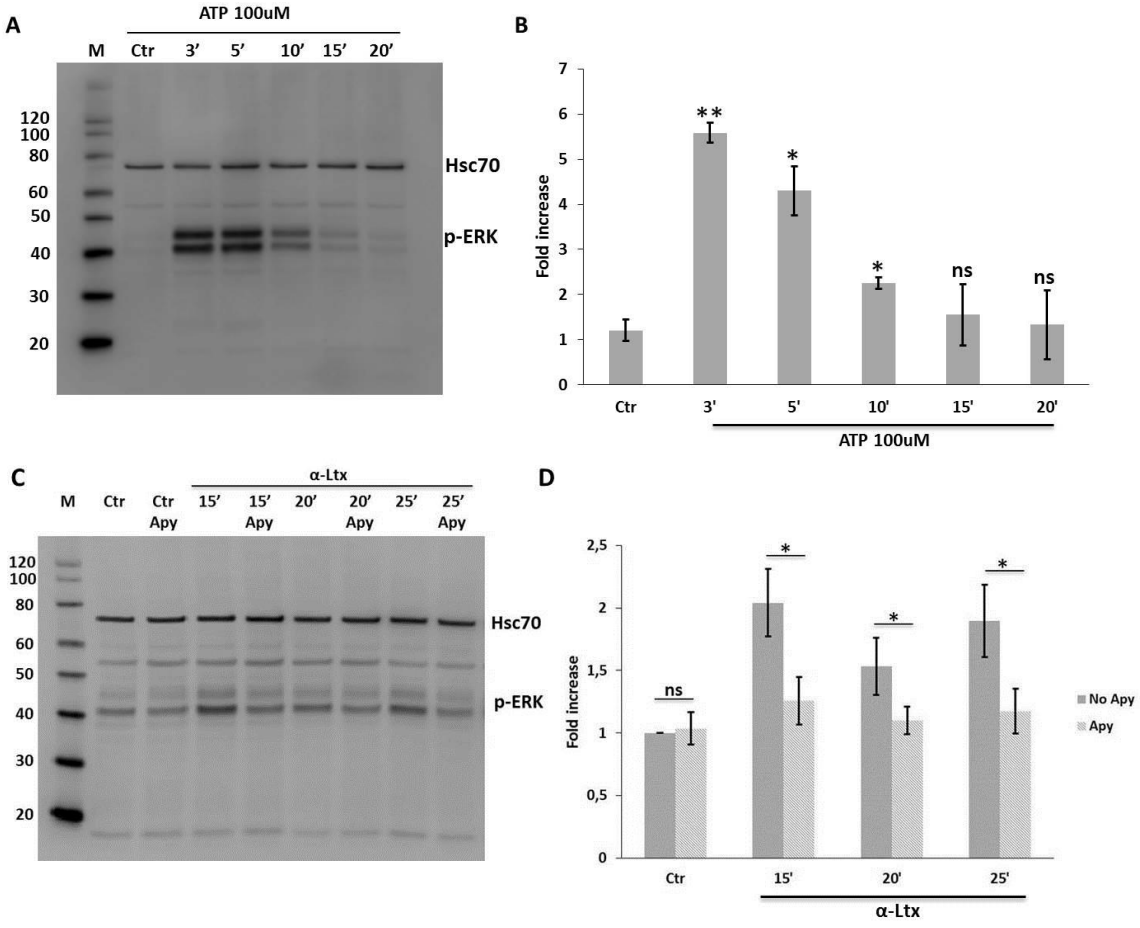

Fig.32. ATP released by intoxicated neurons activates ERK in Schwann cells. A,B: Time-course of ERK phosphorylation induced in primary SCs by ATP (100 µM) (Western blot and quantification). **C,D**: Apyrase pretreatment of cocultures (1,5 U) significantly reduced ERK phosphorylation induced by α-Ltx (0,1 nM) (Western blot and quantification). No ERK phosphorylation is induced in neurons by the toxins. *P < 0.05; ns not significant; n = 3.

Activation of ERK 1/2 and cAMP pathways could modulate CREB-mediated transcription: indeed CREB becomes very rapidly phosphorylated in SCs exposed to ATP (Fig.32A,B), and in SCs in co-cultures upon α-Ltx treatment. The extent of phosphorylation is reduced by the presence of apyrase (Fig.32C,D).

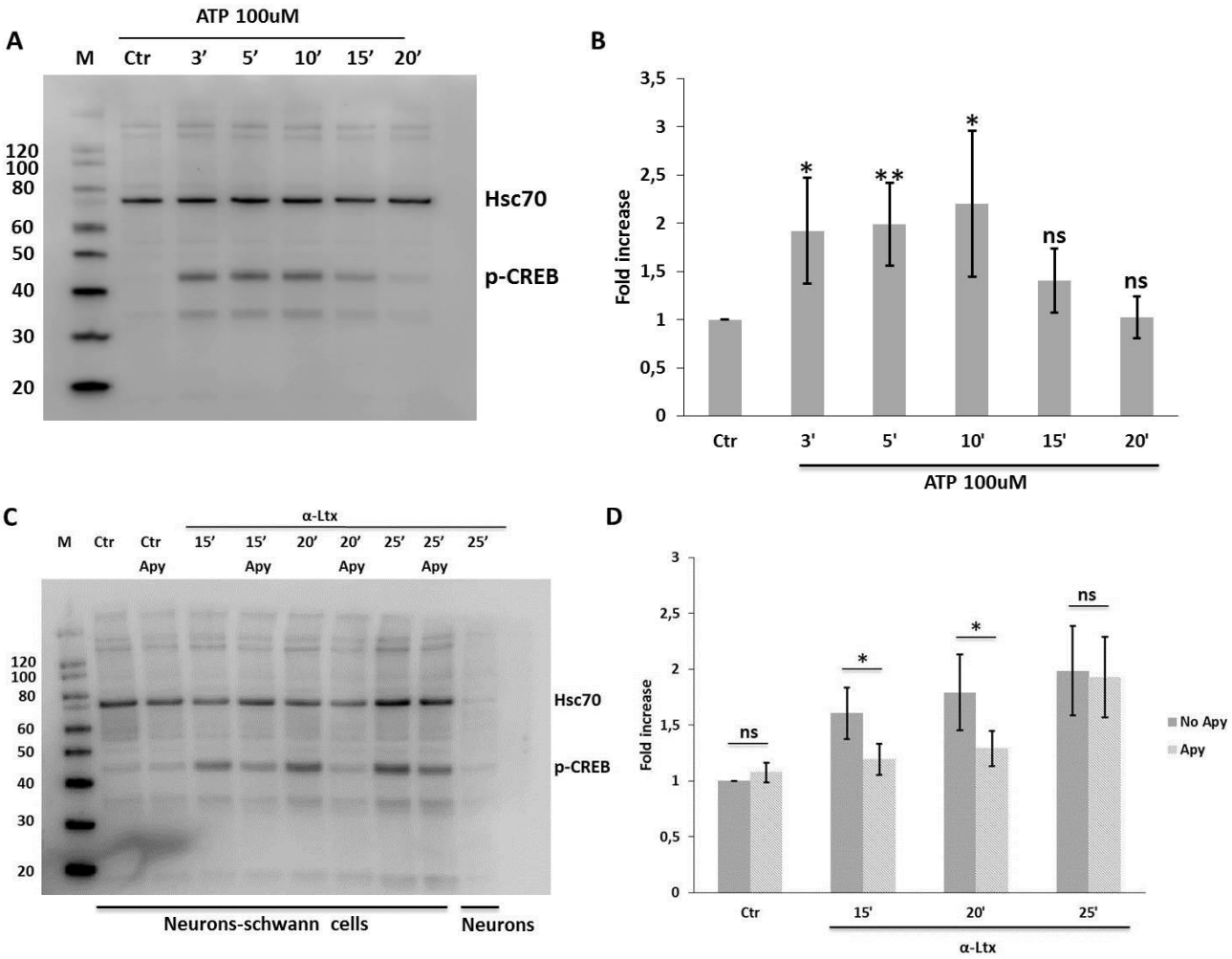

Fig.32. ATP released by intoxicated neurons activates CREB in Schwann cells. A,B: Time-course of CREB phosphorylation induced in primary SCs by ATP (100 µM) (Western blot and quantification). **C,D**: Apyrase pretreatment of cocultures (1,5 U) significantly reduced CREB phosphorylation induced by α-Ltx (0,1nM) (Western blot and quantification). No CREB phosphorylation is induced in neurons by the toxins. *P < 0.05; ns not significant; n = 4.

DISCUSSION

The NMJ is a specialized tripartite synapse formed by MAT, MF, and PSCs. The NMJ has retained throughout vertebrate evolution the capacity to regenerate after nerve injury due to traumas and to the attack of many pathogens including neurotoxins and autoimmune antibodies. Hence, the NMJ is a privileged point of study of the molecular events of inter- and intra-cellular signaling that occur during the degeneration of MAT, due to mechanical injury or neurodegenerative diseases, and, more importantly, of those governing the ensuing regeneration.

The data presented in this thesis were obtained with a model of mouse NMJ degeneration induced by a very specific toxic agent: the presynaptic pore-forming toxin α-Ltx. This model is characterized by a specific biochemical lesion of MAT which induces a rapid Ca^{2+} overload within the nerve terminals. This results in MAT complete degeneration, with consequent activation of the PSCs triggered by at least a several mitochondrial *alarm* molecules (Duregotti et al., 2015). This model is characterized by a high reproducibility and a well defined and rapid time-course of recovery; indeed the entire degeneration and regeneration process induced by α-Ltx is completed within about 5 days. In addition, there is no involvement of the innate immune reaction which would blur and complicate the transcriptomic analysis, as it is the case with the classical cut & crush model.

To identify crucial factors released by PSCs and MF to induce nerve regrowth, we performed a transcriptomic analysis of the NMJ at different time points after injection of α-Ltx. This choice has been very challenging, as a transcriptomic analysis of the NMJ was never reported before.

We succeeded in collecting a number of NMJs suitable for RNA isolation and sequencing of both coding and non–coding RNAs. Among the different mRNAs whose levels increase during degeneration and then progressively return to basal, we selected that encoding for chemokine CXCL12. CXCL12 (stromal cell-derived factor 1/SDF1) is a member of the α-chemokine subfamily; it was originally identified as a stimulatory factor for B-lymphocyte precursor cells (Nagasawa et al., 1994) and, together with its cognate receptor, CXCR4, represents the best-known chemokine ligand/receptor pair. CXCL12 plays an important role during development of the nervous system, where it is necessary for the survival and correct pathfinding of neurons (Arakawa et al., 2003; Pujol et al., 2005). CXCL12 has been found to

facilitate optic nerve regeneration (Heskamp et al., 2013), but its involvement in NMJ recovery of function has been never exploited so far.

By immunostaining we found CXCL12 expressed by PSCs 4h after α-Ltx injection (degeneration phase), while its levels are very low at 24 and 96 hours, when substantial regeneration is attained. Moreover, the protein localizes within intracellular structures Lysotracker- and CD-68-positive, pointing out a possible role of acidic compartments in its secretion, similarly to the secretion route employed by IL-1beta. We are currently investigating the secretion pathway employed by CXCL12. The importance of CXCL12 in nerve recovery is highlighted by the data coming from electrophysiological recordings on *soleus* muscles injected with the toxin in the presence of a neutralizing antibody against the chemokine. Clearly, there is a significant delay in recovery of functionality of those NMJs in which CXCL12 has been inactivated by the antibody. Immunofluorescence analysis on LAL muscles treated as described above show a delay in the reappearance of VAChT staining, a presynaptic marker, in samples exposed to α-Ltx plus anti-CXCL12, compared to muscles injected with α-Ltx alone, thus confirming the electrophysiological results. As expected the antibody did not abolish completely the regeneration process, as several factors are thought to drive NMJ recovery. Moreover, we demonstrated that CXCL12 stimulates motor axon growth. CXCL12 acts via the CXC4R receptor which appears concentrated at the tip of the growing axon. In preliminary experiments performed in *vitro* the CXCR4 antagonist AMD3100 appears to slow down the effects of the chemokine on axon elongation.

In summary, we have collected data about the transcriptional status of the mouse NMJ during degeneration and regeneration, in terms of both coding and non-coding RNAs. We have provided evidence for an important role of the chemokine CXCL12 in NMJ regeneration after an acute damage of MAT. This result might have translational applications for example for the formulation of a mixture of growth factors aimed at improving the recovery of NMJ functionality that is impaired in many human neurodegenerative conditions.

By using α-Ltx as experimental tool, we have also provided evidence that ATP is a signaling molecule involved in the cross-talk between degenerating neurons and SCs. We detected an early release of ATP by cultured primary neurons upon intoxication with α-Ltx, with no loss of plasma membrane integrity. It is generally thought that the main source of ATP acting on purinoreceptors are dying cells, but the present data indicate that this is not the case at least in the present mouse model of peripheral neurodegeneration.

ATP signals through purinergic receptors, whose activation elicits different signaling pathways in target cells including Ca^{2+}, cAMP, inositol-1,4,5-triphosphate, phospholipase C and many others. Since SCs express a range of purinergic receptors (Fields and Burnstock, 2006), we investigated which downstream signaling pathways could be activated in SCs by ATP released by degenerating neurons. Exposure of primary SCs to ATP leads to calcium spikes and cAMP increase. Intoxication of co-cultures with α-Ltx triggers cytosolic Ca^{2+} waves and cAMP rise in SCs. Both effects are reduced by preincubation with apyrase, an ATP-degrading enzyme, indicating that neuronal ATP diffuses to reach nearby SCs, contributing to Ca^{2+} and cAMP response. This supports a role for ATP as *alarm* signal released following PNS injury, able to activate different signaling pathways in SCs, functional to nerve regeneration. Indeed it has been reported that upon neuronal damage SCs undergo a series of cellular changes including dedifferentiation and proliferation, which rely on cAMP signaling. Moreover, given that cAMP has been implicated as an important second messenger regulating phagocytosis (Pryzwansky et al., 1998), it is likely that this signaling cascade could be important also for PSCs, that display macrophagic-like properties during nerve regeneration (Son et al., 1996; Duregotti et al., 2015).

Even the MAPK signaling pathway plays a central role in controlling SC plasticity and peripheral nerve regeneration, and we have recently reported that a major trigger of ERK 1/2 phosphorylation in SCs is hydrogen peroxide, that is produced inside disfunctional mitochondria during MAT degeneration (Duregotti et al., 2015). Here we found that also ATP contributes to ERK 1/2 activation, since intoxicated co-cultures pretreated with apyrase display lower phospho-ERK levels. Both MAPK and PKA engagement can promote CREB transcriptional activity. CREB activates the transcription of target genes in response to a vast array of stimuli including neurotransmitters, hormones, growth factors, synaptic activity, stressors, and inflammatory cytokines (Shaywitz et al., 1999). Indeed we found CREB phosphorylated in the nuclei of isolated SCs exposed to ATP and in our co-culture system: phospho-CREB is detectable at early time points during intoxication, and ATP hydrolysis lowers its levels.

These results highlight the role of ATP as signaling molecules able to activate, in an *in vitro* model of neurodegeneration, a series of intracellullar signaling pathways in SCs including Ca^{2+}, adenylate cyclase, ERK 1/2 and CREB, that are of fundamental importance for the recovery of nerve function.

At the NMJ PSCs and MAT are in close contact: it is likely that in *vivo* ATP released by degenerating axon terminals can reach high local concentrations and activate several pathways in PSCs.

In conclusion the present study has contributed to define the intercellular cross-talk that takes plays at the NMJ during the poisoning by a spider toxin, that could be shared by different forms of neurodegeneration of the presynaptic nerve terminal.

BIBLIOGRAPHY

Angaut-Petit D, Molgo J, Connold AL, Faille L. The levator auris longus muscle of the mouse: a convenient preparation for studies of short- and long-term presynaptic effects of drugs or toxins. *Neurosci Lett*. (1987)

Ansselin AD, Davey DF, Allen DG. Extracellular ATP increases intracellular calcium in cultured adult Schwann cells. *Neuroscience*. (1997)

Arakawa Y, Bito H, Furuyashiki T, Tsuji T, Takemoto-Kimura S, Kimura K, Nozaki K, Hashimoto N, Narumiya S. Control of axon elongation via an SDF-1alpha/Rho/mDia pathway in cultured cerebellar granule neurons. *J Cell Biol*. (2003)

Arce V, Garces A, de Bovis B, Filippi P, Henderson C, Pettmann B, deLapeyrière O. Cardiotrophin-1 requires LIFRbeta to promote survival of mouse motoneurons purified by a novel technique. *J Neurosci Res* (1999).

Arthur-Farraj, P. J. *et al.* c-Jun reprograms Schwann cells of injured nerves to generate a repair cell essential for regeneration. *Neuron.* (2012).

Ashton AC, Volynski KE, Lelianova VG, Orlova EV, Van Renterghem C, Canepari M, Seagar M, Ushkaryov YA. alpha-Latrotoxin, acting via two Ca2+-dependent pathways, triggers exocytosis of two pools of synaptic vesicles. *J Biol Chem*.(2001)

Auld DS, Robitaille R. Perisynaptic Schwann cells at the neuromuscular junction: nerve- and activity-dependent contributions to synaptic efficacy, plasticity, and reinnervation. *Neuroscientist*. (2003)

Baxter RL, Vega-Riveroll LJ, Deuchars J, Parson SH A2A adenosine receptors are located on presynaptic motor nerve terminals in the mouse. *Synapse*. (2005)

Ben-Yaakov Keren, Shachar Y Dagan, Yael Segal-Ruder, Ophir Shalem, Deepika Vuppalanchi, Dianna E Willis, Dmitry Yudin, Ida Rishal, Franziska Rother, Michael Bader, Armin Blesch, Yitzhak Pilpel, Jeffery L Twiss, and Mike Fainzilber. Axonal transcription factors signal retrogradely in lesioned peripheral nerve. *EMBO J*. (2012)

Beirowski B, Adalbert R, Wagner D, Grumme DS, Addicks K, Ribchester RR, Coleman MP. The progressive nature of Wallerian degeneration in wild-type and slow Wallerian degeneration (WldS) nerves. *BMC Neurosci*. (2005)

Bishop, D.L., T. Misgeld, M.K. Walsh, W.B. Gan, J.W. Lichtman Axon branch removal at developing synapses by axosome shedding. *Neuron*. .(2004)

Bourque MJ, Robitaille R. Endogenous peptidergic modulation of perisynaptic Schwann cells at the frog neuromuscular junction. *J Physiol*. (1998)

Bradke F, Fawcett JW, Spira ME. Assembly of a new growth cone after axotomy: the precursor to axon regeneration. *Nat Rev Neurosci*. (2012)

Brill MS, Lichtman JW, Thompson W, Zuo Y, & Misgeld T. Spatial constraints dictate glial territories at murine neuromuscular junctions. *J Cell Biol* (2011).

Brown MC, Hopkins WG.Role of degenerating axon pathways in regeneration of mouse soleus motor axons. *J Physiol*. (1981)

Burden SJ, Sargent PB, McMahan UJ. Acetylcholine receptors in regenerating muscle accumulate at original synaptic sites in the absence of the nerve. *J Cell Biol*. (1979)

Buschow SI, Nolte-'t Hoen EN, van Niel G, Pols MS, ten Broeke T, Lauwen M, Ossendorp F, Melief CJ, Raposo G, Wubbolts R, Wauben MH, Stoorvogel W. MHC II in dendritic cells is targeted to lysosomes or T cell-induced exosomes via distinct multivesicular body pathways. *Traffic*. (2009)

Capogna M, Gähwiler BH, & Thompson SM. Calcium-independent actions of alpha-latrotoxin on spontaneous and evoked synaptic transmission in the hippocampus. *J Neurophysiol*. (1996)

Chen ZL, Strickland S. Laminin gamma1 is critical for Schwann cell differentiation, axon myelination, and regeneration in the peripheral nerve. *J Cell Biol*. (2003)

Chen F, Qian L, Yang ZH, Huang Y, Ngo ST, Ruan NJ, Wang J, Schneider C, Noakes PG, Ding YQ, Mei L, Luo ZG. Rapsyn interaction with calpain stabilizes AChR clusters at the neuromuscular junction. *Neuron*. (2007)

Cheng S, Scigalla FP, Speroni di Fenizio P, Zhang ZG, Stolzenburg JU, Neuhaus J. ATP enhances spontaneous calcium activity in cultured suburothelial myofibroblasts of the human bladder. *PLoS One.* (2011)

Clemence A, Mirsky R, & Jessen KR. Non-myelin-forming Schwann cells proliferate rapidly during Wallerian degeneration in the rat sciatic nerve. *J Neurocytol*. (1989)

Coleman M. Axon degeneration mechanisms: commonality amid diversity. *Nat Rev Neurosci*. (2005)

Collet C, Strube C, Csernoch L, Mallouk N, Ojeda C, Allard B, Jacquemond V. Effects of extracellular ATP on freshly isolated mouse skeletal muscle cells during pre-natal and postnatal development. *Pflugers Arch*. (2002)

Conforti L, Gilley J, Coleman MP. Wallerian degeneration: an emerging axon death pathway linking injury and disease. *Nat Rev Neurosci*. (2014)

Descarries LM, Cai S, Robitaille R, Josephson EM, Morest DK. Localization and characterization of nitric oxide synthase at the frog neuromuscular junction. *J Neurocytol*. (1998)

Duan ZG, Yan XJ, He XZ, Zhou H, Chen P, Cao R, Xiong JX, Hu WJ, Wang XC, Liang SP.Extraction and protein component analysis of venom from the dissected venom glands of Latrodectus tredecimguttatus. *Comp Biochem Physiol B Biochem Mol Biol*. (2006)

Doyu M, Sobue G, Ken E, Kimata K, Shinomura T, Yamada Y, Mitsuma T, Takahashi A. Laminin A, B1, and B2 chain gene expression in transected and regenerating nerves: regulation by axonal signals. *J Neurochem.* (1993)

Duregotti E, Tedesco E, Montecucco C, Rigoni M. Calpains participate in nerve terminal degeneration induced by spider and snake presynaptic neurotoxins. *Toxicon*. (2013)

Duregotti E, Negro S, Scorzeto M, Zornetta I, Dickinson BC, Chang CJ, Montecucco C, Rigoni M. Mitochondrial alarmins released by degenerating motor axon terminals activate perisynaptic Schwann cells. *Proc Natl Acad Sci U S A*. (2015)

Erez H, Malkinson G, Prager-Khoutorsky M, De Zeeuw CI, Hoogenraad CC, Spira ME. Formation of microtubule-based traps controls the sorting and concentration of vesicles to restricted sites of regenerating neurons after axotomy. *J. Cell Biol*. (2007).

Fields R.D. and Burnstock D. Purinergic signalling in neuron–glia interactions. *Nature Reviews Neuroscience* (2006)

Filbin M. T. Myelin-associated inhibitors of axonal regeneration in the adult mammalian CNS. *Nat. Rev. Neurosci.*(2003).

Gaudet AD, Popovich PG, Ramer MS. Wallerian degeneration: gaining perspective on inflammatory events after peripheral nerve injury. *J Neuroinflammation*. (2011)

Glass JD, Culver DG, Levey AI, Nash NR. Very early activation of m-calpain in peripheral nerve during Wallerian degeneration. *J Neurol Sci.* (2002)

Gordon T. The role of neurotrophic factors in nerve regeneration. *Neurosurg Focus*. (2009)

Griffin J. W, George R, Ho T. Macrophage systems in peripheral nerves. A review. *J. Neuropathol. Exp. Neurol.* (1993).

Grishin EV. Black widow spider toxins: the present and the future. *Toxicon*. (1998)

Grishin S, Shakirzyanova A, Giniatullin A, Afzalov R, Giniatullin R. Mechanisms of ATP action on motor nerve terminals at the frog neuromuscular junction. *Eur J Neurosci*. (2005)

Hassan SM, Jennekens FG, Veldman H, Oestreicher BA. GAP-43 and p75NGFR immunoreactivity in presynaptic cells following neuromuscular blockade by botulinum toxin in rat. *JNeurocytol*. (1994)

Heskamp A, Leibinger M, Andreadaki A, Gobrecht P, Diekmann H, Fischer D. CXCL12/SDF-1 facilitates optic nerve regeneration. *Neurobiol Dis*. (2013)

Hoke A, Gordon T, Zochodne D. W, Sulaiman, O. A. A decline in glial cell-line-derived neurotrophic factor expression is associated with impaired regeneration after long-term Schwann cell denervation. *Exp. Neurol.* 173, 77–85 (2002).

Holness CL, Simmons DL. Molecular cloning of CD68, a human macrophage marker related to lysosomal glycoproteins. *Blood*. (1993)

Jessen KR, Mirsky R, Lloyd AC. Schwann Cells: Development and Role in Nerve Repair. *Cold Spring Harb Perspect Biol*. (2015)

Klarenbeek J, Goedhart J, van Batenburg A, Groenewald D, Jalink K. Fourth-Generation Epac-Based FRET Sensors for cAMP Feature Exceptional Brightness, Photostability and Dynamic Range: Characterization of Dedicated Sensors for FLIM, for Ratiometry and with High Affinity. *Plos One* (2015)

Knott E.P, Assi M, Pearse D.D. Cyclic AMP Signaling: A Molecular Determinant of Peripheral Nerve Regeneration. *BioMed Research International Volume* (2014)

Lemons ML, Barua S, Abanto ML, Halfter W, Condic ML. Adaptation of sensory neurons to hyalectin and decorin proteoglycans. *J Neurosci*. (2005)

Levi G, Aloisi F, Ciotti MT, Gallo V. Autoradiographic localization and depolarization-induced release of acidic amino acids in differentiating cerebellar granule cell cultures. *Brain Res* (1984).

Li M, Ransohoff RM. Multiple roles of chemokine CXCL12 in the central nervous system: a migration from immunology to neurobiology. *Prog Neurobiol*. (2008)

Lopez-Verrilli MA, Picou F, Court FA. Schwann cell-derived exosomes enhance axonal regeneration in the peripheral nervous system. *Glia*. (2013)

Love FM, Thompson WJ. Glial cells promote muscle reinnervation by responding to activity-dependent postsynaptic signals. *J Neurosci*. (1999)

McGrath KE, Koniski AD, Maltby KM, McGann JK, Palis J. Embryonic expression and function of the chemokine SDF-1 and its receptor, CXCR4. *Dev Biol*. (1999)

Mallon BS, Shick HE, Kidd GJ, Macklin WB. Proteolipid promoter activity distinguishes two populations of NG2-positive cells throughout neonatal cortical development. *J Neurosci* (2002).

Mathivanan S, Fahner CJ, Reid GE, Simpson RJ. ExoCarta 2012: database of exosomal proteins, RNA and lipids. *Nucleic Acids Res*. **(**2012)

Matteoli M, Haimann C, Torri-Tarelli F, Polak JM, Ceccarelli B, De Camilli P. Differential effect of alpha-latrotoxin on exocytosis from small synaptic vesicles and from large dense-core vesicles containing calcitonin gene-related peptide at the frog neuromuscular junction. *Proc Natl Acad Sci U S A* (1988)

McMahan UJ, Wallace BG. Molecules in basal lamina that direct the formation of synaptic specializations at neuromuscular junctions. *Dev Neurosci*. (1989)

Mehta A, Reynolds ML, Woolf CJ. Partial denervation of the medial gastrocnemius muscle results in growth-associated protein-43 immunoreactivity in sprouting axons and Schwann cells. *Neuroscience*. (1993)

Moloney EB, de Winter F, Verhaagen J. ALS as a distal axonopathy: molecular mechanisms affecting neuromuscular junction stability in the presymptomatic stages of the disease. *Front Neurosci*. (2014)

Nagasawa T. CXC chemokine ligand 12 (CXCL12) and its receptor CXCR4. *J Mol Med (Berl*). (2014)

Nagasawa T, Hirota S, Tachibana K, Takakura N, Nishikawa S, Kitamura Y, Yoshida N, Kikutani H, Kishimoto T. Defects of B-cell lymphopoiesis and bone-marrow myelopoiesis in mice lacking the CXC chemokinePBSF/SDF-1. *Nature*. (1996)

Nagasawa T, Kikutani H, Kishimoto T. Molecular cloning and structure of a pre-B-cell growth-stimulating factor. *Proc Natl Acad Sci U S A*. (1994)

Nobile M, Monaldi I, Alloisio S, Cugnoli C, Ferroni S. ATP-induced, sustained calcium signalling in cultured rat cortical astrocytes: evidence for a non-capacitative, P2X7-like-mediated calcium entry. *FEBS Lett*. (2003)

Opatz J, Küry P, Schiwy N, Järve A, Estrada V, Brazda N, Bosse F, Müller HW.
SDF-1 stimulates neurite growth on inhibitory CNS myelin. *Mol Cell Neurosci*. (2009)

Orlova EV, Rahman MA, Gowen B, Volynski KE, Ashton AC, Manser C, van Heel M, Ushkaryov YA.Structure of alpha-latrotoxin oligomers reveals that divalent cation-dependent tetramers form membrane pores *Nat Struct Biol*. (2000)

Ostrowski M, Carmo NB, Krumeich S, Fanget I, Raposo G, Savina A, Moita CF, Schauer K, Hume AN, Freitas RP, Goud B, Benaroch P, Hacohen N, Fukuda M, Desnos C, Seabra MC, Darchen F, Amigorena S, Moita LF, Thery C. Rab27a and Rab27b control different steps of the exosome secretion pathway. *Nat Cell Biol*. (2010)

Park JW, Vahidi B, Taylor AM, Rhee SW, Jeon NL. Microfluidic culture platform for neuroscience research. *Nat Protoc*. (2006)

Perrin FE, Lacroix S, Avilés-Trigueros M, David S .Involvement of monocyte chemoattractant protein-1, macrophage inflammatory protein-1alpha and interleukin-1beta in Wallerian degeneration. *Brain*. (2005)

Piccioli P, Rubartelli A. The secretion of IL-1β and options for release. *Semin Immunol*. (2013)

Pinard A, Lévesque S, Vallée J, Robitaille R. Glutamatergic modulation of synaptic plasticity at a PNS vertebrate cholinergic synapse. *Eur J Neurosci.* (2003)

Press C, Milbrandt J. Nmnat delays axonal degeneration caused by mitochondrial and oxidative stress. *J. Neurosci.* (2008).

Previtali SC, Feltri ML, Archelos JJ, Quattrini A, Wrabetz L, Hartung H. Role of integrins in the peripheral nervous system. *Prog Neurobiol*. (2001)

Pryzwansky KB, Kidao S, Merricks EP. Compartmentalization of PDE-4 and cAMP-dependent protein kinase in neutrophils and macrophages during phagocytosis. *Cellular biochemistry and biophysics*. (1998)

Pujol F, Kitabgi P, Boudin H. The chemokine SDF-1 differentially regulates axonal elongation and branching in hippocampal neurons. *J Cell Sci*. (2005)

Ramprasad MP, Terpstra V, Kondratenko N, Quehenberger O, Steinberg D. Cell surface expression of mouse macrosialin and human CD68 and their role as macrophage receptors for oxidized low density lipoprotein. *Proc Natl Acad Sci U S A*. (1996)

Reddy LV, Koirala S, Sugiura Y, Herrera AA, Ko CP. Glial cells maintain synaptic structure and function and promote development of the neuromuscular junction in vivo. *Neuron*. (2003)

Reynolds ML, Woolf CJ. Terminal Schwann cells elaborate extensive processes following denervation of the motor endplate. *J Neurocytol*. (1992)

Rigoni M, Schiavo G, Weston AE, Caccin P, Allegrini F, Pennuto M, Valtorta F, Montecucco C, Rossetto O. Snake presynaptic neurotoxins with phospholipase A2 activity induce punctate swellings of neurites and exocytosis of synaptic vesicles. *J Cell Sci*. (2004)

Rigoni M, Caccin P, Gschmeissner S, Koster G, Postle AD, Rossetto O, Schiavo G, Montecucco C.Equivalent effects of snake PLA2 neurotoxins and lysophospholipid-fatty acid mixtures. *Science* (2005).

Rigoni M, Pizzo P, Schiavo G, Weston AE, Zatti G, Caccin P, Rossetto O, Pozzan T, Montecucco C. Calcium influx and mitochondrial alterations at synapses exposed to snake neurotoxins or their phospholipid hydrolysis products. *J Biol Chem*. (2007)

Riley DA. Spontaneous elimination of nerve terminals from the endplates of developing skeletal myofibers. *Brain Res*. (1977)

Robitaille R. Purinergic receptors and their activation by endogenous purines at perisynaptic glial cells of the frog neuromuscular junction. *J Neurosci*. (1995)

Robitaille R, Bourque MJ, Vandaele S. Localization of L-type Ca2+ channels at perisynaptic glial cells of the frog neuromuscular junction. *J Neurosc*i. (1996)

Robitaille R, Jahromi BS, Charlton MP. Muscarinic Ca2+ responses resistant to muscarinic antagonists at perisynaptic Schwann cells of the frog neuromuscular junction. *J Physiol*. (1997)

Rochon D, Rousse I, Robitaille R. Synapse-glia interactions at the mammalian neuromuscular junction. *J Neurosci*. (2001)

Rotshenker, S. Wallerian degeneration: the innate-immune response to traumatic nerve injury. *J. Neuroinflammation* 8, 109 (2011).

Rudolf R, Khan MM, Labeit S, Deschenes MR. Degeneration of neuromuscular junction in age and dystrophy. *Front Aging Neurosci*. 2014

Sanes JR, Lichtman JW. Development of the vertebrate neuromuscular junction. *Annu Rev Neurosci*. (1999)

Silinsky EM. On the association between transmitter secretion and the release of adenine nucleotides from mammalian motor nerve terminals. *J Physiol*. (1975)

Simons M, Raposo G. Exosomes--vesicular carriers for intercellular communication. *Curr Opin Cell Biol.* (2009)

Schaefer AW, Schoonderwoert VT, Ji L, Mederios N, Danuser G, Forscher P.. Coordination of actin filament and microtubule dynamics during neurite outgrowth. *Dev. Cell* (2008).

Scheer H, Prestipino G, Meldolesi J. Reconstitution of the purified alpha-latrotoxin receptor in liposomes and planar lipid membranes. Clues to the mechanism of toxin action.
EMBO J. (1986)

Shaywitz AJ, Greenberg ME. CREB: a stimulus-induced transcription factor activated by a diverse array of extracellular signals. *Annu Rev Biochem*. (1999)
Scheib J, Höke A. Advances in peripheral nerve regeneration. *Nat Rev Neurol*. (2013)

Shen, Y. J., DeBellard, M. E., Salzer, J. L., Roder, J. & Filbin, M. T. Myelin-associated glycoprotein in myelin and expressed by Schwann cells inhibits axonal regeneration and branching. *Mol. Cell. Neurosci.* (1998).

Simpson RJ, Jensen SS, Lim JW. Proteomic profiling of exosomes: current perspectives. *Proteomics*. (2008)

Son YJ & Thompon WJ. Schwann cell processes guide regeneration of peripheral axons. *Neuron*. (1995)

Son YJ & Thompson WJ. Nerve sprouting in muscle is induced and guided by processes extended by Schwann cells. *Neuron.* (1995).
Son YJ, Trachtenberg JT, Thompson WJ. Schwann cells induce and guide sprouting and reinnervation of neuromuscular junctions. *Trends Neurosci*. (1996)

Song JW, Misgeld T, Kang H, Knecht S, Lu J, Cao Y, Cotman SL, Bishop DL, Lichtman JW.. Lysosomal activity associated with developmental axon pruning. *J Neurosci*. (2008)

Sotelo-Silveira, J. R., Calliari, A., Kun, A., Koenig, E. & Sotelo, J. R. RNA trafficking in axons. *Traffic* (2006).

Stoll G, Griffin JW, Li CY, Trapp BD. Wallerian degeneration in the peripheral nervous system: participation of both Schwann cells and macrophages in myelin degradation. *J Neurocytol*. (1989)

Stoll G, Jander S, Myers RR. Degeneration and regeneration of the peripheral nervous system: from Augustus Waller's observations to neuroinflammation. *J Peripher Nerv Syst*. (2002)

Subang MC, Richardson PM. Influence of injury and cytokines on synthesis of monocyte chemoattractant protein-1 mRNA in peripheral nervous tissue. *Eur J Neurosci*. (2001)

Tedesco E, Rigoni M, Caccin P, Grishin E, Rossetto O, Montecucco C. Calcium overload in nerve terminals of cultured neurons intoxicated by alpha-latrotoxin and snake PLA2 neurotoxins. *Toxicon*. (2009)

Tetta C, Ghigo E, Silengo L, Deregibus MC, Camussi G. Extracellular vesicles as an emerging mechanism of cell-to-cell communication. *Endocrine*. (2013)

Todd KJ, Robitaille R. Neuron-glia interactions at the neuromuscular synapse. *Novartis Found Symp*. 2006

Tofaris GK, Patterson PH, Jessen KR, Mirsky R. Denervated Schwann cells attract macrophages by secretion of leukemia inhibitory factor (LIF) and monocyte chemoattractant protein-1 in a process regulated by interleukin-6 and LIF. *J Neurosci*. (2002)

Tucker BA, Mearow KM. Peripheral sensory axon growth: from receptor binding to cellular signaling. *Can J Neurol Sci*. (2008)

Ushkaryov YA, Rohou A, & Sugita S. Alpha-Latrotoxin and its receptors. *Handb Exp Pharmacol*. (2008)

Van Niel G, Porto-Carreiro I, Simoes S, Raposo G. Exosomes: a common pathway for a specialized function. *J Biochem*. (2006)

Vargas ME, Barres BA. Why is Wallerian degeneration in the CNS so slow? *Annu Rev Neurosci*. (2007)

Volynski KE, Capogna M, Ashton AC, Thomson D, Orlova EV, Manser CF, Ribchester RR, Ushkaryov YA .Mutant alpha-latrotoxin (LTXN4C) does not form pores and causes secretion by receptor stimulation: this action does not require neurexins. *J Biol Chem*. 2003

Vrbova G, Mehra N, Shanmuganathan H, Tyreman N, Schachner M, Gordon T. Chemical communication between regenerating motor axons and Schwann cells in the growth pathway. *Eur J Neurosci*. (2009)

Wallquist W, Patarroyo M, Thams S, Carlstedt T, Stark B, Cullheim S, Hammarberg H. Laminin chains in rat and human peripheral nerve: distribution and regulation during development and after axonal injury. *J Comp Neurol*. (2002)

Wolpowitz D, Mason TB, Dietrich P, Mendelsohn M, Talmage DA, Role LW.
Cysteine-rich domain isoforms of the neuregulin-1 gene are required for maintenance of peripheral synapses. *Neuron*. (2000)

Wood SJ, Slater CR. Safety factor at the neuromuscular junction. *Prog Neurobiol*. (2001)

Woolf CJ, Reynolds ML, Chong MS, Emson P, Irwin N, Benowitz LI. Denervation of the motor endplate results in the rapid expression by terminal Schwann cells of the growth-associated protein GAP-43. *J Neurosci*. (1992)

Yan F, Wu X, Crawford M, Duan W, Wilding EE, Gao L, Nana-Sinkam SP, Villalona-Calero MA, Baiocchi RA, Otterson GA.The Search for an Optimal DNA, RNA, and Protein

Detection by *in situ* Hybridization, Immunohistochemistry, and Solution-Based Methods. *Methods.* (2010)

Ydens E, Cauwels A, Asselbergh B, Goethals S, Peeraer L, Lornet G, Almeida-Souza L, Van Ginderachter JA, Timmerman V, Janssens S.. Acute injury in the peripheral nervous system triggers an alternative macrophage response. *J. Neuroinflammation.* (2012).

Yoo, S., van Niekerk, E. A., Merianda, T. T. & Twiss, J. L. Dynamics of axonal mRNA transport and implications for peripheral nerve regeneration. *Exp. Neurol*. (2010).

You, S., Petrov, T., Chung, P. H. & Gordon, T. The expression of the low affinity nerve growth factor receptor in long-term denervated Schwann cells. *Glia* 20, 87–100 (1997).

Yu B, Zhou S, Yi S, Gu X.The regulatory roles of non-coding RNAs in nerve injury and regeneration. *Prog Neurobiol*. (2015)

Yurchenco PD, Cheng YS, Campbell K, Li S. Loss of basement membrane, receptor and cytoskeletal lattices in a laminin-deficient muscular dystrophy. *J Cell Sci*. (2004)

Zhu Y, Matsumoto T, Mikami S, Nagasawa T, Murakami F. SDF1/CXCR4 signalling regulates two distinct processes of precerebellar neuronal migration and its depletion leads to abnormal pontine nuclei formation. *Development*. (2009)

Zlotnik A, Yoshie O. Chemokines: a new classification system and their role in immunity. *Immunity*. (2000)

Mitochondrial alarmins released by degenerating motor axon terminals activate perisynaptic Schwann cells

Elisa Duregotti[a], Samuele Negro[a], Michele Scorzeto[a], Irene Zornetta[a], Bryan C. Dickinson[b,c,1], Christopher J. Chang[b,c], Cesare Montecucco[a,d,2], and Michela Rigoni[a,2]

[a]Department of Biomedical Sciences, University of Padua, Padua 35131, Italy; [b]Department of Chemistry and Molecular and Cell Biology and [c]Howard Hughes Medical Institute, University of California, Berkeley, CA 94720; and [d]Italian National Research Council Institute of Neuroscience, Padua 35131, Italy

Edited by Thomas C. Südhof, Stanford University School of Medicine, Stanford, CA, and approved December 22, 2014 (received for review September 5, 2014)

An acute and highly reproducible motor axon terminal degeneration followed by complete regeneration is induced by some animal presynaptic neurotoxins, representing an appropriate and controlled system to dissect the molecular mechanisms underlying degeneration and regeneration of peripheral nerve terminals. We have previously shown that nerve terminals exposed to spider or snake presynaptic neurotoxins degenerate as a result of calcium overload and mitochondrial failure. Here we show that toxin-treated primary neurons release signaling molecules derived from mitochondria: hydrogen peroxide, mitochondrial DNA, and cytochrome c. These molecules activate isolated primary Schwann cells, Schwann cells cocultured with neurons and at neuromuscular junction in vivo through the MAPK pathway. We propose that this inter- and intracellular signaling is involved in triggering the regeneration of peripheral nerve terminals affected by other forms of neurodegenerative diseases.

motor axon degeneration | presynaptic neurotoxins | mitochondrial alarmins | Schwann cells

The venoms of the black widow spider *Latrodectus mactans*, the Australian taipan snake *Oxyuranus scutellatus scutellatus*, and the Taiwan krait *Bungarus multinctus* cause the paralysis of peripheral skeletal and autonomic nerve terminals in envenomated subjects. Such paralysis is completely reversible, and within a month or so, patients, supported by mechanical ventilation, recover completely (1–3). Paralysis in mice/rodents has a shorter duration, and again recovery is complete (4, 5). Major presynaptic toxins of these venoms are α-latrotoxin (α-Ltx), taipoxin (Tpx), and β-bungarotoxin (β-Btx), respectively (6, 7). α-Ltx induces a very rapid nerve terminal paralysis by forming transmembrane ion channels that cause a massive Ca^{2+} entry, with exocytosis of synaptic vesicles and mitochondrial damage (7–11). This is followed by Ca^{2+}-induced degeneration of motor axon terminals, which is remarkably limited to the unmyelinated endplate. Complete regeneration is achieved in mice within 8–10 d (4). Tpx and β-Btx are representative of a large family of presynaptic snake neurotoxins endowed with phospholipase A2 activity (SPANs), which are important, although neglected, human pathogens (12–15). We have contributed to the definition of their mechanism of action, which involves generation of lysophospholipids and fatty acids on the external layer of the plasma membrane (16, 17). The mixture of these lipid products favors exocytosis of ready-to-release synaptic vesicles and mediates the rise of cytosolic Ca^{2+}, presumably via transient lipid ion channels (16, 18). In turn, this Ca^{2+} influx causes a massive release of synaptic vesicles and mitochondrial damage, with ensuing complete degeneration of axon terminals (5, 18–20). Similar to α-Ltx, SPANs-induced peripheral paralysis is followed by a complete recovery: regeneration and functional reinnervation are almost fully restored in rats by 5 d (20). The similar outcome and time-course of the paralysis induced by the two types of presynaptic neurotoxins suggest that the common property of inducing Ca^{2+} entry into the nerve terminals is the main cause of nerve terminal degeneration (21). Indeed, these neurotoxins cause activation of the calcium-activated calpains that contribute to cytoskeleton fragmentation (22).

Although clearly documented (4, 5, 20), the regeneration of the motor axon terminals after presynaptic neurotoxins injection is poorly known in its cellular and molecular aspects. Available evidence indicates that, in general, regeneration of mechanically damaged motor neuron terminals relies on all three cellular components of the neuromuscular junction (NMJ): the neuron, the perisynaptic Schwann cells (PSCs), and the muscle cells (23, 24). The regeneration steps that take place on animal neurotoxin poisoning are likely to be similar to those after the cut or crush of nerves, as a closely similar cascade of toxic events occurs in both conditions (i.e., calcium overload, mitochondrial impairment, and cytoskeleton degradation). Similar neurodegenerative events are also shared by traumatized patients. However, the model system used here provides the advantage of being much more controlled and more reproducible. In addition, it does not involve the death of many cell types, as it follows a well-characterized biochemical lesion of the end plate only (7, 8, 10–12, 16, 18). Therefore, the mouse NMJ treated with α-Ltx, Tpx, or β-Btx represents a relevant model of acute motor axon terminal

Significance

The neuromuscular junction is the site of transmission of the nerve impulse to the muscle. This finely tuned synapse relies on at least three components: the motor neuron, the muscle fiber, and the Schwann cells, which assist nerve recovery after injury. Using animal neurotoxins to induce an acute and reversible nerve degeneration, we have identified several mitochondrial molecules through which the damaged nerve terminal communicates with nearby cells, activating signaling pathways in Schwann cells involved in nerve regeneration. Among these messengers, hydrogen peroxide appears to be crucial at the initial stages of regeneration, because its inactivation delays the functional recovery of the damaged neuromuscular junction in vivo. These findings provide important indications about the pharmacological treatment of traumatized patients.

Author contributions: C.M. and M.R. designed research; E.D., S.N., M.S., and I.Z. performed research; B.C.D. and C.J.C. contributed new reagents/analytic tools; E.D., S.N., M.S., I.Z., C.M., and M.R. analyzed data; and E.D., S.N., M.S., I.Z., B.C.D., C.J.C., C.M., and M.R. wrote the paper.

The authors declare no conflict of interest.

This article is a PNAS Direct Submission.

Freely available online through the PNAS open access option.

[1]Present address: Gordon Center for Integrative Sciences, University of Chicago, Chicago, IL 60637.

[2]To whom correspondence may be addressed. Email: michela.rigoni@unipd.it or cesare.montecucco@unipd.it.

This article contains supporting information online at www.pnas.org/lookup/suppl/doi:10.1073/pnas.1417108112/-/DCSupplemental.

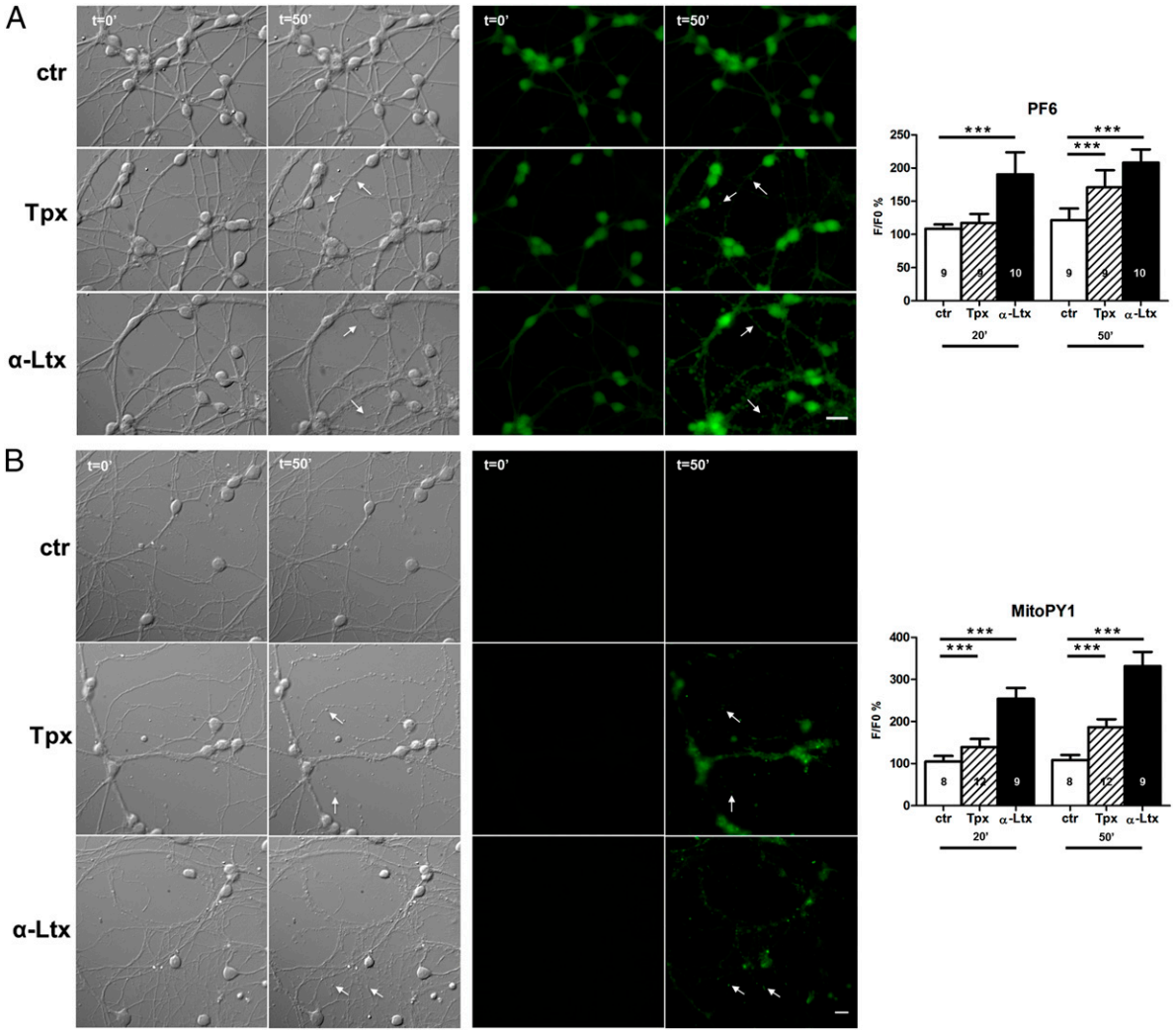

Fig. 1. Live-imaging of neuronal hydrogen peroxide production. Rat CGNs were loaded with the H_2O_2-specific probes PF6-AM (*A*) or MitoPY1 (*B*), washed, and then exposed to Tpx 6 nM or α-Ltx 0.1 nM for 50 min. Changes in fluorescence resulting from H_2O_2 production were monitored with time and expressed as a percentage of the fluorescence value at $t = 0$ (*Right*). ***$P < 0.001$. Arrows in bright-field images and in the green channel point to neuronal bulges. (Scale bars: 10 μm.)

degeneration and regeneration, which is likely to provide information useful to the understanding of the pathogenesis not only of envenomation but also, more in general, of other human pathological syndromes.

Cell death and injury often lead to the release or exposure of intracellular molecules called damage-associated molecular patterns (DAMPs) or alarmins. Recently, mitochondria have emerged as major sources of DAMPs (25). Mitochondria are abundant subcellular components of the NMJ that have been recently shown to release mitochondrial DNA (mtDNA) and cytochrome c (Cyt c) after trauma or snake myotoxin-induced muscle damage, thus contributing to the systemic or local inflammatory responses associated with such conditions (26, 27). In this study, we tested whether α-Ltx and SPANs induce the release of mitochondrial signaling molecules from primary neuronal cultures and found that, in addition to mtDNA and Cyt c, hydrogen peroxide (H_2O_2) is released. First candidate targets of these mitochondrial mediators released by damaged neurons are nonmyelinating PSCs, which are intimately associated with the end plate. They play an active role in the formation, function, maintenance, and repair of the NMJ (28–33). PSC activation parallels nerve degeneration and contributes to neuronal regeneration by phagocytosis of cellular debris and by extension of processes that guide reinnervation (34, 35). We therefore investigated whether mitochondrial DAMPs released by injured neurons were able to activate SCs, and through which downstream pathway. Using isolated primary cells, neuron-Schwann cell cocultures, and the NMJ in vivo, we found that PSCs are activated by mitochondrial alarmins and that the MAPK signaling pathway is involved in this process.

Results

Hydrogen Peroxide Is Produced by Neurons Exposed to Spider or Snake Presynaptic Neurotoxins. Given that mitochondria of stressed cells produce superoxide anion, which is rapidly converted into H_2O_2, and that in neurons exposed to the neurotoxins, mitochondria functionality is impaired, we asked whether intoxication of neurons by α-Ltx or SPANs leads to H_2O_2 production, an ideal candidate as intercellular signaling molecule (36–38). We therefore loaded rat cerebellar granular neurons (CGNs) with specific H_2O_2 probes with different cellular localization and monitored the samples for up to an hour. MitoPY1 is a bifunctional molecule that combines a chemoselective boronate-based switch and a mitochondrial-targeting phosphonium moiety for the detection

of H_2O_2 localized to mitochondria (39). PF6-AM takes advantage of multiple masked carboxylates to increase cellular retention, and hence sensitivity to low levels of peroxide. In its ester-protected form, PF6-AM can readily enter cells. Once inside cells, the protecting groups are rapidly cleaved by intracellular esterases to produce their anionic carboxylate forms, which are effectively trapped within cells (40).

After exposure to α-Ltx or Tpx, H_2O_2 levels increased with time, markedly at the level of neurite enlargements (so-called bulges), which are a hallmark of intoxication (16, 41), as shown in Fig. 1. Bulges are sites of calcium overload and accumulation of depolarized mitochondria (18), and the MitoPY1 signal indicates that these mitochondria produce H_2O_2. Quantification of the signals indicates a more pronounced effect of α-Ltx with respect to Tpx, in agreement with the fact that the pore formed by the former neurotoxin mediates a larger Ca^{2+} entry than Tpx (21). Similar results were obtained following intoxication of rat spinal cord motor neurons (MNs; Fig. S1). That mitochondria are the major source of H_2O_2 is reinforced by the finding that toxins failed to induce membrane translocation of cytoplasmic p47phox, a regulatory component of the NADPH oxidase complex, which excludes a role of the NADPH oxidase system (Fig. S2).

Hydrogen Peroxide Released by Degenerating Nerve Terminals Activates Schwann Cells and Stimulates Regeneration. Growing evidence indicates that H_2O_2 is a largely used intercellular signaling molecule regulating kinase-driven pathways (37, 38, 42): it triggers ERK phosphorylation in different cell types (43), with consequent activation of downstream gene transcription, and ERK signaling was recently shown to play a central role in the orchestration of axon repair by SCs (44, 45).

In preliminary experiments, we checked whether primary SCs isolated from rat sciatic nerves were responsive to H_2O_2 by analyzing ERK phosphorylation by Western blotting and immunofluorescence. Exposure of primary SCs to H_2O_2 led to ERK phosphorylation and translocation of p-ERK into the nucleus (Fig. S3 *A* and *B*). Cocultures of primary spinal cord motor neurons and sciatic nerve-derived SCs were then exposed to α-Ltx or Tpx: bulges appeared within few minutes along neuronal processes, and p-ERK was detected in the cytoplasm and nucleus of SCs (Fig. 2*A*). Phospho-ERK-positive cells were also positive for S-100, a specific SC marker (Fig. S3*C*). In cocultures, the score of S-100-positive cells that become p-ERK-positive is 59% on intoxication with β-Btx ($n = 81$) and 78% in the case of α-Ltx ($n = 69$). These percentages were obtained by counting many S-100-positive cells randomly distributed in different fields, but the value is actually much higher if one considers only clustered SCs in close proximity of intoxicated neurites; this observation further supports the conclusion that molecules released by injured neurons reach nearby SCs, thus activating them.

ERK phosphorylation was reduced in cocultures preincubated with catalase, which converts H_2O_2 into water and O_2, indicating that H_2O_2 produced inside neurons diffuses to reach nearby SCs, contributing to their ERK activation (Fig. 2*B*). Residual p-ERK signal might be a result of mediators other than H_2O_2 released on neuronal injury. Toxins failed to induce a direct ERK phosphorylation either in isolated SCs (Fig. S3*D*) or in isolated primary neurons (Fig. 2*B*).

Next we tested whether the ERK pathway is activated also within PSCs at the NMJs of intoxicated mice. Sublethal doses of the neurotoxins were s.c. injected in transgenic mice expressing a cytoplasmic GFP specifically in SCs under the *plp* promoter (46, 47), in proximity to the levator auris longus (LAL) (48), a thin muscle ideal for imaging. Twenty-four hours later, muscles were collected and processed for indirect immunohistochemistry. A clear p-ERK signal was detected at the level of PSCs in treated NMJs, thus extending in vivo the results obtained in cocultures

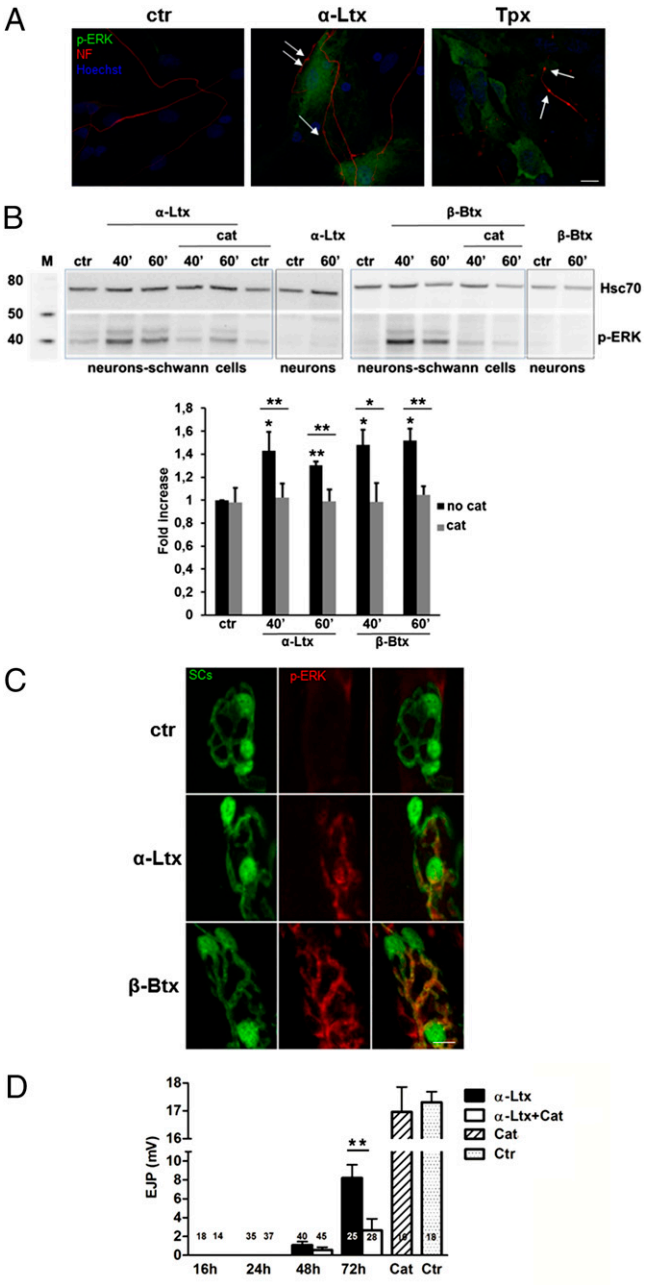

Fig. 2. Hydrogen peroxide released after nerve terminal degeneration activates ERK in Schwann cells and stimulates regeneration. Phospho-ERK (green) was detected in primary SCs cocultured with spinal cord MNs on exposure to α-Ltx (0.1 nM) or SPANs (6 nM) for 50 min by immunofluorescence (*A*), as well as by Western blots of total lysates (*B*). Arrows in *A* point to neuronal bulges stained with an antibody against neurofilaments (NF; red). Nuclei are stained with Hoechst (blue). (Scale bars: 10 μm.) (*B*) Catalase pretreatment of cocultures (1,000 U) significantly reduced ERK phosphorylation induced by the toxins (Western blot and quantification). No ERK phosphorylation is induced in neurons by the toxins. $*P < 0.05$; $**P < 0.01$; $n = 4$. (*C*) α-Ltx or β-Btx s.c. injections in LAL muscle of transgenic mice trigger ERK phosphorylation (p-ERK; red) in PSCs (green). Muscles were collected 24 h after injection. (Scale bars: 10 μm.) *(D)* Electrophysiological recordings of EJPs at soleus NMJs treated with α-Ltx alone (5 μg/kg; black bars) or with α-Ltx plus catalase (750 U; white bars). At 72 h EJP amplitudes of fibers exposed to toxin plus catalase are significantly smaller than those exposed to the sole toxin ($**P < 0.01$).

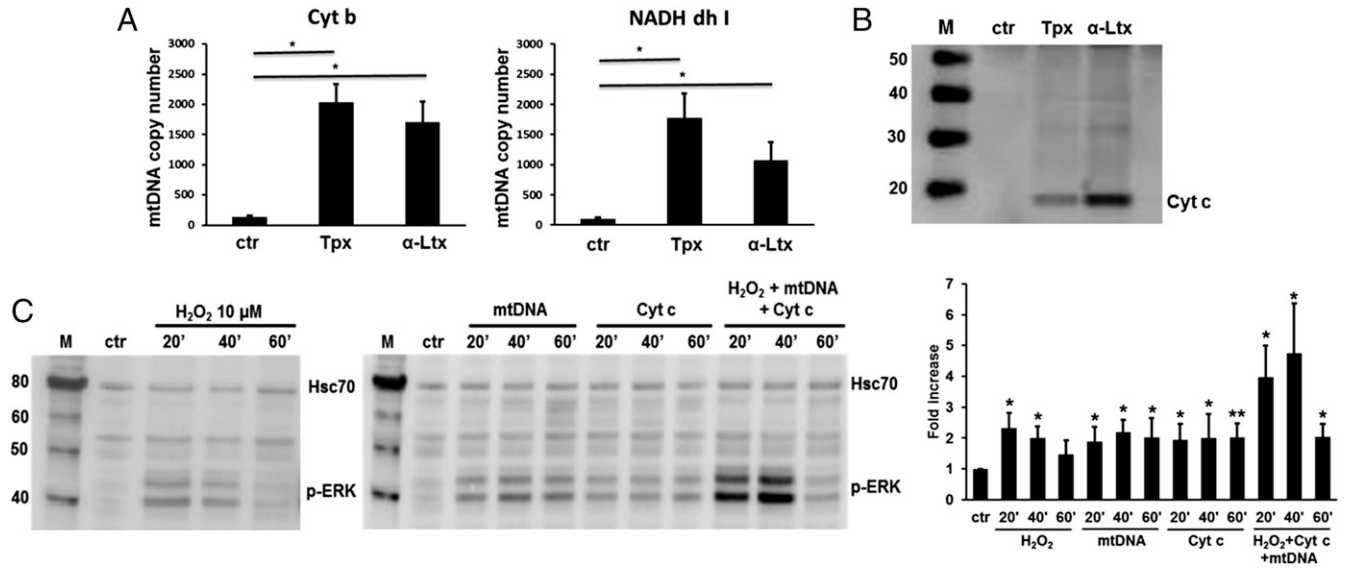

Fig. 3. Mitochondrial DNA and cytochrome *c* are released by degenerating neurons and activate the ERK pathway, together with hydrogen peroxide. (*A*) Real-time qPCR performed on CGNs supernatants from control and toxin-treated samples (Tpx 6 nM or α-Ltx 0.1 nM for 50 min), using primers specific for rat mitochondrial genes Cyt b and NADH dhI. DNA copy numbers of control and treated samples have been quantified. $*P < 0{,}05$; $n = 11$. (*B*) Supernatants from control and neurons treated as described earlier were precipitated with TCA and probed for Cyt c immunoreactivity in Western blot. (*C*) Time-course of ERK-phosphorylation induced in primary SCs by H_2O_2 (10 μM), mtDNA (10 μg/mL), and Cyt c (1 μg/mL) added alone or in a mixture and the relative quantification. Phospho-ERK signal was normalized to the Hsc70 band. $*P < 0.05$; $**P < 0.01$; $n = 3$.

(Fig. 2*C*). The importance of ERK pathway for SCs activation and regeneration was addressed by a pharmacologic approach: SCs-MNs cocultures exposed to the neurotoxins show a decreased ERK phosphorylation in the presence of the MEK 1 inhibitor PD98059 (Fig. S4 *A* and *B*); moreover, soleus muscles of mice pretreated with PD98059 and then locally injected with α-Ltx show a delayed recovery from paralysis with respect to mice injected with toxin only (Fig. S4*C*).

PSCs respond to neurotoxin-induced nerve degeneration by forming long sproutings and bridges between junctions of different fibers by the first day of injection (Fig. S5). This response has been long known to follow nerve terminal damage (35), and therefore, the present toxin-based model of acute nerve degeneration reproduces the known crucial aspects of regeneration.

To test whether H_2O_2 production by injured nerve terminals is important for functional regeneration, we performed electrophysiological recordings at soleus NMJs 16, 24, 48, and 72 h after i.m. injections of α-Ltx alone or α-Ltx plus catalase. Three days after treatment, fibers injected with α-Ltx plus catalase showed evoked junction potentials (EJPs) with significantly smaller amplitudes than those injected only with the toxin, indicating a slowdown of the regeneration process; muscles treated with catalase alone showed EJPs indistinguishable from the control (Fig. 2*D*). Immunohistochemistry on LAL muscles treated as described earlier confirmed the electrophysiological results, showing a delay in the recovery of synaptosomal-associated protein 25 (SNAP-25) staining, a presynaptic marker, in samples exposed to α-Ltx plus catalase compared with muscles injected with α-Ltx only (Fig. S6). At 24 h, SNAP-25 staining is recovered in 80% of the NMJs treated with α-Ltx (90% at 48 h) compared with 17% of the NMJs treated with α-Ltx plus catalase (33% at 48 h; $n = 40$). The disappearance of SNAP-25 during the degeneration steps takes place with a closely similar kinetic under the two conditions (Fig. S6). Four hours after intoxication, SNAP-25 displays a spotty distribution in nearly all NMJs analyzed (indicative of nerve terminal degeneration), both in the presence and absence of catalase; at 16 h, 68% of α-Ltx-treated NMJs have no more SNAP-25 versus 60% of catalase and α-Ltx-treated NMJs ($n = 30$).

mtDNA and Cyt C Are Released by Degenerating Neurons and Activate the ERK Pathway in Schwann Cells. We next tested whether mtDNA and Cyt c could act together with H_2O_2 as neuronal mediators of PSCs activation. For mtDNA detection, primary neurons were intoxicated, the supernatants collected, and DNA purified. The eluates were subjected to real-time PCR, using primers specific for the rat mitochondrial genes Cyt b and NADH dhI. Fig. 3*A* shows that mtDNA is indeed released in the neuronal supernatant after treatment with Tpx or α-Ltx. In another set of experiments, TCA-precipitated cell supernatants (sham or toxin-treated) were loaded in SDS/PAGE, followed by Western blotting. Samples were probed with an antibody against Cyt c: only toxin-treated samples showed a clear band corresponding to the intact, monomeric form of the protein (Fig. 3*B*). Control experiments showed no amplification when primers for the nuclear gene GAPDH were used (Fig. S7*A*), and the LDH assay on neuronal supernatant excluded a loss of membrane integrity (Fig. S7*B*). Thioredoxin 2, a mitochondrial protein with a molecular weight similar to Cyt c, was undetectable by Western blot of toxin-treated supernatants precipitated with TCA, thus supporting the conclusion that neuronal alarmins are released from intact membranes (Fig. S7*C*). Moreover, CGNs loaded with calcein-AM did not lose dye during 50 min incubation with both the toxins, indicating conservation of plasma membrane integrity (Fig. S7*D*).

Exposure of isolated SCs to mtDNA or Cyt c led to a sustained ERK phosphorylation, whereas a peak of p-ERK followed by progressive decline was observed upon H_2O_2 stimulation. When the three mitochondrial alarmins were added together, an additive effect on ERK phosphorylation was observed (Fig. 3*C*).

Mitochondrial Alarmins Exit from Neurons. H_2O_2 is permeable to biological membranes (49), whereas mtDNA and Cyt c must be released from mitochondrial and plasma membranes to reach the extracellular medium. Pretreatment of neurons with cyclosporin A, a drug that desensitizes the mitochondrial permeability transition pore (PTP) via its binding to cyclophilin D (50), reduces both mtDNA and Cyt c release triggered by the toxins (Fig. 4 *A* and *B*), suggesting these molecules can exit mitochondria and

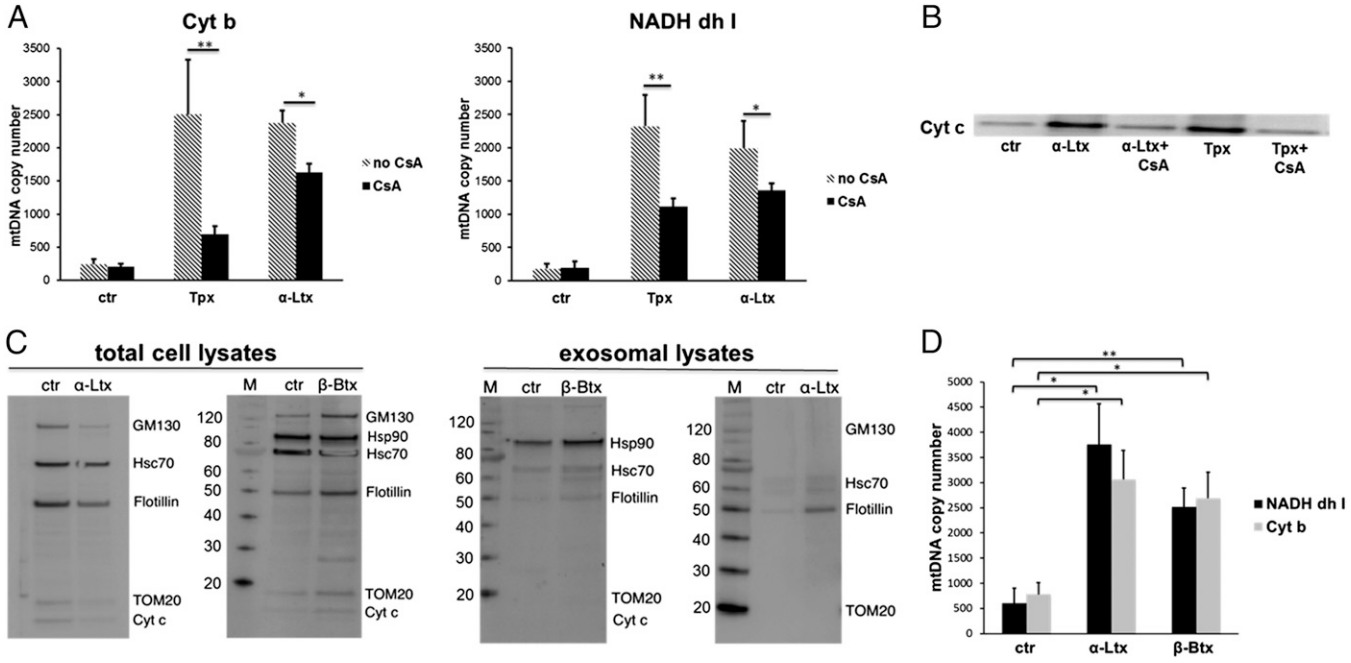

Fig. 4. Mitochondrial alarmins exit from neurons. Preincubation with cyclosporine A (5 μM for 30 min) significantly reduced both mtDNA (*A*) and Cyt c release (*B*) induced by exposure of CGNs to Tpx or α-Ltx (6 nM and 0.1 nM for 50 min, respectively). $*P < 0.05$; $**P < 0.01$; $n = 3$. (*C*) Exosomes were purified from CGNs supernatants and probed for the exosome-enriched proteins flotillin, Hsc70, and Hsp90. The absence of the Golgi marker GM130 and of the mitochondrial one Tom20 is indicative of uncontaminated preparations (*Right*). Cellular lysates are positive for all markers tested (*Left*). (*D*) DNA was extracted from exosomes purified from the supernatants of α-Ltx- and β-Btx-treated CGNs (0.1 and 6 nM for 50 min, respectively) and subjected to real-time qPCR for the detection of mtDNA. $*P < 0.05$; $**P < 0.01$; $n = 5$.

reach the cytoplasm through the PTP, whose opening is indeed induced by snake neurotoxins (51).

Because neuronal plasma membrane integrity is preserved, how do these alarmins reach the extracellular medium? We posited that exosomes might be involved and have purified them from control and treated neuronal supernatants. Purified exosomes were found enriched in Hsp90, Hsc70, flotillin, and CD63; no contamination with Golgi, mitochondrial, or plasma membranes was detected (Fig. 4*C* and Fig. S8 *A* and *B*). Electron microscopy and immunogold labeling of purified exosomes confirmed their correct morphology, size, and positivity for Hsp90 (Fig. S8*C*). Next, we purified total DNA from exosomes and performed real-time PCR to check for their mtDNA content. Fig. 4*D* shows that exosomes released by α-Ltx- and β-Btx-intoxicated neurons do contain mtDNA. Similar mtDNA copy numbers were found before and after DNase treatment of exosomal fractions, indicating that mtDNA is indeed inside exosomes (Fig. S8*D*). In contrast, no Cyt c was detected in exosomes by Western blotting; this is likely to be a result of the much lower sensitivity of Western blotting with respect to RT-PCR, but the possibility that Cyt c is released from damaged nerve terminals via other mechanisms cannot be discarded.

Phagocytosis Is Induced in PSCs During Nerve Terminal Injury. During toxin-induced neurodegeneration, PSCs at poisoned NMJs undergo evident morphological changes, showing a number of intracellular structures appearing dense by light microscopy (Fig. 5*A*, *Lower*). These structures are particularly evident at 4 h after α-Ltx injection, with a reduction in number and size with time (Fig. 5*A*).

The appearance and life span of these structures parallel nerve terminal degeneration, suggesting they might be phagosomes involved in the clearance of nerve debris. Accordingly, immunostaining of sham or poisoned LAL muscles for the scavenger macrophage receptor CD68 was performed. After α-Ltx injection, perineural SCs of LAL NMJs do express CD68 on these intracellular structures, supporting their phagocytic role (Fig. 5*B*). CD68-positive structures also appear after β-Btx treatment, but at a later time (16 h), as expected on the basis of the different time course of pathogenesis of the two neurotoxins (Fig. 5*B*). Lysotracker-positive staining confirmed the acidic nature of such compartments (Fig. 5*C*). CD68-positive macrophages were also recruited in the proximity of neurotoxin-treated NMJs, with a typical migrating phenotype (Fig. S9); this is consistent with the chemoattractant role of H_2O_2 (52–54). In contrast, polymorphonuclear leukocytes, which are recruited by axonal degradation (54), were rarely seen in the many samples we have inspected.

Four hours after α-Ltx injection, the distribution of the presynaptic markers neurofilaments (NF) and SNAP-25 is altered, with clear fragmentation in many junctions, as a result of the specific and localized nerve terminal degeneration induced by the neurotoxins (Fig. 6 *A* and *B*). SNAP-25-positive spots localize within PSCs phagosomes (the same holds true for NF), as shown by orthogonal projections (Fig. 6*C*), confirming that phagocytosis by PSCs and macrophages is taking place during nerve terminal degeneration.

Discussion

The present article describes an original approach to study motor axon terminals degeneration and regeneration. This model system is based on the use of animal presynaptic neurotoxins highly specific for nerve terminals with a well-defined biochemical mechanism of action (10, 12, 16, 18). Here, these neurotoxins are used as tools to induce localized and reversible nerve degeneration, followed by complete regeneration. This system is more controllable than the classical cut and crush approaches, which are invasive and inevitably damage several cell types, triggering a pronounced inflammatory response (55). Moreover, this model avoids some adverse effects of techniques such as laser ablation (high temperatures, photooxidation, etc). The model proposed here is therefore better suited to

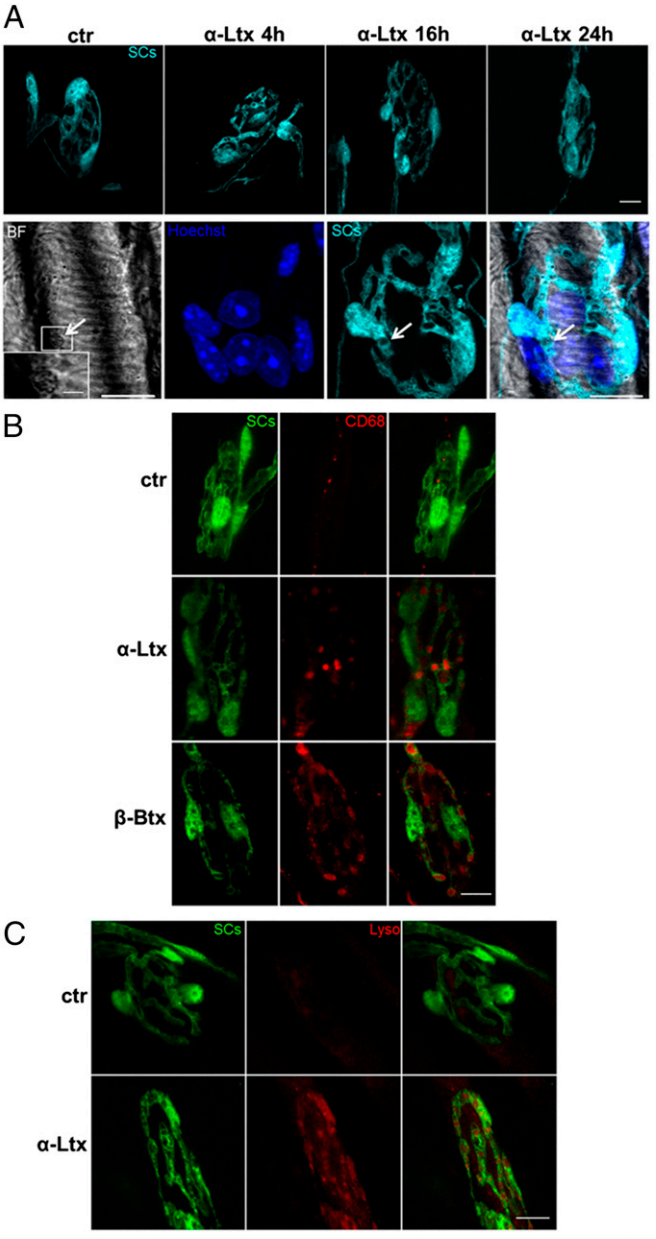

Fig. 5. Nerve terminal degeneration triggers phagocytosis in terminal SCs at the NMJ. (*A*) LAL muscles from transgenic mice were injected with α-Ltx (5 μg/kg), collected at different time points (4, 16, 24 h), and processed for indirect immunohistochemistry. PSCs (cyan) show intracellular structures of different size that are particularly evident after 4 h of intoxication. These structures appear dense by light microscopy (brightfield, *Lower*, arrows). Nuclei are stained with Hoechst (blue). (Scale bars: 10 μm.) (*B*) PSCs (green) at α-Ltx- and β-Btx-treated NMJs (4 and 16 h of intoxication, respectively) are positive for the phagocytic marker CD68 (red), which stains intracellular vesicular structures. A very low CD68 signal is detected in control NMJs. (Scale bars: 10 μm.) (*C*) Ex vivo Lysotracker staining (red) of α-Ltx-treated LAL (4 h) confirms the acidic nature of intracellular vacuoles. (Scale bar: 10 μm.)

study the inter- and intracellular signaling and transcriptomic events involved in the regeneration process.

Spider and snake presynaptic neurotoxins induce, by different biochemical mechanisms, a large entry of calcium in axon terminals, which in turn leads to mitochondrial failure and nerve terminal degeneration. At the same time, PSCs perceive the damage occurring to the motor axons and respond by dedifferentiating to a progenitor-like state, proliferating and assisting nerve regeneration. They acquire macrophagic-like activities that contribute to the removal of nerve cell debris and facilitate reinnervation, similar to what was found previously after nerve crush (23). Moreover, upon extensive cytoskeletal reorganization, PSCs send out long projections, along which the regenerating nerve terminals extend sprouts, which originate from the nonmyelinated axon terminal to innervate adjacent denervated junctions (34, 35).

It was recently shown that the MAPK signaling pathway has a central role in controlling SC plasticity and peripheral nerve regeneration via the activation of ERK1/2 and JNK, which activate the transcription complex activator protein 1, of which c-Jun is a key component (44, 45, 56). The major result obtained here, using p-ERK as a read-out, is that alarmins released by mitochondria of degenerating axon terminals activate SCs. Mitochondria are abundant components of the motor axons terminals, and here we define them as a source of mediators that are released under cytosolic calcium overload. The rapid accumulation of Ca^{2+} inside mitochondria causes the opening of the PTP and the exit of alarmins (50). Mitochondrial alterations are hallmarks of nerve terminal damage (19, 20), and therefore the present findings can be extrapolated to several other nerve terminal pathological conditions.

Mitochondria of stressed cells produce reactive oxygen species (ROS), among which H_2O_2 is the most stable species (37, 38, 57). It is a very reactive molecule that can permeate biological membranes. As PSCs and axon terminals are in close contact within the NMJ, significant amounts of H_2O_2 released by axon terminals can reach PSCs before it becomes inactivated by cellular antioxidant defense systems. Once within the target cell, H_2O_2 can act as a second messenger via chemoselective oxidation of cysteine residues in signaling proteins and via ERK phosphorylation. Collectively, these properties make H_2O_2 an ideal mediator of signal transduction processes (36–38, 42, 58). Recent experimental

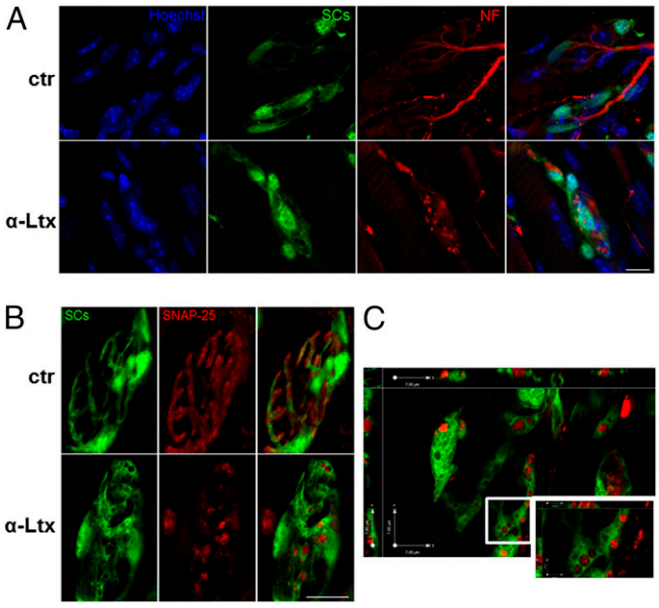

Fig. 6. Degenerating terminals are engulfed by perisynaptic SCs. (*A*) PSCs engulf presynaptic components, as shown by NF-positive staining of PSCs phagosomes at NMJs treated for 4 h with α-Ltx (red, *Lower*). (*Upper*) control NMJs. Nuclei are stained with Hoechst (blue). (Scale bars: 10 μm.) (*B*) Control NMJs with typical SNAP-25 presynaptic localization (red). In α-Ltx-treated NMJs (4 h), SNAP-25 aggregates localize within PSC phagosomes. (Scale bars: 10 μm.) (*C*) Orthogonal projections of α-Ltx-treated NMJs show that SNAP-25 positive aggregates are inside PSCs phagosomes. (Scale bars: 10 μm.)

evidence in different animal models demonstrated that a rapid concentration gradient of H_2O_2 is generated during injury and that H_2O_2 is a powerful chemoattractant of leukocytes (53, 54). Moreover, lowering ROS levels by pharmacologic or genetic approaches reduces cell proliferation and impairs regeneration (59). We therefore have imaged H_2O_2 in living neurons exposed to neurotoxins with novel specific fluorescent probes (39, 40) and found that the degenerating nerve terminals release H_2O_2 of mitochondrial origin. This H_2O_2 activates PSCs in vitro and in vivo. We also found that macrophages are recruited around the neurotoxin-treated NMJs. It is therefore likely that these macrophages are attracted by H_2O_2, as well as by molecules released by activated PSCs, as previously found (60, 61). The prominent role of H_2O_2 in neurotoxin-induced nerve degeneration and repair is proved by the impaired regeneration we observed in the presence of catalase.

In addition to H_2O_2, we found that mtDNA and Cyt c can act as mediators of neuronal damage and activate SCs via ERK pathway. When added in a mixture with H_2O_2, an additive effect on ERK phosphorylation is observed. As neuronal membrane integrity is preserved, the question arises of how mtDNA and Cyt c, coming from the mitochondrial matrix or the intermembrane space, respectively, can exit the cell. Several pieces of evidence indicate that mitochondria are central sensors for axonal degenerative stimuli (62), and the release of mtDNA fragments from PTP in isolated mitochondria has been documented (63). Here, the mitochondrial PTP was found to be involved in the exit of both mtDNA and Cyt c from mitochondria, with a significant reduction in the presence of the PTP desensitizing molecule cyclosporin A. Once in the cytosol, mtDNA and Cyt c could be released via the nonclassical or unconventional secretory route, including secretory lysosomes, membrane blebbing, multivesicular body-derived exosomes, or autophagy (64). Here, we found that exosomes purified from intoxicated neuronal supernatants contain mtDNA, whereas Cyt c was not detected, possibly because of the insufficient sensitivity of Western blot. It is also possible that Cyt c is released directly via contact sites between mitochondria and the presynaptic membrane, similar to those observed by electron microscopy in a closely similar pathological condition caused by autoimmune anti-ganglioside antibodies (65).

The present work has identified three mitochondrial alarmins involved in PSCs activation after an acute nerve injury and proposes H_2O_2 as the strongest inducer of PSCs response. Inactivation of H_2O_2 by catalase reduces ERK phosphorylation in SCs in culture and delays NMJ recovery in vivo after toxin-induced neuroparalysis and degeneration, supporting a crucial role of this molecule in the regeneration process.

Nerve damage triggers important morphologic and functional changes in PSCs aimed at promoting NMJ regeneration, confirming their endowed high plasticity and their crucial role in the clearance of nerve debris. Indeed, during nerve terminal degeneration, PSCs become CD68-positive, indicating an acquired phagocytic activity. Together with macrophages, but not neutrophils, activated PSCs were found here to remove nerve debris, thus permitting a functional nerve regeneration. This is at variance from what was found during axonal degeneration, where a pronounced neutrophil infiltration was detected (54).

The phagocytic features of PSCs described here represent an additional early read-out of PSCs activation at the injured NMJ. PSCs respond to axonal damage caused by neurotoxin poisoning by engulfing degenerating terminals, by extending long processes, and by activating intracellular signaling pathways crucial for regeneration. On the basis of these perspectives, we plan to study more in detail the intracellular signaling and transcriptomic events taking place inside activated PSCs. More in general, it appears that the present experimental approach can be extended to the investigation of other motor neuron diseases, including the non-cell-autonomous and dying-back axonopathy of ALS and autoimmune neuropathies including Guillain-Barré and Miller-Fisher syndromes (66, 67). Such studies are likely to provide relevant insights for future therapeutic endeavors.

Materials and Methods

Animal Strains. C57BL/6 mice expressing cytosolic GFP under the *plp* promoter (46, 47) were kindly provided by W. B. Macklin (Aurora, CO) via the collaboration of T. Misgeld (Munchen, Germany). All experiments were performed in accordance with the European Communities Council Directive n° 2010/63/UE and approved by the Italian Ministry of Health.

Hydrogen Peroxide Detection. Hydrogen peroxide generation in primary neurons was measured using Mitochondria Peroxy Yellow 1 (MitoPY1) (39) or Peroxyfluor 6 acetoxymethyl ester (PF6-AM) (40), synthesized in the C.J.C. laboratory (Berkeley, CA), specific probes of H_2O_2 production in mitochondria and cytoplasm, respectively. Both probes were loaded at 5 μM for 30 min at 37 °C in Krebs ringer buffer (KRH: Hepes 25 mM at pH 7.4, NaCl 124 mM, KCl 5 mM, $MgSO_4$ 1.25 mM, CaCl2 1.25 mM, KH_2PO_4 1.25 mM, glucose 8 mM). Images were acquired at different points after toxin exposure with a DMI6000 inverted epifluorescence microscope (Leica) equipped with a 63× HCX PL APO oil immersion objective NA 1.4. Filter cubes (Chroma Technology) have an excitation range of 470/40 nm, a dichroic mirror 495LPXR, and an emission of 525/50 nm. Images were acquired with an Orca-Flash4 digital camera (Hamamatsu). Illumination was kept at a minimum to avoid ROS generation because of phototoxicity. To detect neuronal bulges, we took advantage of differential interference contrast microscopy. Fluorescence intensity quantification was carried out with ImageJ, and the statistical analysis with Prism (GraphPad).

Cell Treatments. CGNs (6 d in culture) plated onto 35-mm dishes (1.2 million cells per well) were exposed for 50–60 min to SPANs (6 nM) or to α-Ltx (0.1 nM) at 37 °C. In some experiments, neurons were preincubated for 30 min with cyclosporin A 5 μM before toxin addition. Supernatants or cell lysates were collected and then processed for real-time quantitative PCR (qPCR) or Western blot.

Primary SCs were exposed to different mitochondrial alarmins [H_2O_2 10–100 μM, Cyt c (R&D) 1 μg/mL, mtDNA 10 μg/mL] or to the toxins for different times and lysed in Lysis Buffer [Hepes 10 mM, NaCl 150 mM, SDS 1%, EDTA 4 mM, protease inhibitors mixture (Roche), and phosphatase inhibitor mixture].

Cocultures were treated with the toxins and then lysed after different points; in a set of experiments, 1,000 U per well catalase was added 5 min before intoxication and kept throughout the experiment; in another set, cocultures were incubated with the MEK1 inhibitor PD98059 (Cell Signaling; 80 μM) 1 h before toxins addition. Samples were then probed for p-ERK.

Immunofluorescence. After treatments, isolated SCs or cocultures were fixed for 15 min in 4% (wt/vol) paraformaldehyde (PFA) in PBS, quenched (0.38% glycine, 0.24% NH_4Cl in PBS), and permeabilized with 0.3% Triton X-100 in PBS for 5 min at room temperature (RT). After saturation with 3% (vol/vol) goat serum in PBS for 1 h, samples were incubated with primary antibodies [anti-Phospho-p44/42 MAPK (Cell Signaling), 1:1,000; anti- anti-NF200 (Sigma), 1:200; anti-S100 (Sigma), 1:1,000] diluted in 3% (vol/vol) goat serum in PBS overnight at 4 °C, washed, and then incubated with the correspondent secondary antibodies (Alexa-conjugated, 1:200; Life Technologies) for 1 h at RT. Coverslips were mounted in Mowiol and examined by confocal (Leica SP5) or epifluorescence (Leica CTR6000) microscopy.

In a set of experiments, CGNs were exposed to α-Ltx (0.1 nM, 50 min) or PMA (phorbol 12-myristate 13-acetate, 1 μg/mL, 20 min) and processed for immunofluorescence as described earlier. p47phox was detected by a monoclonal antibody (Santa Cruz; 1:200).

NMJ Immunohistochemistry. α-Ltx (5 μg/kg) or β-Btx (10 μg/kg) were diluted in 25 μL physiological saline (0.9% wt/vol NaCl in distilled water) and injected s.c. in proximity of the LAL muscle of anesthetized transgenic C57BL/6 male mice (expressing a cytosolic GFP under the *plp* promoter) (46, 47) of around 20–25 g. Control animals were injected with saline. LAL muscles were dissected at different points after injections and fixed in 4% (wt/vol) PFA in PBS for 30 min at RT. Samples were quenched, permeabilized, and saturated for 2 h in 15% (vol/vol) goat serum, 2% (wt/vol) BSA, 0.25% gelatin, 0.20% glycine, and 0.5% Triton X-100 in PBS. Incubation with the following primary antibodies was carried out for at least 48 h in blocking solution: anti-neurofilaments (mouse monoclonal, anti-NF200, 1:200; Sigma), anti-SNAP-25 (SMI81 mouse monoclonal, 1:200; Covance), and anti-CD68 (mouse monoclonal, 1:200; Santa Cruz). Muscles were then washed and incubated with secondary antibodies (Alexa-conjugated, 1:200 in PBS; Life Technologies). Nuclei were stained with Hoechst. For p-ERK detection incubation with the

primary antibody (anti-Phospho-p44/42 MAPK, 1:1,000; Cell Signaling) was carried out for 72 h and the tyramide signal amplification kit (Perkin-Elmer) was used (45).

To stain acidic compartments, LAL muscles collected after 4 h of intoxication were loaded ex vivo with LysoTracker Red DND-99 (1:5,000; Life Technologies) for 2–3 min (68) while being continuously perfused with oxygenated Neurobasal A medium (Life Technologies). Samples were then fixed and processed for indirect immunohistochemistry, as described earlier. Images were collected with a Leica SP5 confocal microscope equipped with a 63× HCX PL APO NA 1.4. Laser excitation line, power intensity, and emission range were chosen according to each fluorophore in different samples to minimize bleed-through.

Electrophysiological Recordings. Electrophysiological recordings were performed in oxygenated Krebs-Ringer solution on sham or α-Ltx-injected soleus muscles (α-Ltx 5 μg/kg, with or without 750 U catalase), using intracellular glass microelectrodes (WPI) filled with one part 3 M KCl and two parts 3 M CH_3COOK. In another set of experiments, muscles were locally injected with PD98059 (50 μg in DMSO) 1 h before α-Ltx injection.

Evoked neurotransmitter release was recorded in current-clamp mode, and resting membrane potential was adjusted with current injection to −70 mV. EJPs were elicited by supramaximal nerve stimulation at 0.5 Hz, using a suction microelectrode connected to a S88 stimulator (Grass). To prevent muscle contraction after dissection, samples were incubated for 10 min with 1 μM μ-Conotoxin GIIIB (Alomone).

Signals were amplified with intracellular bridge mode amplifier (BA-01X, NPI), sampled using a digital interface (NI PCI-6221, National Instruments) and recorded by means of electrophysiological software (WinEDR; Strathclyde University). EJPs measurements were carried out with Clampfit software (Molecular Devices).

Statistical Analysis. The sample size (N) of each experimental group is described in each corresponding figure legend, and at least three biological replicates were performed. Prism (GraphPad Software) was used for all statistical analyses. Quantitative data displayed as histograms are expressed as means ± SEM (represented as error bars). Results from each group were averaged and used to calculate descriptive statistics. Significance was calculated by Student's *t* test (unpaired, two-side). *P* values less than 0.05 were considered significant.

ACKNOWLEDGMENTS. We gratefully thank Dr. W. B. Macklin and Dr. T. Misgeld for providing the C57BL/6 transgenic mice strain and Dr. P. Caccin for the kind help with EM experiments. This work was supported by the Cariparo Foundation and the Provincia autonoma di Trento, Bando Grandi Progetti 2012 (to C.M.). M.R. is the recipient of Young Investigators Grant GR-2010-2320779 from the Italian Ministry of Health. C.J.C. is an Investigator with the Howard Hughes Medical Institute, and his contributions are supported by NIH Grant GM79465.

1. Pearn JH (1971) Survival after snake-bite with prolonged neurotoxic envenomation. *Med J Aust* 2(5):259–261.
2. Connolly S, et al. (1995) Neuromuscular effects of Papuan Taipan snake venom. *Ann Neurol* 38(6):916–920.
3. Kularatne SA, Senanayake N (2014) Venomous snake bites, scorpions, and spiders. *Handb Clin Neurol* 120:987–1001.
4. Duchen LW, Gomez S, Queiroz LS (1981) The neuromuscular junction of the mouse after black widow spider venom. *J Physiol* 316:279–291.
5. Dixon RW, Harris JB (1999) Nerve terminal damage by beta-bungarotoxin: Its clinical significance. *Am J Pathol* 154(2):447–455.
6. Chang CC, Chen TF, Lee CY (1973) Studies of the presynaptic effect of -bungarotoxin on neuromuscular transmission. *J Pharmacol Exp Ther* 184(2):339–345.
7. Rosenthal L, Zacchetti D, Madeddu L, Meldolesi J (1990) Mode of action of alpha-latrotoxin: Role of divalent cations in Ca2(+)-dependent and Ca2(+)-independent effects mediated by the toxin. *Mol Pharmacol* 38(6):917–923.
8. Hurlbut WP, Ceccarelli B (1979) Use of black widow spider venom to study the release of neurotransmitters. *Adv Cytopharmacol* 3:87–115.
9. Ceccarelli B, Hurlbut WP (1980) Vesicle hypothesis of the release of quanta of acetylcholine. *Physiol Rev* 60(2):396–441.
10. Südhof TC (2001) alpha-Latrotoxin and its receptors: Neurexins and CIRL/latrophilins. *Annu Rev Neurosci* 24:933–962.
11. Ushkaryov YA, Rohou A, Sugita S (2008) alpha-Latrotoxin and its receptors. *Handbook Exp Pharmacol* (184):171–206.
12. Rossetto O, Montecucco C (2008) Presynaptic neurotoxins with enzymatic activities. *Handbook Exp Pharmacol* (184):129–170.
13. Gutiérrez JM, Theakston RD, Warrell DA (2006) Confronting the neglected problem of snake bite envenoming: The need for a global partnership. *PLoS Med* 3(6):e150.
14. Pungercar J, Krizaj I (2007) Understanding the molecular mechanism underlying the presynaptic toxicity of secreted phospholipases A2. *Toxicon* 50(7):871–892.
15. Kasturiratne A, et al. (2008) The global burden of snakebite: A literature analysis and modelling based on regional estimates of envenoming and deaths. *PLoS Med* 5(11): e218.
16. Rigoni M, et al. (2005) Equivalent effects of snake PLA2 neurotoxins and lysophospholipid-fatty acid mixtures. *Science* 310(5754):1678–1680.
17. Paoli M, et al. (2009) Mass spectrometry analysis of the phospholipase A(2) activity of snake pre-synaptic neurotoxins in cultured neurons. *J Neurochem* 111(3):737–744.
18. Rigoni M, et al. (2007) Calcium influx and mitochondrial alterations at synapses exposed to snake neurotoxins or their phospholipid hydrolysis products. *J Biol Chem* 282(15):11238–11245.
19. Cull-Candy SG, Fohlman J, Gustavsson D, Lüllmann-Rauch R, Thesleff S (1976) The effects of taipoxin and notexin on the function and fine structure of the murine neuromuscular junction. *Neuroscience* 1(3):175–180.
20. Harris JB, Grubb BD, Maltin CA, Dixon R (2000) The neurotoxicity of the venom phospholipases A(2), notexin and taipoxin. *Exp Neurol* 161(2):517–526.
21. Tedesco E, et al. (2009) Calcium overload in nerve terminals of cultured neurons intoxicated by alpha-latrotoxin and snake PLA2 neurotoxins. *Toxicon* 54(2):138–144.
22. Duregotti E, Tedesco E, Montecucco C, Rigoni M (2013) Calpains participate in nerve terminal degeneration induced by spider and snake presynaptic neurotoxins. *Toxicon* 64:20–28.
23. Son YJ, Trachtenberg JT, Thompson WJ (1996) Schwann cells induce and guide sprouting and reinnervation of neuromuscular junctions. *Trends Neurosci* 19(7): 280–285.
24. Feng Z, Ko CP (2008) The role of glial cells in the formation and maintenance of the neuromuscular junction. *Ann N Y Acad Sci* 1132:19–28.
25. Krysko DV, et al. (2011) Emerging role of damage-associated molecular patterns derived from mitochondria in inflammation. *Trends Immunol* 32(4):157–164.
26. Zhang Q, et al. (2010) Circulating mitochondrial DAMPs cause inflammatory responses to injury. *Nature* 464(7285):104–107.
27. Zornetta I, et al. (2012) Envenomations by Bothrops and Crotalus snakes induce the release of mitochondrial alarmins. *PLoS Negl Trop Dis* 6(2):e1526.
28. Robitaille R (1998) Modulation of synaptic efficacy and synaptic depression by glial cells at the frog neuromuscular junction. *Neuron* 21(4):847–855.
29. Rochon D, Rousse I, Robitaille R (2001) Synapse-glia interactions at the mammalian neuromuscular junction. *J Neurosci* 21(11):3819–3829.
30. Auld DS, Robitaille R (2003) Perisynaptic Schwann cells at the neuromuscular junction: Nerve- and activity-dependent contributions to synaptic efficacy, plasticity, and reinnervation. *Neuroscientist* 9(2):144–157.
31. Todd KJ, Auld DS, Robitaille R (2007) Neurotrophins modulate neuron-glia interactions at a vertebrate synapse. *Eur J Neurosci* 25(5):1287–1296.
32. Todd KJ, Darabid H, Robitaille R (2010) Perisynaptic glia discriminate patterns of motor nerve activity and influence plasticity at the neuromuscular junction. *J Neurosci* 30(35):11870–11882.
33. Griffin JW, Thompson WJ (2008) Biology and pathology of nonmyelinating Schwann cells. *Glia* 56(14):1518–1531.
34. Son YJ, Thompson WJ (1995) Schwann cell processes guide regeneration of peripheral axons. *Neuron* 14(1):125–132.
35. Son YJ, Thompson WJ (1995) Nerve sprouting in muscle is induced and guided by processes extended by Schwann cells. *Neuron* 14(1):133–141.
36. Paulsen CE, Carroll KS (2010) Orchestrating redox signaling networks through regulatory cysteine switches. *ACS Chem Biol* 5(1):47–62.
37. Dickinson BC, Chang CJ (2011) Chemistry and biology of reactive oxygen species in signaling or stress responses. *Nat Chem Biol* 7(8):504–511.
38. Murphy MP, et al. (2011) Unraveling the biological roles of reactive oxygen species. *Cell Metab* 13(4):361–366.
39. Dickinson BC, Chang CJ (2008) A targetable fluorescent probe for imaging hydrogen peroxide in the mitochondria of living cells. *J Am Chem Soc* 130(30):9638–9639.
40. Dickinson BC, Peltier J, Stone D, Schaffer DV, Chang CJ (2011) Nox2 redox signaling maintains essential cell populations in the brain. *Nat Chem Biol* 7(2):106–112.
41. Rigoni M, et al. (2004) Snake presynaptic neurotoxins with phospholipase A2 activity induce punctate swellings of neurites and exocytosis of synaptic vesicles. *J Cell Sci* 117(Pt 16):3561–3570.
42. Gough DR, Cotter TG (2011) Hydrogen peroxide: A Jekyll and Hyde signalling molecule. *Cell Death Dis* 2:e213.
43. Kemmerling U, et al. (2007) Calcium release by ryanodine receptors mediates hydrogen peroxide-induced activation of ERK and CREB phosphorylation in N2a cells and hippocampal neurons. *Cell Calcium* 41(5):491–502.
44. Harrisingh MC, et al. (2004) The Ras/Raf/ERK signalling pathway drives Schwann cell dedifferentiation. *EMBO J* 23(15):3061–3071.
45. Napoli I, et al. (2012) A central role for the ERK-signaling pathway in controlling Schwann cell plasticity and peripheral nerve regeneration in vivo. *Neuron* 73(4): 729–742.
46. Mallon BS, Shick HE, Kidd GJ, Macklin WB (2002) Proteolipid promoter activity distinguishes two populations of NG2-positive cells throughout neonatal cortical development. *J Neurosci* 22(3):876–885.
47. Brill MS, Lichtman JW, Thompson W, Zuo Y, Misgeld T (2011) Spatial constraints dictate glial territories at murine neuromuscular junctions. *J Cell Biol* 195(2):293–305.
48. Angaut-Petit D, Molgo J, Connold AL, Faille L (1987) The levator auris longus muscle of the mouse: A convenient preparation for studies of short- and long-term presynaptic effects of drugs or toxins. *Neurosci Lett* 82(1):83–88.
49. Miller EW, Dickinson BC, Chang CJ (2010) Aquaporin-3 mediates hydrogen peroxide uptake to regulate downstream intracellular signaling. *Proc Natl Acad Sci USA* 107(36):15681–15686.

50. Rasola A, Sciacovelli M, Pantic B, Bernardi P (2010) Signal transduction to the permeability transition pore. *FEBS Lett* 584(10):1989–1996.
51. Rigoni M, et al. (2008) Snake phospholipase A2 neurotoxins enter neurons, bind specifically to mitochondria, and open their transition pores. *J Biol Chem* 283(49): 34013–34020.
52. Klyubin IV, Kirpichnikova KM, Gamaley IA (1996) Hydrogen peroxide-induced chemotaxis of mouse peritoneal neutrophils. *Eur J Cell Biol* 70(4):347–351.
53. Niethammer P, Grabher C, Look AT, Mitchison TJ (2009) A tissue-scale gradient of hydrogen peroxide mediates rapid wound detection in zebrafish. *Nature* 459(7249): 996–999.
54. Li L, Yan B, Shi YQ, Zhang WQ, Wen ZL (2012) Live imaging reveals differing roles of macrophages and neutrophils during zebrafish tail fin regeneration. *J Biol Chem* 287(30):25353–25360.
55. Conforti L, Gilley J, Coleman MP (2014) Wallerian degeneration: An emerging axon death pathway linking injury and disease. *Nat Rev Neurosci* 15(6):394–409.
56. Arthur-Farraj PJ, et al. (2012) c-Jun reprograms Schwann cells of injured nerves to generate a repair cell essential for regeneration. *Neuron* 75(4):633–647.
57. Lambert AJ, Brand MD (2009) Reactive oxygen species production by mitochondria. *Methods Mol Biol* 554:165–181.
58. Holmström KM, Finkel T (2014) Cellular mechanisms and physiological consequences of redox-dependent signalling. *Nat Rev Mol Cell Biol* 15(6):411–421.
59. Love NR, et al. (2013) Amputation-induced reactive oxygen species are required for successful *Xenopus* tadpole tail regeneration. *Nat Cell Biol* 15(2):222–228.
60. Tofaris GK, Patterson PH, Jessen KR, Mirsky R (2002) Denervated Schwann cells attract macrophages by secretion of leukemia inhibitory factor (LIF) and monocyte chemoattractant protein-1 in a process regulated by interleukin-6 and LIF. *J Neurosci* 22(15): 6696–6703.
61. Martini R, Fischer S, López-Vales R, David S (2008) Interactions between Schwann cells and macrophages in injury and inherited demyelinating disease. *Glia* 56(14): 1566–1577.
62. Court FA, Coleman MP (2012) Mitochondria as a central sensor for axonal degenerative stimuli. *Trends Neurosci* 35(6):364–372.
63. Patrushev M, et al. (2004) Mitochondrial permeability transition triggers the release of mtDNA fragments. *Cell Mol Life Sci* 61(24):3100–3103.
64. Frühbeis C, Fröhlich D, Krämer-Albers EM (2012) Emerging roles of exosomes in neuron-glia communication. *Front Physiol* 3:119.
65. Halstead SK, et al. (2005) Anti-disialosyl antibodies mediate selective neuronal or Schwann cell injury at mouse neuromuscular junctions. *Glia* 52(3):177–189.
66. Vinsant S, et al. (2013) Characterization of early pathogenesis in the SOD1(G93A) mouse model of ALS: Part II, results and discussion. *Brain Behav* 3(4):431–457.
67. Plomp JJ, Willison HJ (2009) Pathophysiological actions of neuropathy-related anti-ganglioside antibodies at the neuromuscular junction. *J Physiol* 587(Pt 16): 3979–3999.
68. Song JW, et al. (2008) Lysosomal activity associated with developmental axon pruning. *J Neurosci* 28(36):8993–9001.

Supporting Information

Duregotti et al. 10.1073/pnas.1417108112

SI Materials and Methods

Toxins. α-Ltx and Tpx were purchased from Alomone, and β-Btx from Sigma. The purity of the toxins was checked by SDS/PAGE, and their neurotoxicity by ex vivo mouse nerve-hemidiaphragm preparation, as previously described (1).

Chemicals. Unless otherwise stated, all reagents were purchased from Sigma.

Primary Cell Cultures. Rat cerebellar granular neurons and rat spinal motoneurons were purified as described in ref. 2. Primary SCs were purified from sciatic nerves of six P3 Wistar rats. Briefly, sciatic nerves were dissected and tissues digested in 0.1% wt/vol collagenase and 0.25% wt/vol trypsin in L15 medium (Life Technologies), plus 0.3% BSA for 1 h. Dissociated cells were seeded onto uncoated Petri dishes in DMEM 10% (vol/vol) FBS; 24 h after seeding, 10 μM arabinoside C was added to the medium and kept for 2 d to prevent fibroblasts mitosis. Five days after seeding, an immunopanning with an anti-Thy1.1 antibody followed by rabbit complement addition was performed to eliminate contaminating fibroblasts. Purified SCs were subsequently plated on poly-L-lysine-coated dishes and allowed to grow in expansion medium consisting of DMEM, supplemented with 10% (vol/vol) FBS, 2 μM forskolin, and 10 nM heregulin β-1.

Primary Neurons-SCs Cocultures. CGNs and spinal MNs were used to set up cocultures with primary SCs. Briefly, 4 d after primary neurons seeding, primary SCs were added to neuronal cultures at an average density of 1×10^4 cells/cm^2. Cocultures were kept for 2–3 d in CGNs or MNs medium, respectively, and then processed for immunofluorescence or Western blotting.

Sample Preparation for Western Blotting.

Cyt c detection. CGNs were intoxicated as previously described, the supernatant was collected, and total proteins were precipitated with TCA [10% (vol/vol) final concentration]. The resulting pellet was suspended in loading sample buffer and denatured at 95 °C for 5 min. Samples were loaded on Precast 4–12% SDS-polyacrylamide gels (Life Technologies) and transferred to a nitrocellulose in a refrigerated chamber. After saturation, membranes were incubated overnight with a mouse monoclonal anti-Cyt c antibody (BD Biosciences; 1:1,000) followed by a secondary anti-mouse antibody HRP-conjugated (Life Technologies; 1:2,000). Chemiluminescence was developed with the Luminata TM Crescendo (Millipore) or ECL Advance Western blotting detection system (GE Healthcare) and was emission measured with ChemiDoc XRS (Bio-Rad). Band intensities were quantified on the original files with the software Quantity One (Bio-Rad). None of the bands reached signal saturation. In another set of experiments, TCA-precipitated supernatants were probed with a monoclonal antibody specific for thioredoxin 2 (Abcam; 1:1,000).

Phospho-ERK detection. Seven to 10 μg of total lysates from SCs or cocultures were loaded on SDS/PAGE. Protein concentration was quantified using the BCA assay (Protein Assay Kit; Pierce). Phospho-ERK was detected with a rabbit polyclonal antibody (anti-Phospho-p44/42 MAPK, 1:1,000; Cell Signaling). For densitometric quantification, the bands of interest were normalized to the housekeeping protein Hsc70 (monoclonal anti-Hsc70, 1:10,000; Synaptic Systems).

Real-Time qPCR. Supernatants of intoxicated neurons were collected and total DNA was extracted using the DNeasy Blood & Tissue kit (Qiagen) following manufacturer's instructions and subjected to real-time PCR. Primers for rat cytochrome B (forward 5′- TCCACTTCATCCTCCCATTC-3′ and reverse 5′-CTGCGTCGGAGTTTAATCCT-3′), rat NADH dehydrogenase I (forward 5′- CAATACCCCACCCCCTTATCAA-3′ and reverse 5′- GAGGCTCATCCCGATCATAGAA-3′), and rat GAPDH (forward 5′-ATTTCCTTTAATAAAGCCGGT-3′ and reverse 5′- TAAGAGACTTAAAATGACTTTG-3′) were synthesized by Life Technologies. Primer sequences have no significant homology with DNA found in any bacterial species published on BLAST.

Standards for quantification were obtained by PCR on total DNA isolated from cultured CGNs. Samples that produced no PCR products after 33 cycles were considered undetectable. Real-time qPCR was performed using iCyclerH thermal cycler (Bio-Rad). Amplification conditions were the following: 10 min at 95 °C, 40 cycles: 10 s at 95 °C, 30 s at 47.6 °C. A melting curve analysis, consisting of an initial step of 10 s at 65 °C and a slow elevation of temperature (0.5 °C/s) to 95 °C, was performed at the end of the amplification cycles to check for the absence of primer dimers and nonspecific products, using iQ SYBR Green supermix (BioRad). Results were expressed as copy numbers of target genes.

Mitochondrial DNA Purification. Mitochondrial DNA was extracted from 25 μg mice tibialis muscle, using the DNeasy Blood & Tissue kit (Qiagen), following manufacturer's instructions. DNA concentration was determined by spectrophotometer. No protein contamination was found. We checked the purity of mtDNA by real-time PCR, using primers for nuclear GAPDH.

Lactate Dehydrogenase Assay. Lactate dehydrogenase (LDH) activity was measured on the supernatants of CGNs plated on 96-well plates (150,000 cells/well) and exposed to the toxins as previously described, following manufacturer's instructions (Sigma). LDH activity measured in the total cell lysate was taken as 100% ($n = 3$).

Calcein Imaging. CGNs were loaded with calcein-AM (Life Technologies), 1 μM for 15 min at 37 °C in KRH, washed, and then exposed to α-Ltx 0.1 nM or Tpx 6 nM for 50 min. Fluorescence was monitored with time. Loss of calcein dye because of membrane permeabilization was achieved by the addition of 0.1% saponin. Images were acquired by epifluorescence (Leica CTR6000) microscopy.

Exosomes Purification. Exosomes were obtained from CGNs isolated from four rat cerebella (P6) following standard protocols (3). The mean total cell yield was 50–60 million cells (Mc). Cells plated on poly-L-lysine-coated 100-mm Petri dishes (10 Mc/dish) were grown till 6 d in culture; on the day of the experiment, plates were washed three to four times with warm KRH to remove the culture medium. α-Ltx 0.1 nM or β-Btx 6 nM were incubated in KRH for 45–60 min, and control samples were incubated with saline. Supernatants were then collected and subjected to cycles of centrifugations ($300 \times g$ for 10 min at 4 °C and $16,500 \times g$ for 20 min at 4 °C). The supernatant was then filtered through a 0.2-μm filter and centrifuged again at $120,000 \times g$ for 70 min at 4 °C to pellet exosomes, which were resuspended in loading buffer for SDS/PAGE analysis or in lysis buffer for DNA extraction. Each lane of SDS/PAGE corresponds to exosomes obtained from the medium of 10^7 neurons. Proteins enriched in exosomes such as flotillin, Hsc70, Hsp90, and CD63 were detected in both the exosomal and the total lysate fractions [anti-flotillin, 1:500 (BD

Biosciences); anti-Hsc70, 1:10,000 (Synaptic Systems); anti-Hsp90, 1:1,000 (BD Biosciences); and anti-CD63, 1:200 (Santa Cruz)]. To exclude contamination with other cell compartments, the exosomal fraction was assayed for Golgi (anti-GM130, 1:1,000; BD Transduction laboratories), mitochondrial (anti-TOM20, 1:1,000; Santa Cruz), and plasma membrane markers (anti-syntaxin 1A, 1:2,000; Synaptic Systems). DNA extraction from exosomes and real-time qPCR were performed as described earlier. In a set of experiments, exosomes were pretreated with purified DNase (1 U/μL, 1 h at 37 °C); DNase was inactivated at 65 °C for 10 min before DNA extraction and real-time qPCR.

Exosomes Identification by Electron Microscopy

The exosome-enriched pellet (purified from 60 Mc) was resuspended in PBS and ultracentrifuged at 120,000g for 70 min at 4 °C to repellet the exosomes. The pellets were immediately fixed by 2% (wt/vol) paraformaldehyde and applied to formvar-carbon-coated EM grids. For immunogold labeling, grids were incubated with anti-Hsp90 primary antibodies, which were then revealed using 5-nm gold-conjugated secondary antibodies (Sigma, 1:100). The exosomes were then stained with 1% uranyl acetate for 30 min. Observations were made using a transmission electron microscope (TECNAI G12, FEI) at 100 kV, equipped with a digital camera (Veleta, OSIS).

1. Rigoni M, et al. (2005) Equivalent effects of snake PLA2 neurotoxins and lysophospholipid-fatty acid mixtures. *Science* 310(5754):1678–1680.
2. Rigoni M, et al. (2007) Calcium influx and mitochondrial alterations at synapses exposed to snake neurotoxins or their phospholipid hydrolysis products. *J Biol Chem* 282(15):11238–11245.
3. Lachenal G, et al. (2011) Release of exosomes from differentiated neurons and its regulation by synaptic glutamatergic activity. *Mol Cell Neurosci* 46(2):409–418.

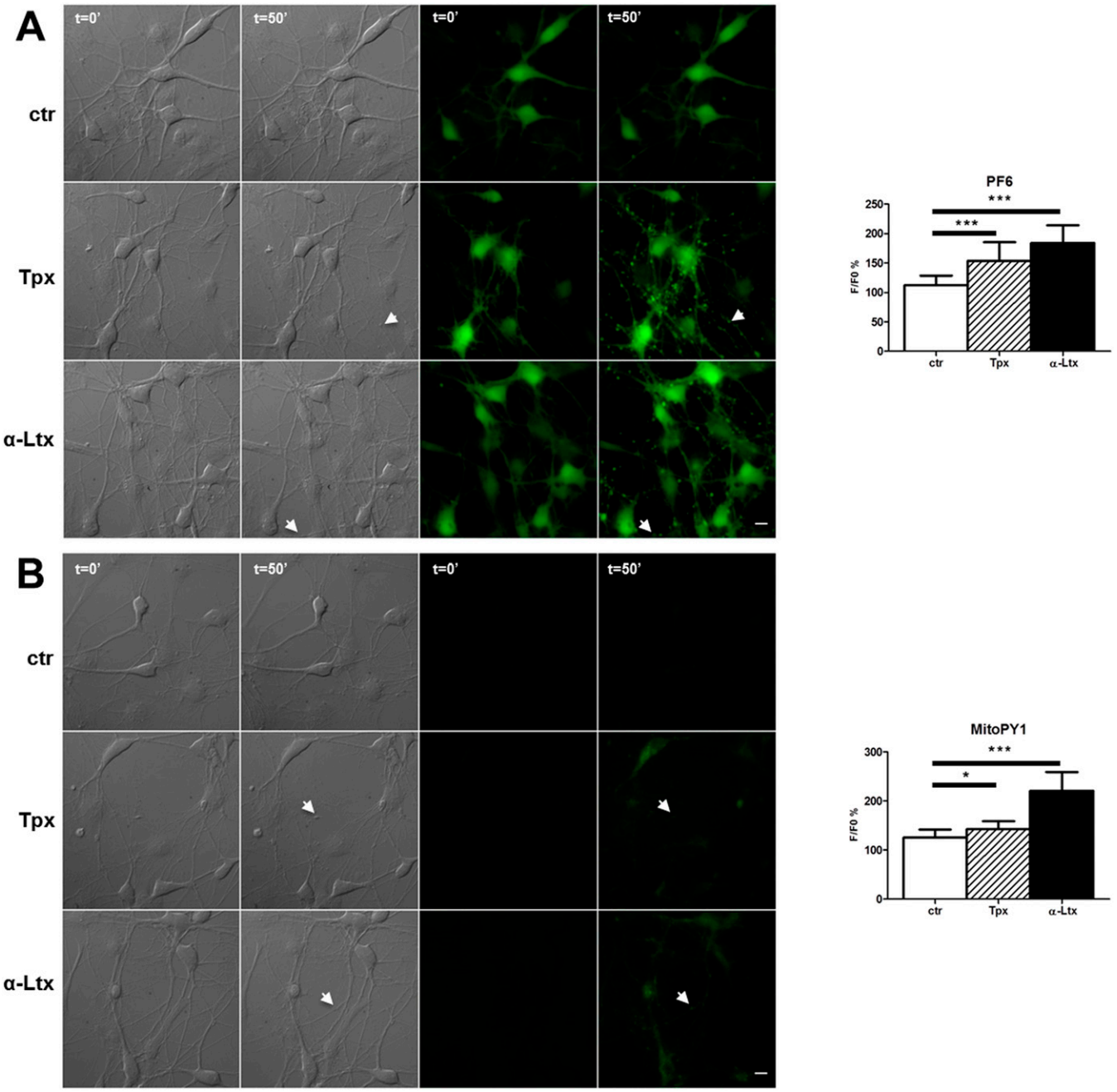

Fig. S1. *Live-imaging* of hydrogen peroxide production in spinal cord MNs. Rat MNs were loaded with the H_2O_2-specific probes PF6-AM (*A*) or MitoPY1 (*B*), washed, and then exposed to Tpx 6 nM or α-Ltx 0.1 nM for 50 min. Changes in fluorescence resulting from H_2O_2 production were measured at $t = 50$ min and expressed as a percentage of the fluorescence value at $t = 0$ (*Right*). $^*P < 0.05$; $^{***}P < 0.001$; $n = 15$. Arrows in bright-field images and in the green channel point to neuronal bulges. (Scale bars: 10 μm.)

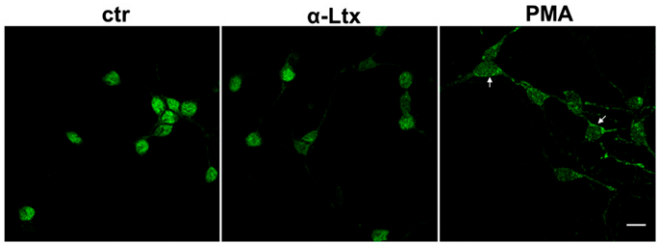

Fig. S2. NADPH oxidase is not involved in hydrogen peroxide production. p47phox staining was performed in CGNs exposed to α-Ltx (0.1 nM for 50 min) or to PMA (1 μg/mL for 20 min) as positive control for p47phox translocation. Arrows point to membrane accumulation of p47phox signal in PMA-treated cells. (Scale bar: 10 μm.)

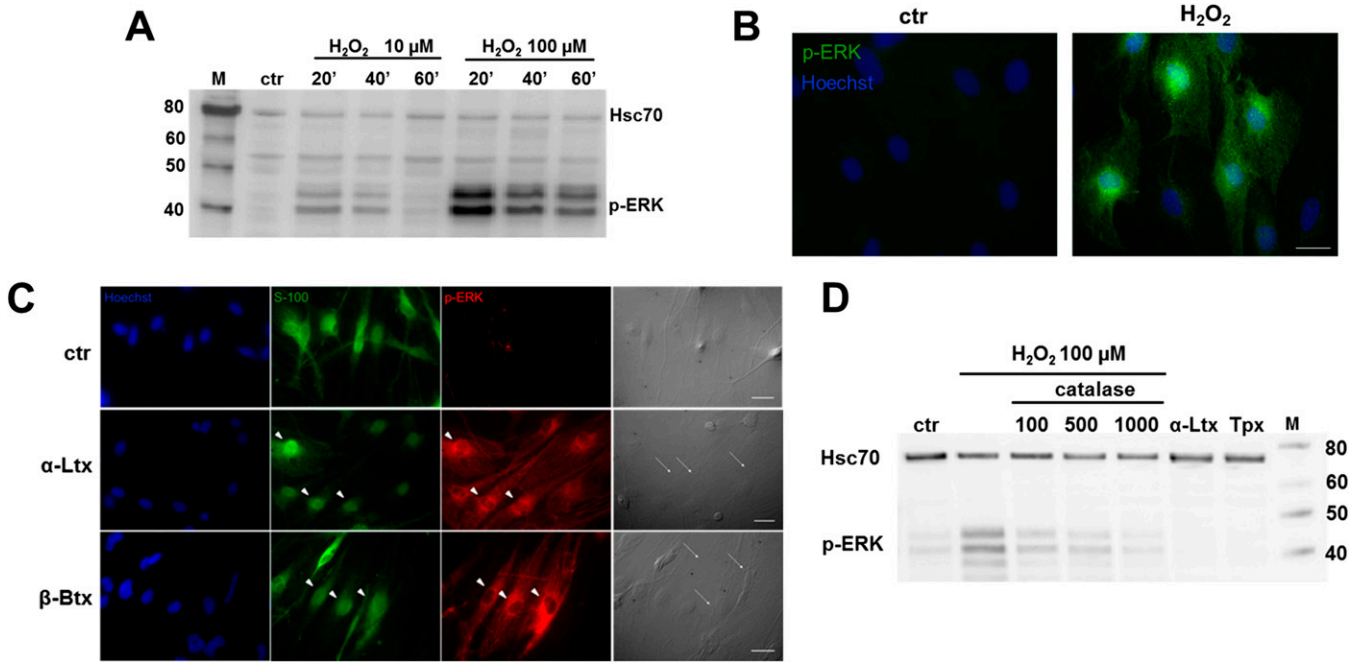

Fig. S3. Primary SCs respond to hydrogen peroxide by phosphorylating ERK. (*A*) Kinetic and dose-dependence of ERK phosphorylation induced in primary SCs by H_2O_2. (*B*) Immunofluorescence of p-ERK (green) in SCs after exposure to H_2O_2 (100 μM for 60 min). Nuclei are stained in blue. (Scale bar: 10 μm.) (*C*) Phospho-ERK positive cells (red) in SCs-MNs cocultures exposed to the neurotoxins are positive for the SCs marker S-100 (green, arrowheads). Arrows in bright-field panels point to bulges. (Scale bar: 20 μm.) (*D*) Preincubation of SCs with increasing amounts of catalase prevents ERK-phosphorylation by H_2O_2 to a different extent. Both α-Ltx and SPANs are ineffective in phosphorylating ERK in SCs.

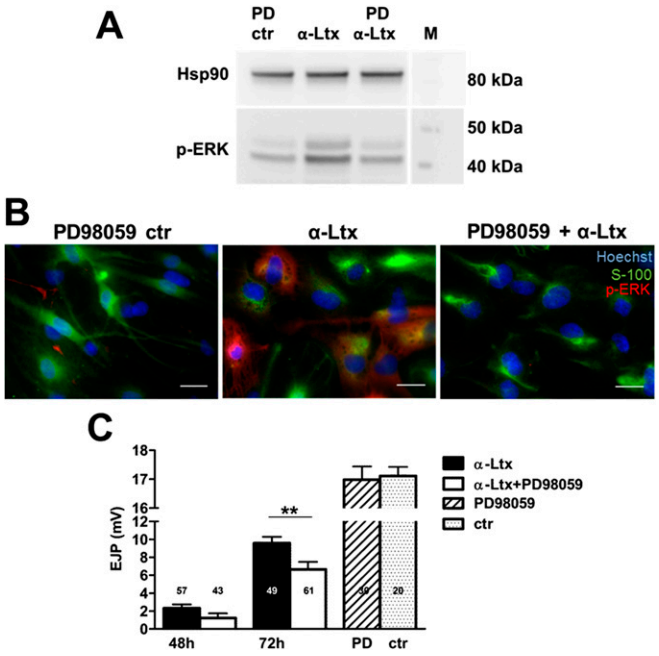

Fig. S4. ERK pathway is involved in SCs activation and subsequent nerve regeneration. SCs-MNs cocultures were pretreated with the MEK1 inhibitor PD98059 before α-Ltx exposure and then probed for p-ERK both in Western blot (*A*) and in immunofluorescence (*B*). The red channel represents p-ERK, and the green one the S-100 marker. Nuclei are stained with Hoechst. (Scale bar in *B*: 20 μm.) (*C*) Electrophysiological recordings of EJPs at soleus NMJs treated with α-Ltx alone (5 μg/kg, black bars) or pretreated with PD98059 (50 μg) before α-Ltx injection (white bars). At 72 h, EJP amplitudes of fibers pretreated with the inhibitor are significantly smaller than those exposed to toxin only (**$P < 0.01$).

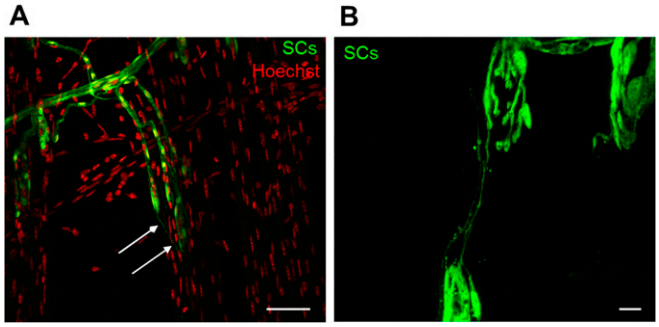

Fig. S5. PSCs activation after toxin-induced nerve terminal degeneration. (*A*) PSCs sproutings (green), typical hallmarks of regeneration, are observed at poisoned LAL NMJs by 24 h from α-Ltx injection. Nuclei are stained with Hoechst (red). In some instances, PSCs sproutings form bridges between adjacent junctions (*B*). (Scale bar: 50 μm in *A*, 10 μm in *B*.)

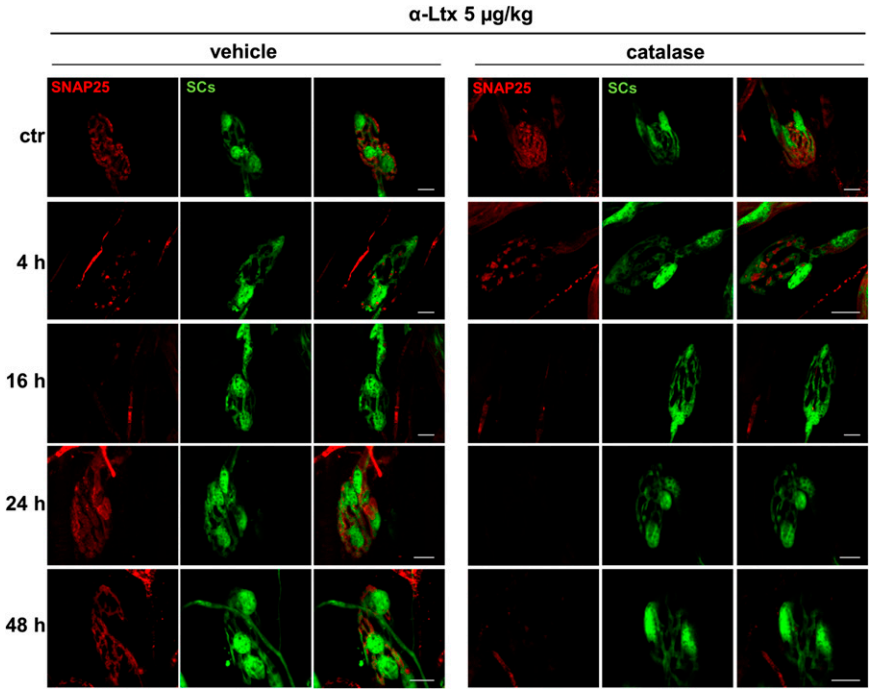

Fig. S6. Regeneration of poisoned presynaptic nerve terminals is delayed by catalase. SNAP-25 labeling (red) was used as read-out to monitor degeneration and regeneration of nerve terminals at the NMJs of LAL muscles s.c. injected with α-Ltx or α-Ltx plus catalase (750 U). Muscles were collected after 4, 16, 24, and 48 h, and representative images are shown. (Scale bars: 10 μm.)

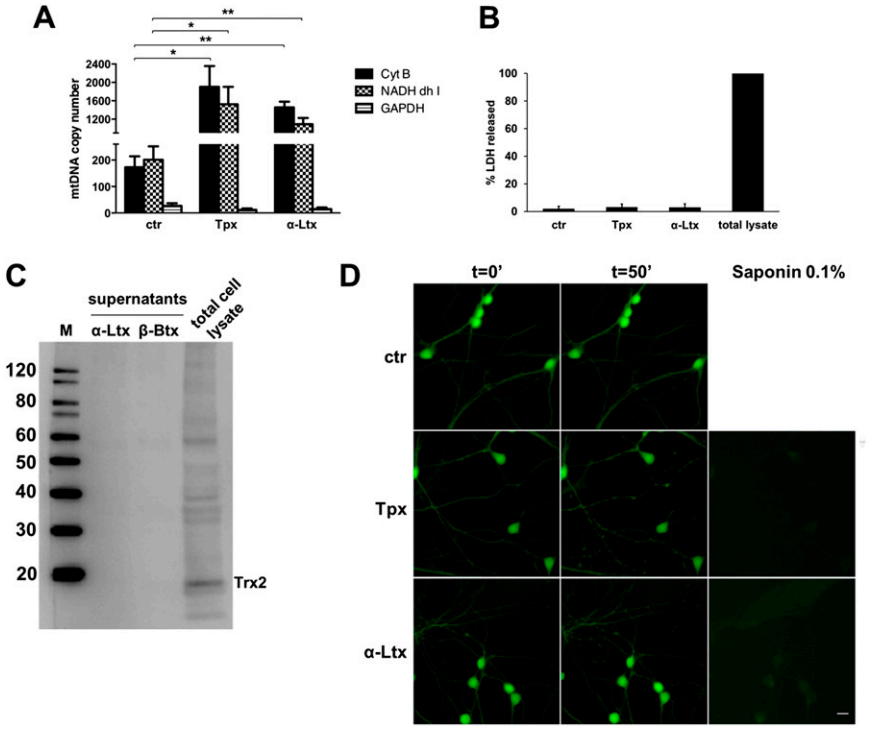

Fig. S7. Neuronal DAMPs are released from intact membranes. (*A*) No GAPDH amplification (nuclear housekeeping gene) was detected by real-time qPCR in neuronal supernatants after 50 min intoxication with α-Ltx or SPANs. $*P < 0.05$; $**P < 0.01$; $n = 3$. (*B*) LDH enzymatic activity was determined in the supernatants of neurons exposed for 50 min to Tpx or to α-Ltx. LDH release is an index of loss of membrane integrity. Data represent the mean of three independent experiments. (*C*) Thioredoxin 2, a mitochondrial protein of similar size to Cyt c, is detectable by Western blot only in CGNs lysates, but not in supernatants of neurons treated with α-Ltx or β-Btx (0.1 or 6 nM for 50 min, respectively) after TCA precipitation. (*D*) Membrane integrity was also assessed by calcein-AM retention in CGNs treated with Tpx or α-Ltx for 50 min. Calcein staining is lost after saponin-induced membrane permeabilization. (Scale bar: 10 μm.)

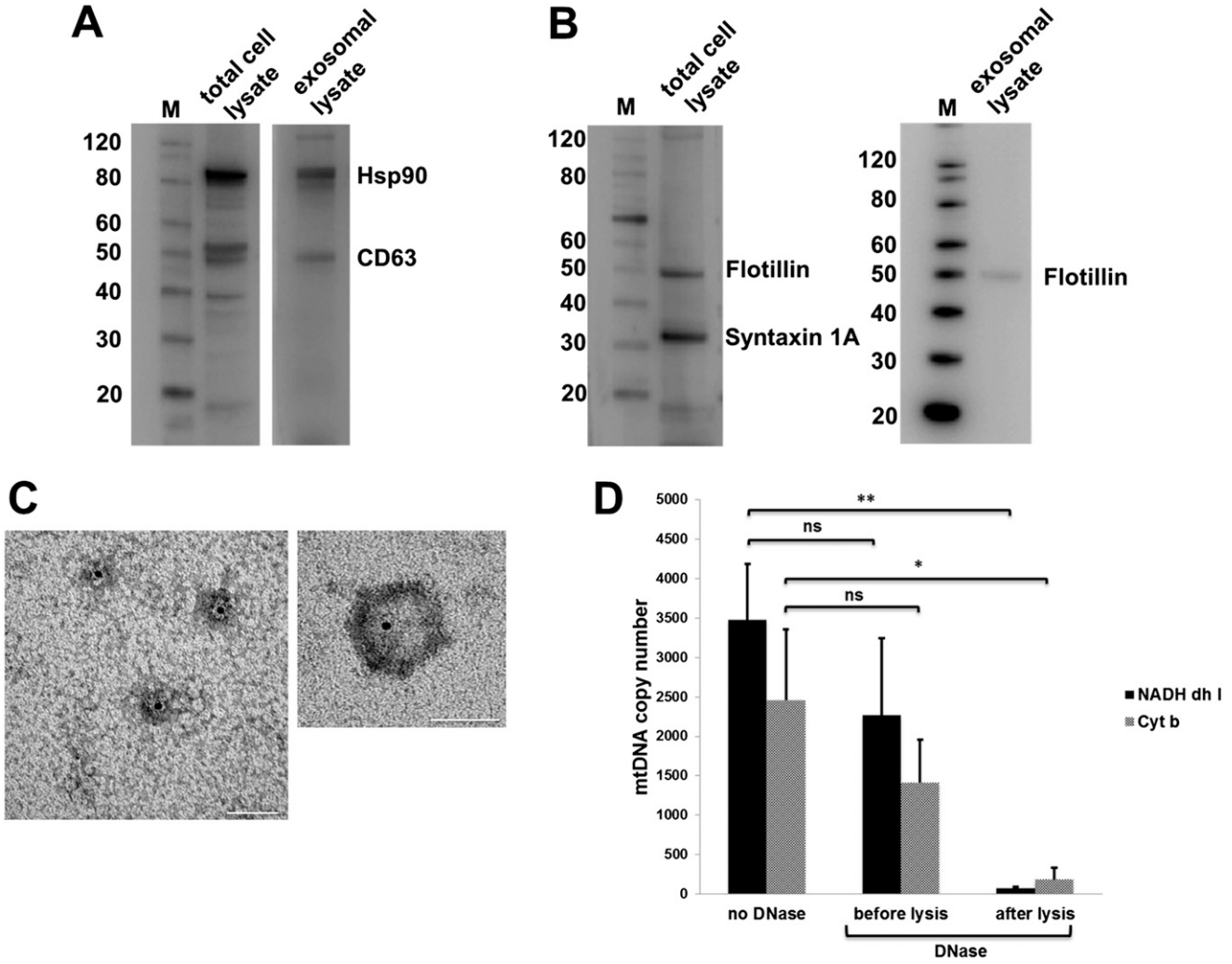

Fig. S8. Mitochondrial DNA is carried inside exosomes. Purified exosomes are positive for the exosomal marker CD63 (*A*) and negative for the plasma membrane marker syntaxin 1A (*B*). (*C*) Immunogold labeling of purified exosomes shows positivity for the exosomal marker Hsp90 and confirms their correct size and morphology. (Scale bars: 50 nm.) (*D*) Real-time PCR for the detection of mtDNA in exosomes treated with DNase (1 U/μL for 60 min). Exosomes were incubated with DNase before or after lysis and DNA purification. $*P < 0.05$; $**P < 0.01$; $n = 3$.

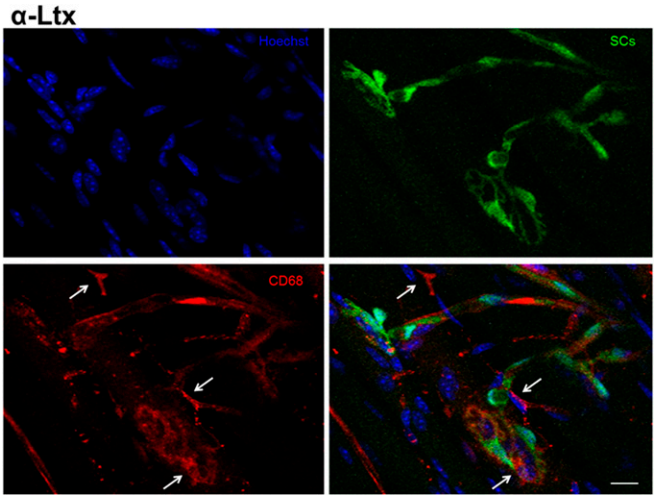

Fig. S9. Macrophages are recruited at the poisoned NMJ. CD68-positive macrophages (red, white arrows) are observed at the NMJs of LAL muscles injected with α-Ltx during nerve terminal degeneration (16 h intoxication). (Scale bar: 10 μm.)